Mitigation of Distortion in WDM Systems Based on Optical Phase Conjugation

A Thesis Submitted to the Institute of Laser for Postgraduate Studies, University of Baghdad in Partial Fulfillment of the Requirements for the Degree of Doctor of Philosophy in Laser / Electronics and Communication Engineering

By
Adnan Sabbar Abbas

B.Sc. Electrical Engineering - 2005
M. Sc. Electronics and Communication - 2012

2017 AD   **1439 AH**

Mitigation of Distortion in WDM Systems Based on Optical Phase Conjugation

A Thesis Submitted to the Institute of Laser for Postgraduate Studies, University of Baghdad in Partial Fulfillment of the Requirements for the Degree of Doctor of Philosophy in Laser / Electronics and Communication Engineering

By

Adnan Sabbar Abbas

B.Sc. Electrical Engineering - 2005
M. Sc. Electronics and Communication - 2012

Supervisor
Prof. Dr. Mazin M. Elias

2017 AD   **1439 AH**

بِسْمِ اللَّهِ الرَّحْمَٰنِ الرَّحِيمِ

نَرْفَعُ دَرَجَاتٍ مَّن نَّشَاءُ
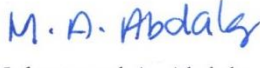
وَفَوْقَ كُلِّ ذِي عِلْمٍ

عَلِيمٌ

سورة يوسف (٧٦)
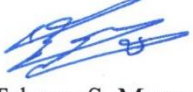
Examination Committee Certificate

We certify that we have read this thesis "Mitigation of Distortion in WDM Systems Based on Optical Phase Conjugation" and as examination committee we examined the student in its contents and in our opinion it is adequate with standards as a thesis for the degree of Doctor of Philosophy in Laser/ Electronic and Communication Engineering.

Signature
Name: Dr. Abdul Hadi M. Al-Janabi
Title: Professor
Address: Institute of Laser for Postgraduate Studies,
University of Baghdad
Date: /   /2017

(Chairman)

Signature
Name: Dr. Abdulkareem A. Kadhim
Title: Assistant Professor
Address: Department of Computer Engineering,
Al-Nahrain University
Date: 22 / 11 /2017

(Member)

Signature: M. A. Abdala
Name: Dr. Mohammed A. Abdala
Title: Assistant Professor
Address: Medical Instrumentation Engineering,
Al-Hussein University College
Date: 25 / 11 /2017

(Member)

Signature:
Name: Dr. Shelan K. Tawfeeq
Title: Assistant Professor
Address: Institute of Laser for Postgraduate Studies,
University of Baghdad
Date: 78 / 11 /2017

(Member)

Signature:
Name: Dr. Tahreer S. Mansour
Title: Assistant Professor
Address: Institute of Laser for Postgraduate Studies,
University of Baghdad
Date: 20 / 11 /2017

(Member)

Signature:
Name: Dr. Mazin M. Elias
Title: Professor
Address: Institute of Laser for Postgraduate Studies,
University of Baghdad
Date: /   /2017

(Supervisor)

Approval by the Deanship of Institute of Laser for Postgraduate Studies, University of Baghdad,

Signature:
Name: Dr. Abdul Hadi M. Al-Janabi
Title: Dean of Institute of Laser for Postgraduate Studies,
University of Baghdad
Date: /   /2017

Certification

I certify that this thesis was prepared under my supervision at the institute of laser for postgraduate studies, university of Baghdad as a partial requirement for the degree of a Doctor of Philosophy in Laser / Electronic and Communication Engineering.

Signature

Name: Dr. Mazin M. Elias

Title: Professor

Address: Institute of Laser for Postgraduate Studies

         University of Baghdad

Date: / /2017

(Supervisor)

In view of an available recommendation, I forward this thesis for debate by the examination committee.

Signature

Name: Dr. Shelan Khasro Tawfeeq

Title: Asst. Professor

Address: Head of Scientific committee

         Institute of Laser for Postgraduate Studies

         University of Baghdad

Date: 19/7/2017

Dedication

To my family

Acknowledgements

Abstract

Today, fiber-optic communication systems are considered the backbone of telecommunication systems and networks. Optical fiber is an excellent transmission medium due to its low loss, high bandwidth and robustness. However, linear and nonlinear impairments of an optical fiber lead to signal distortions. Propagation impairments accumulate over fiber distance and seriously distort the signal in high-capacity, long-haul fiber-optic communication systems. Transmission performance can be significantly improved by compensating for fiber dispersion and nonlinear distortions.

This thesis investigates the performance of advanced fiber-optic communication systems incorporating Optical Phase Conjugations (OPC) technique for mitigation of linear and nonlinear signal phase distortions. The OPC is achieved using Four-Wave Mixing (FWM) process in Highly Nonlinear Fiber (HNLF). Two compensation configurations are investigated and compared, one uses one OPC inserted in the mid-link point (Mid-Span OPC (MS-OPC)) while the other configuration uses multiple OPCs distributed along the link.

The work in this thesis falls into two main parts. In the first part, the effect of polarization on the performance of a dual-pump HNLF-based OPC (HNLF-OPC) is investigated analytically using a set of eight Nonlinear Schrödinger Equations (NLSEs). These equations describe the propagation of the orthogonal components of the two pumps, signal, and the generated idler. Practical assumptions are applied to derive expressions describing the dependence of FWM gain and conversion efficiency on the States Of Polarization (SOP) of the four waves. The results reveal that the use of two orthogonal linearly-polarized pumps leads to an OPC whose characteristics is independent of the signal polarization.

The second part of the thesis simulates the performance of two high-bit rate, long-haul, and Wavelength Division Multiplexing (WDM) systems incorporating HNLF-OPC compensation technique. The results are obtained using Optisystem v14.1 software package for both MS-and multiple-OPC configurations. Both WDM systems use long-haul distributed Raman amplified (DRA) link with 320 Gbps (8×40 Gbps) Polarization Division Multiplexing (PDM) Non-Return-to-Zero On-Off-Keying (NRZ-OOK) and 2.048 Tbps (8×256 Gbps) PDM 16-states quadrature-amplitude modulation (16-QAM).

Simulation results show that the use of multiple-OPC compensation technique offers an improvement in system performance over a MS-OPC compensation technique.

In single channel PDM NRZ-OOK 40 Gbps transmission, the use of multiple-OPC compensation technique provides an improvement in achieved maximum Q-factor of ~2 dB compared to the MS-OPC compensation technique. Furthermore, the transmission reach at the Hard Decision-Forward Error Correction (HD-FEC) limit is enlarged by 24.2% when the multiple-OPC configuration is used. In WDM system, the Q-factor is improves by 0.62 dB when a multiple-OPC compensation technique is used over the MS-OPC technique.

In single channel PDM 16QAM 256 Gbps transmission, the use of multiple-OPC shows a 1.35 dB improvement in Q-factor over the MS-OPC case. In the WDM system, using multiple-OPC increased the nonlinear threshold by ~2 dB compared to the case of MS-OPC, showing 0.62 dB improvement in Q-factor over the MS-OPC compensation scheme.

List of Contents

List of Symbols

Symbols	Description
A	Amplitude of the optical field
A_{eff}	Effective fiber core area
$\boldsymbol{B}$	Magnetic flux density
B	Bit rate
B_m	Modal birefringence
c	Speed of light in vacuum
D	Dispersion parameter
$\boldsymbol{D}$	Electric flux density
d_{sp}	Walk-off parameter
$\boldsymbol{E}$	Electric field vector
F	Frequency
g	Parametric gain coefficient
g_R	Raman-gain coefficient
$\boldsymbol{H}$	Magnetic field vector
$\boldsymbol{J}$	Current density
k	Effective phase mismatch
Δk	Phase-matching parameter
L	Length of the optical fiber
L_{eff}	Effective length
$\boldsymbol{M}$	Magnetic polarization
n	Linear refractive index
n_2	Nonlinear refractive index
$\boldsymbol{P}$	Electric polarization
P_0^{cr}	Critical Raman power
Q_{spm}	Nonlinear phase shift due to cross phase modulation

Symbols	Description
S	Dispersion slope parameter
v_G	Group velocity
T_R	Slope of the Raman gain
ΔT	Maxwellian distributed of pulse
α	Attenuation coefficient
β	Propagation constant
β_1	First order dispersion parameter
β_2	Group velocity dispersion parameter
β_3	Dispersion slope parameter
γ	Nonlinearity coefficient
ϵ_0	Vacuum permittivity
η_c	Conversion efficiency
θ_{P1}	Polarization angle of the pump1
θ_{P2}	Polarization angle of the pump2
θ_s	Polarization angle of the signal wave
θ_i	Polarization angle of the idler wave
λ	Optical wavelength
λ_0	Zero-dispersion wavelength
μ_0	Vacuum permeability
v	Velocity
v_G	Group velocity
$\chi^{(n)}$	nth-order susceptibility
ω	Optical angular frequency
ω_0	Zero-dispersion frequency

List of Abbreviations

Abbreviation	Description
ASE	Amplified Spontaneous Emission
ASK	Amplitude Shift Keying
BER	Bit Error Rate
BPSK	Binary Phase Shift Keying
BSG	Bit-Sequence Generator
CD	Chromatic Dispersion
DBP	Digital Back Propagation
DCF	Dispersion Compensation Fiber
DD	Direct Detection
DFWM	Degenerate Four-Wave Mixing
DGD	Differential Group Delay
DRA	Distributed Raman Amplifier
DSF	Dispersion Shifted Fiber
DSP	Digital Signal Processing
EDFA	Erbium-Doped Fiber Amplifier
FDM	Frequency-Division Multiplexing
FEC	Forward Error Correction
FOPA	Fiber Optic Parametric Amplifier
FWM	Four-Wave Mixing
GVD	Group Velocity Dispersion
HD-FEC	Hard Decision-Forward Error Correction
HDF	Highly Dispersion Fiber
HNLF	Highly Nonlinear Fiber
HNLF-OPC	Highly Nonlinear Fiber Based-Optical Phase Conjugation
IM	Intensity Modulation
IM-DD	Intensity Modulation-Direct Detection

Abbreviation	Description
LPF	Low-Pass Filter
LSE	Linear Schrödinger Equation
MPSK	M-ary Phase Shift Keying
MS-OPC	Mid-Span Optical Phase Conjugation
MSSI	Mid-Span Spectral Inversion
MZI	Mach-Zehnder Interferometer
MZM	Mach-Zehnder Modulator
NDFWM	Non-Degenerate Four-Wave Mixing
NLSE	Nonlinear Schrödinger Equation
NRZ-OOK	Non-Return-to-Zero On-Off-Keying
OA	Optical Amplifier
OBP	Optical Back Propagation
OBPF	Optical Band-Pass Filter
OFDM	Orthogonal Frequency Division Multiplexing
OOK	On-Off Keying
OPC	Optical Phase Conjugation
OPLL	Optical Phase Locked Loop
OSNR	Optical Signal-to-Noise Ratio
PC	Polarization Controller
PCTW	Phase Conjugated Twin Waves
PDM	Polarization Division Multiplexing
PLL	Phase Locked Loop
PM-IM	Phase-Modulation to Intensity-Modulation
PMD	Polarization Mode Dispersion
PSK	Phase Shift Keying
QAM	Quadrature Amplitude Modulation
QPSK	Quadrature Phase Shift Keying
RZ-DQPSK	Return-to-Zero Differential Quadrature Phase Shift keying

Abbreviation	Description
SBS	Stimulated Brillouin Scattering
SOP	States Of Polarization
SPM	Self-Phase Modulation
SRS	Stimulated Raman Scattering
SSMF	Standard Single-Mode Fiber
TE	Transverse Electric
TM	Transverse Magnetic
WDM	Wavelength Division Multiplexing
WSS	Wavelength Selective Switch
XPM	Cross-Phase Modulation

List of Tables

List of Figures

CHAPTER ONE

Introduction

CHAPTER ONE

Introduction

1.1 Overview

The fiber-optic communication system is the simplest kind of lightwave system, consists of a transmitter, followed by an optical fiber as a transmission channel, and then a receiver. The evolution of fiber-optic communications has been promoted along with the advent of the above three major components. In 1960, the invention and the realization of laser [1] provided a coherent source for transmitting information using lightwaves. In 1966, the optical fiber was firstly used as a lightwave transmission medium despite the fact that optical fiber at that time suffered unacceptable loss (over 1000 dB/Km). Since then, strenuous efforts have been made to reduce the losses of the optical fiber. In 1979, the low loss fiber was realized at the operating wavelength of 1550 nm with a loss of 0.2 dB/Km. The simultaneous availability of stable optical source (laser) and a low-loss optical fiber led to a rapid development of fiber-optic communication systems, which can be grouped into five distinct generations. A commonly used figure of merit for point-to-point communication systems is the bit rate-distance product, BL, where B is the bit rate and L is the repeater spacing. In every generation, BL increases initially but then begins to saturate as the technology matures. Each new generation brings a fundamental change that helps to improve the system performance further [2].

The first-generation of lightwave systems operated near 800 nm and used GaAs semiconductor lasers. The operating bit rate was 45 Mb/s and allowed repeater spacings of up to 10 Km. The repeater spacing of the first-

generation lightwave systems was limited by fiber dispersion which lead to pulse-spreading at the operating wavelength of 800 nm. In 1970s that the repeater spacing increased considerably by operating the lightwave system in the wavelength region near 1300 nm, where optical fibers exhibit minimum dispersion, furthermore, fiber loss is below 1 dB/Km. This realization led to a worldwide effort for the development of InGaAsP semiconductor lasers and detectors operating near 1300 nm [3].

The second generation of fiber-optic communication systems became available in the early 1980s, but the bit rate of early systems was limited to below 100 Mb/s because of intermodal dispersion in multimode fibers. This limitation was overcome by the use of single-mode fibers. By 1987, second-generation lightwave systems, operating at bit rates of up to 1.7 Gb/s with a repeater spacing of about 50 Km, were commercially available. The repeater spacing of the second-generation lightwave systems was limited by the fiber losses at the operating wavelength of 1300 nm (typically 0.5 dB/km). Losses of silica fibers become minimum near 1550 nm. Indeed, a 0.2 dB/Km loss was realized in 1979 in this spectral region. The drawbacks of 1550 nm systems were a large fiber dispersion near 1550 nm, and the conventional InGaAsP semiconductor lasers could not be used because of pulse spreading occurring as a result of simultaneous oscillation of several longitudinal modes. The dispersion problem can be overcome either by using dispersion-shifted fibers designed to have minimum dispersion near 1550 nm or by limiting the laser spectrum to a single longitudinal mode. For a Dispersion Shifted Fiber (DSF) the zero Chromatic Dispersion (CD) is shifted to minimum-loss window at 1550 nm from 1300 nm by controlling the waveguide dispersion and dopant-dependent material dispersion such that transmission fiber with both low dispersion and low attenuation can be achieved. Third-generation lightwave systems operating at 2.5 Gb/s became available commercially in 1990. Such systems are capable of operating at a

bit rate of up to 10 Gb/s. The best performance is achieved using dispersion-shifted fibers in combination with lasers oscillating in a single longitudinal mode [4].

A drawback of third-generation 1550 nm systems is that the signal is regenerated periodically by using optoelectronic repeaters, spaced apart typically by 60 - 70 Km, in which the optical signal is first convert to the electrical current and then regenerate by modulating an optical source. The repeater spacing can be increased by making use of a homodyne or heterodyne detection schemes because its use improves receiver sensitivity. These optoelectronic regenerating procedures are not suitable for multi-channel lightwave systems because each single wavelength needs a separate optoelectronic repeater, which leads to high cost and excessive system complexity. Another obstacle of using electronic repeaters is that due to high data rate in fiber-optic communication systems, the high speed electronic devises are required which is very hard and expensive to make [2].

The fourth generation of lightwave systems makes use of optical amplification for increasing the repeater spacing and of WDM for increasing the bit rate. The advent of optical amplifiers, which amplify the optical bit stream directly without requiring conversion of the signal to the electric domain, revolutionized the development of fiber-optic communication systems. Only adding noise to the signal, optical amplifiers are especially valuable for WDM lightwave systems as they can amplify many channels simultaneously. The optical amplification was first realized using semiconductor laser amplifiers in 1983, then Raman amplifiers in 1986 [5], and later using optically pumped rare earth Erbium-Doped Fiber Amplifier (EDFA) in 1987 [6]. The low-noise, high-gain and wide-band amplification characteristics of EDFAs stimulated the development of transmitting signal using multiple carriers simultaneously, which can be implemented using a WDM scheme. WDM is basically the same as the Frequency-Division

Multiplexing (FDM) as the wavelength and frequency are related $\lambda = v/f$ where v is the speed of light and f is the frequency. The advent of the WDM technique started a revolution in fiber-optic communication networks due to the fact that the capacity of the system can be increased simply by increasing the number of channels without deploying more fibers. That resulted in doubling of the system capacity every 6 months or so, and led to lightwave systems operating at a bit rate of 10 Tb/s by 2001 [3]. Commercial terrestrial systems with the capacity of 1.6 Tb/s were available by the end of 2000, and the plans were underway to extend the capacity toward 6.4 Tb/s. Given that the first-generation systems had a capacity of 45 Mb/s in 1980, it is remarkable that the capacity has jumped by a factor of more than 10,000 over a period of 20 years [2].

The fifth-generation of fiber-optic communication systems is concerned with extending the wavelength range over which a WDM system can operate simultaneously. While WDM systems can greatly improve the capacity of fiber optic transmission systems by increasing the number of channels, achievable data rate is limited by the bandwidth of optical amplifiers and ultimately by the fiber itself. The conventional wavelength window, known as the C-band, covers the wavelength range 1530 – 1570 nm. It is being extended on both the long- and short-wavelength sides, resulting in the L- and S-bands, respectively. The Raman amplification technique can be used for signals in all three wavelength bands. Moreover, a new kind of fiber, known as the dry fiber has been developed with the property that fiber losses are small over the entire wavelength region extending from 1300 to 1650 nm. Availability of such fibers and new amplification schemes may lead to lightwave systems with thousands of WDM channels [2].

The fifth-generation systems also attempt to increase the data rate of each channel within the WDM signal. This could be addressed by improving

the signal spectral efficiency [7]. The signal spectral efficiency is measured in bit/s/Hz, and can be increased using various spectrally efficient modulation schemes, such as M-ary Phase Shift Keying (MPSK), Quadrature Amplitude Modulation (QAM), and PDM technique. In fiber-optical transmission systems the transmitted signal power cannot be arbitrary large due to the fiber nonlinearity and therefore it requires a high-sensitivity optical receiver for a noise-limited transmission system. The power efficiency can be improved by minimizing the required average signal power or Optical Signal to Noise Ratio (OSNR) at a given level of Bit Error Rate (BER). In a conventional fiber optic communication system, the intensity of the optical carrier is modulated by the electrical information signal and at the receiver, the optical signal, transmitted through fiber link, is directly detected by a photo-diode acting as a square law detector, and converted into the electrical domain.

This simple deployment of Intensity Modulation (IM) on the transmitter side and Direct Detection (DD) at the receiver end called Intensity Modulation-Direct Detection (IM-DD) scheme. Apparently, due to the power law of a photo-diode, the phase information of the transmitted signal is lost when direct detection is used, which prevents the use of phase-modulated modulation schemes, like MPSK and QAM. Therefore, both spectral efficiency and power efficiency are limited in a fiber-optic system using direct detection [2].

In contrast, like many wireline and wireless telecommunication systems, homodyne or heterodyne detection schemes can be introduced to fiber-optic communications. This kind of system are referred to as coherent fiber-optic systems. The coherent fiber-optic communication systems have been extensively studied during 1980s due to high receiver sensitivity [8]. However, coherent communication systems were not commercialized because of the practical issues associated with Phase Locked Loops (PLLs)

to align the phase of local oscillator with the output of the fiber optic link and with the emergence of the EDFA, the former advantage of a higher receiver sensitivity compared to direct detection disappeared, the more so as the components were complex and costly [9].

Nowadays however, coherent optical systems are reappearing as an area of interest. The linewidth requirements have relaxed and sub-megahertz linewidth lasers have recently been developed. More recently, the high-speed Digital Signal Processing (DSP) available allows for the implementation of critical operations like phase locking, frequency synchronization and polarization control in the electronic domain through digital means. Former concepts for carrier synchronization with Optical Phase Locked Loops (OPLL) can be replaced by subcarrier OPLLs or digital phase estimation. Thus, under the new circumstances, the chances of cost effectively manufacturing stable coherent receivers are increasing.

In addition to the already mentioned potentials of spectral efficiency, coherent detection provides several advantages. Coherent detection is very beneficial within the design of optical high-order modulation systems, because all the optical field parameters (amplitude, phase frequency and polarization) are available in the electrical domain. Therefore, the demodulation schemes are not limited to the detection of phase differences as for direct detection, but arbitrary modulation formats and modulation constellations can be received.

Furthermore, the preservation of the temporal phase enables more effective methods for the adaptive electronic compensation of transmission impairments like chromatic dispersion and nonlinearities. When used in WDM systems, coherent receivers can offer tunability and enable very small channel spacings, since channel separation can be performed by high-selective electrical filtering [10].

It is expected that the demand in the growing system and the capacity of the network remain to deal with more-bandwidth requiring technologies such as voice and video over internet protocol, TV satellite channels, and video conferences. To stay in step with the growth of the data capacity requirement, new technologies to improve the fiber-optic communication systems are in great need. On the other hand, systems must be carefully studied and designed [11].

The major transmission performance degradation of long-haul, large-capacity fiber-optic communication systems comes from fiber non ideal transmission characteristics (such as attenuation, dispersion, optical fiber nonlinearity caused by Kerr effect, polarization-mode dispersion), optical amplifier noise accumulation, and interaction among them [12,13].

The way to achieve high performance fiber-optic communication systems has been studied widely by different research groups around the world. However, the complicated interaction between system impairments makes the study of fiber-optic communication systems a difficult task. This thesis focuses on the study of the fiber dispersion and nonlinearity mitigation in fiber-optic communication systems.

1.2 Objectives of the Thesis

The main objective of this work is to compensate linear and nonlinear distortions in large-capacity, long-haul fiber-optic communication systems. These distortions are originated from the interaction of fiber dispersion and fiber nonlinearity that is caused by Kerr effect. This goal may be achieved through the following steps

- Developing numerical and analytical models to characterize fiber transmission characteristics in the presence of dispersion and optical nonlinearities.

- Implementation of compensation methods to compensate the fiber nonlinearities in fiber-optic communication systems.

- Applying the proposed mitigation methods to fiber-optic communication systems with different modulation formats.

1.3 Fiber-optic communication Systems Impairments

The effects that degrade the optical signal when it is propagating in an optical fiber are usually divided into linear and nonlinear effects. This section discusses briefly these effects in fiber-optic communication systems.

1.3.1 Linear Impairments

Linear Schrödinger Equation (LSE) well describes the linear impairments in optical fiber, where the propagation constant (β) is firstly expanded into a Taylor series about the carrier frequency, here in, the series expansion includes only the first three terms. Under this assumption, the LSE can be given by [14]

$$\frac{\partial A}{\partial z} + \frac{\alpha}{2} A + \beta_1 \frac{\partial A}{\partial t} + \frac{j}{2} \beta_2 \frac{\partial^2 A}{\partial t^2} - \frac{1}{6} \beta_3 \frac{\partial^3 A}{\partial t^3} = 0 \tag{1.1}$$

where A is the amplitude of the optical field, α is the attenuation coefficient, β_1 is associated to the group velocity, while the parameter β_2 represents dispersion of the group velocity and is responsible for pulse broadening, and β_3 is the third-order dispersion parameter.

1.3.1.1 Fiber Attenuation

The optical wave propagation in optical fiber is accompanied by power loss. The main reasons behind power loss are due to material light absorption, Rayleigh and Mie linear scattering. Beer's law governs the decay of optical power in a lossy fiber extended in the z direction and it can be written as

$$P(z) = P(0) \exp(-\alpha z) \tag{1.2}$$

where $P(0)$ is the launched power into the fiber.

Optical fibers are designed with low levels of attenuation coefficients with α of about 0.17 dB/km at 1550 nm is reported. Figure (1.1) shows the spectrum of the losses caused by different sources of a fused silica fiber. This fiber shows minimum losses value in the region near 1550 nm. At shorter wavelengths, losses show higher values reaching a few dB/km in the visible region [15].
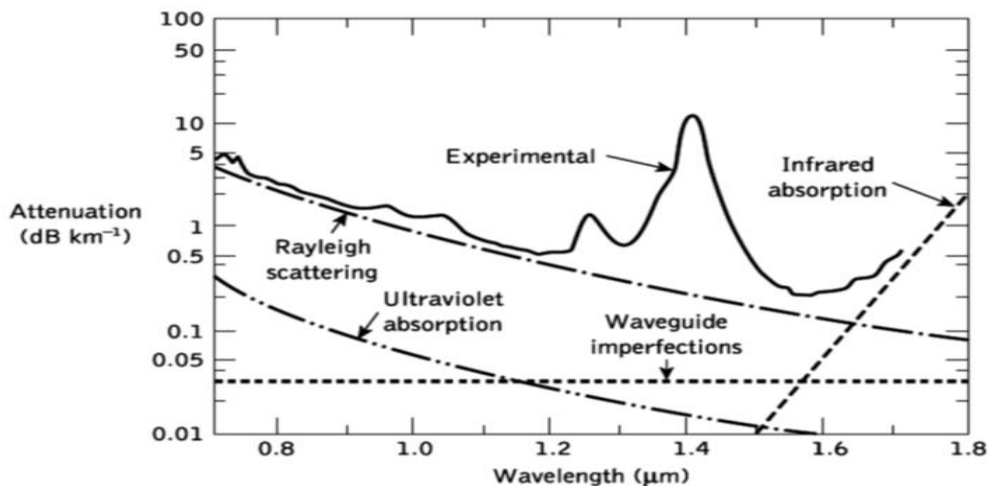
Figure (1.1): Measured loss spectrum of a single-mode silica fiber (solid line) with the calculated spectra for some of the loss mechanisms contributing to the overall fiber attenuation (dashed and dotted lines) [16].

1.3.1.2 Chromatic Dispersion

After attenuation, dispersion is considered the next limiting factor that determines how much and how far information can be transmitted on the fiber link. From Eqn. (1.1), β_1 controls the propagation speed of the envelope of the optical pulse along the fiber [14]

$$\beta_1 = \frac{1}{v_G} = \frac{1}{c}\left(n + \omega\frac{dn}{d\omega}\right) \tag{1.3}$$

where n is the linear refractive index, ω is the optical frequency, and c is the speed of light in vacuum. The Group Velocity Dispersion (GVD) is the main reason behind optical pulse broadening during the propagation. In Eqn. (1.1), β_2 is the GVD parameter and given by [14]

$$\beta_2 = \frac{1}{c}\left(2\frac{dn}{d\omega} + \omega\frac{d^2n}{d\omega^2}\right) \tag{1.4}$$

β_1 is related to the dispersion parameter D which can be obtained by taking the first derivative of β_1 with respect to the wavelength

$$D = \frac{d\beta_1}{d\lambda} = -\frac{2\pi c}{\lambda^2}\beta_2 \approx \frac{\lambda}{c}\cdot\frac{d^2n}{d\lambda^2} \tag{1.5}$$

Return to Eqn. (1.1) again, $\beta_3 = d\beta_2/d\omega$ is considered as the GVD slope parameter, which is associated to the dispersion slope parameter S [16]

$$S = \frac{d\beta_2}{d\lambda} = -\frac{4\pi c^2}{\lambda^3}\beta_2 + \left(\frac{2\pi c}{\lambda^2}\right)^2\beta_3 \tag{1.6}$$

For transmission in the region of zero dispersion i.e. $\beta_2 = 0$, the GVD slope becomes dominant and must be taken into account.

If one introduces a retarded time frame $T = t - z/v_G$, which moves with the signal at the group velocity, then β_1 will be eliminated from Eqn. (1.1). Furthermore, when Standard Single-Mode Fibers (SSMFs) or other

types with sufficiently high GVD are used, then the effect of the GVD slope can be neglected. Under these conditions Eqn. (1.1) can be written as [16]

$$\frac{\partial A}{\partial z} + \frac{\alpha}{2}A + \frac{j}{2}\beta_2\frac{\partial^2 A}{\partial t^2} = 0 \qquad (1.7)$$

In silica SSMF, the total dispersion profile is determined by the waveguide dispersion and the material dispersion. The summation of those two parameters gives the dispersion profile depicted in Fig. (1.2). The zero dispersion wavelength is located at 1324 nm and D = 16 ps/km/nm at 1550 nm. The material dispersion is related to the nature of the fused silica, and hence it cannot be changed. However, the effective refractive index of the fiber controls the waveguide dispersion. By changing the index profile, different fibers such as Dispersion Compensating Fiber (DCF) with $D = -80\ ps/km/nm$ and non-zero dispersion shifted fiber with $D = 4\ ps/km/nm$ can be manufactured. [16].
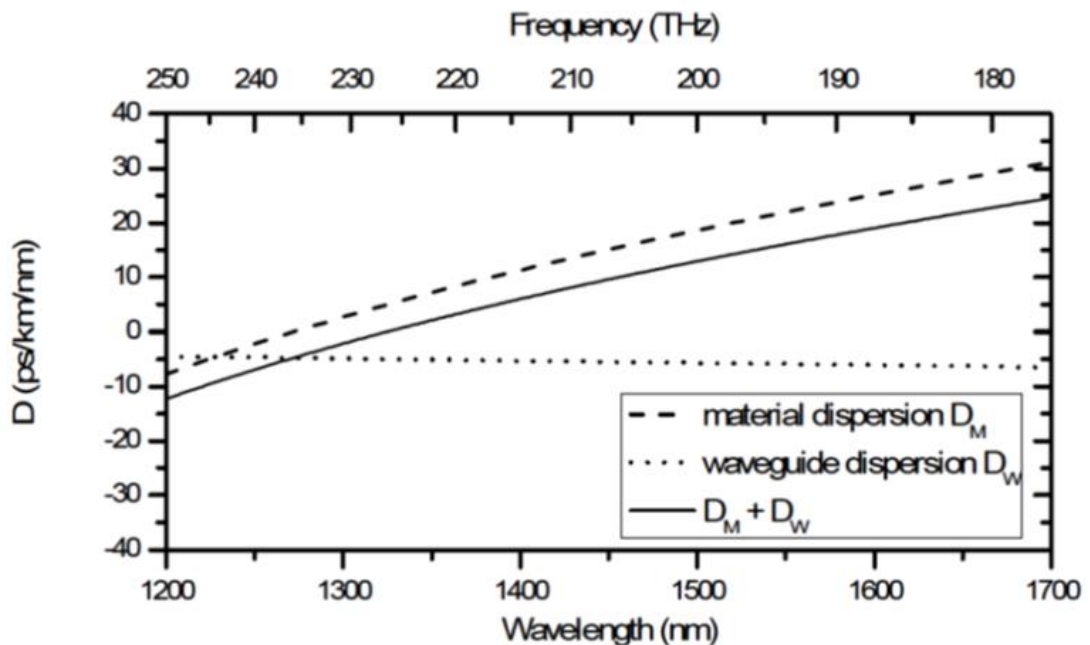
Figure (1.2): Dispersion characteristic of a typical standard single mode fiber as a function of wavelength and frequency [8].

1.3.1.3 Polarization Mode Dispersion

Polarization of light is an electromagnetic wave property that describes the direction of fluctuation of the transverse electric field. In SSMF, there exists two orthogonal polarization states, which are denoted here as x and y. Polarization of light can be described by representation of Stokes parameters, which can be straight forward expressed by using Poincaré sphere. The Poincaré sphere consists of four stocks parameters in terms of optical power as shown in Fig. (1.3) to visualize the SOP. SSMFs support two polarization modes simultaneously transmitting. These two polarization modes are orthogonal to each other. But the modes orthogonality can be changed due to temperature fluctuations and fiber birefringence caused by mechanical stress [2,17].
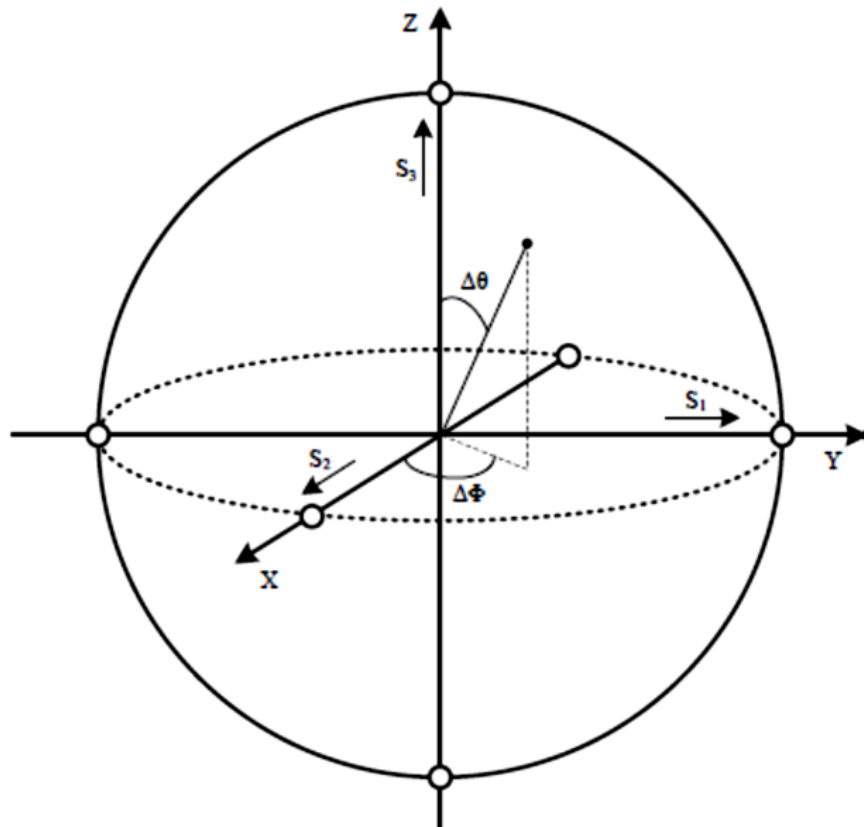
Figure (1.3): Poincaré sphere. S_1, S_2, and S_3 are the stockes parameters. The forth parameter S_4 is calculated from $S_4^2 = S_1^2 + S_2^2 + S_3^2$ [17].

The SOP variation occurs typically with fiber length ranges from hundreds meters and extends up to a few kilometers. Mathematically, one can define modal birefringence, B_m as [16]

$$B_m = \frac{|\beta_x - \beta_y|}{2\pi} = |n_x - n_y| \tag{1.8}$$

with n_x and n_y being the effective refractive index of both modes and β_x and β_y the equivalent propagation constants. The axis with larger group velocity is usually denoted as the fast axis while the axis with smaller group velocity is referred to as the slow axis. Consider a linearly polarized pulse, which is launched into a fiber at a 45 degree ($\pi/4$ rad) angle with respect to the slow axis as depicted in Fig. (1.4). In this case, the optical pulse excites two orthogonal modes of equal power, one in the slow axis and one in the fast axis. Whilst propagating along the fiber, the energy splits randomly between these two polarization states and the receiver detects two pulses, one in each polarization. The difference between the arrival-times of the two pulses is denoted as Differential Group Delay (DGD) ΔT and exhibits a Maxwellian distribution around the mean DGD-value $\langle \Delta T \rangle$. The mean DGD scales with L^2 (square of the fiber length) and is directly related to the Polarization Mode Dispersion (PMD) parameter of the fiber, which typically varies between 0.01 and 0.5 $ps/\sqrt{km}$ [16]
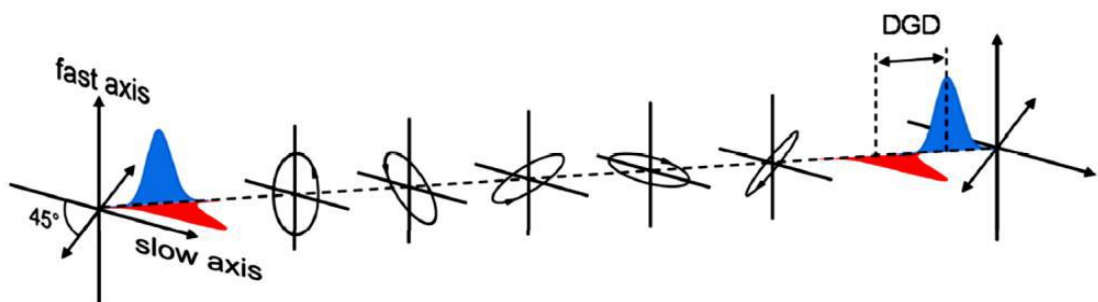
Figure (1.4): Random birefringence and the resulted DGD for a pulse launched into a fiber at 45° [16].

1.3.2 Nonlinear Impairments

The response of the optical fiber and all the dielectric materials to the light becomes nonlinear for intense electromagnetic fields. The silica is not considered in nature as a highly nonlinear material, but sometimes the fiber geometry that leads to confine the light to a small cross-section for long fiber lengths can makes nonlinear effects [10]. Fiber nonlinearities consist generally of two main groups. The first group is related to nonlinear refractive index, and these nonlinearities are called (Kerr effect). The other type of nonlinearities is associated to the nonlinear optical scattering. The fiber refractive index depends on the light intensity, and hence due to this dependency, the Kerr effect is produced. Fiber nonlinearities in this category are represented by Self-Phase Modulation (SPM), Cross-Phase Modulation (XPM), and FWM. On other hand, parametric interaction between the light and materials is caused by the stimulated scattering effects. Stimulated scattering effects occur in two types, the first is called Stimulated Raman Scattering (SRS) and the other is Stimulated Brillouin Scattering (SBS). The stimulated scattering effect has threshold power level as a condition at which the nonlinear effects manifest themselves. However, Kerr effect does not have such threshold [18]. The Raman backscattering and SBS may cause severe performance degradations in dense bidirectional WDM systems. By extending Eqn. (1.1) to include the nonlinear propagation effects, one obtains the NLSE defined in Eqn. (1.9) [14]

$$\frac{\partial A}{\partial z} + \frac{\alpha}{2}A + \beta_1\frac{\partial A}{\partial t} + \frac{j}{2}\beta_2\frac{\partial^2 A}{\partial t^2} - \frac{1}{6}\beta_3\frac{\partial^3 A}{\partial t^3} = j\gamma|A|^2 A \qquad (1.9)$$

The refractive index (ñ) of an optical fiber consists of a linear part n and a nonlinear part n_2, the later depends on the optical intensity in the fiber (Kerr effect) [14]

$$\tilde{n} = n + n_2 |A|^2 \tag{1.10}$$

The fiber nonlinearity coefficient γ in Eqn. (1.9) is related to n_2 and the effective core area A_{eff} at the center frequency ω_0 by [14]

$$\gamma(\omega_0) = \frac{\omega_0 \, n_2}{c \, A_{eff}} \tag{1.11}$$

The amplitude of the optical field $\boldsymbol{A}$ in Eqn. (1.1) can be decomposed into three interacting field components $\boldsymbol{A}_0$, $\boldsymbol{A}_1$ and $\boldsymbol{A}_2$ which describe the two pumps and signal with $\Delta\beta$ describing the phase relationship between them. To explain the influence of nonlinearity, one can restrict the analysis to small-signal distortions, and separate Eqn. (1.1) into three coupled equations. For $\boldsymbol{A}_0$ component, the NLSE becomes [14]

$$\frac{\partial \boldsymbol{A}_0}{\partial z} + \frac{\alpha}{2} \boldsymbol{A}_0 + \frac{j}{2} \beta_2 \frac{\partial^2 \boldsymbol{A}_0}{\partial t^2} = j\gamma |\boldsymbol{A}_0|^2 \boldsymbol{A}_0 + 2j\gamma(|\boldsymbol{A}_1|^2 + |\boldsymbol{A}_2|^2)\boldsymbol{A}_0$$

$$+j\gamma \sum_{l \neq m} \boldsymbol{A}_l \boldsymbol{A}_m \boldsymbol{A}_{l+m}^* e^{j\Delta\beta z} \tag{1.12}$$

where $\Delta\beta$ is the linear phase mismatch.

In Eqn. (1.12), the SPM, XPM, and FWM are represented by the three parts of the right hand side, respectively. In SPM, the nonlinear phase shift caused by the power of the $\boldsymbol{A}_0$ component itself is considered, while XPM describes the nonlinear phase shift that induced due to the contribution of the optical powers of neighboring channels. FWM describes a mixing process between all channels satisfying $k = l + m - n$ [16].

1.3.2.1 Self-Phase Modulation

If one assumes single signal propagation, (i.e. no XPM and FWM as defined in Eqn. (1.1)) and neglect chromatic dispersion, the solution to Eqn. (1.1) has the following form [2]

$$A(z.T) = A(0.T) \, exp\left(-\frac{\alpha}{2} \, z\right) exp\left(j\emptyset_{spm}\right) \qquad (1.13)$$

where T is the pulse duration, α is attenuation coefficient, and $\emptyset_{spm}$ is the nonlinear phase distortion caused by the SPM. The nonlinear phase shift acquired due to SPM is dependent on the intensity profile of the waveform and the fiber effective length, and it is proportional directly to the optical power [16]

$$\emptyset_{spm} = \gamma L_{eff} |A|^2 \qquad (1.14)$$

Furthermore, $\emptyset_{spm}$ scales with the effective fiber length L_{eff}, which includes the exponential decay of power profile [16]

$$L_{eff} = \frac{1 - exp(-\alpha L)}{\alpha} \approx \frac{1}{\alpha} \quad \text{(for suifficiently long fibers)} \qquad (1.15)$$

Note that in absence of chromatic dispersion, SPM does not change the pulse shape, while the interaction of SPM with dispersion results in pulse distortion due to Phase-Modulation to Intensity-Modulation (PM-IM) conversion of the phase distortion $\emptyset_{spm}$. In the latter case, the time dependent nonlinear phase shift induces carrier frequency fluctuations, which are referred to as chirp [16]

$$\delta\omega(T) = -\frac{\partial \delta\emptyset_{spm}(T)}{\partial T} \qquad (1.16)$$

The chirp generates new frequency components leading to spectral broadening in dispersive media, increasing for fast pulse rise times since the shape of $\phi_{spm}(T)$ is proportional to the pulse shape. In a response to the SPM phase shift, the leading edge of the pulses experiences a frequency reduction and the trailing edge a frequency increase.

1.3.2.2 Cross-Phase Modulation

By analogy to SPM, XPM is also a result of a nonlinear phase shift in an optical field. With SPM, the nonlinear phase shift in an optical signal is due to time-dependent power fluctuations in the wavelength channel itself. XPM, in contrast, covers the influence of the nonlinear phase shift induced by an orthogonal polarization (polarization multiplex) or neighboring wavelength channels (wavelength division multiplexing). Referring to Eqn. (1.12) and consider the second term on the right hand side. One can find an expression for the nonlinear phase shift due to two neighboring channels A_2 and A_3 [16]

$$\emptyset_{XPM}(z.T) = \gamma L_{eff}^2 \left(\int_0^z \left| A_2\left(0.T + d_{sp}z'\right)\exp\left(\frac{j}{2}\beta_2\omega_2^2 z'\right) \right|^2 dz' \right.$$

$$\left. + \int_0^z \left| A_3\left(0.T + d_{sp}z'\right)\exp\left(\frac{j}{2}\beta_2\omega_3^2 z'\right) \right|^2 dz' \right) \qquad (1.17)$$

This expression can be generalized to express the nonlinear phase shift induced on central channel A_s due to XPM, by summing up the contributions of all neighboring waves [16]

$$\emptyset_{XPM}(z.T) = \gamma L_{eff}^2 \sum_{p \neq 1} \left| A_p\left(0.T + d_{sp}z'\right)\exp\left(\frac{j}{2}\beta_2\omega_p^2 z'\right) \right|^2 dz' \qquad (1.18)$$

where ω_p is the angular frequency of the neighboring wave that caused the nonlinear phase shift on the signal due to XPM.

Due to the different group velocities of each WDM-channel the symbol patterns of the interacting channels walk-off from the central channel as displayed in figure (1.5). This effect is described by the walk-off parameter d_{sp} [16]

$$d_{sp} \approx D \cdot (\lambda_s - \lambda_p) \qquad\qquad (1.19)$$

where D is the dispersion parameter, λ_s and λ_p are the wavelengths of the central and the neighboring waves, respectively.

A higher walk-off parameter helps decorrelate XPM contributions along the transmission link and reduces the variance of the XPM distortion. Eqn. (1.18) shows that $\emptyset_{XPM}$ depends on the adjacent channels power profile and is therefore, similarly to SPM, stronger within the effective length of the fiber. Furthermore, the nonlinear phase shift depends also on the accumulated dispersion of the interfering channels. Since the signal peak-to-average power ratio is generally smaller for larger values of accumulated dispersion. It is justified to say that highly dispersed channels induce less severe XPM-distortions [16].
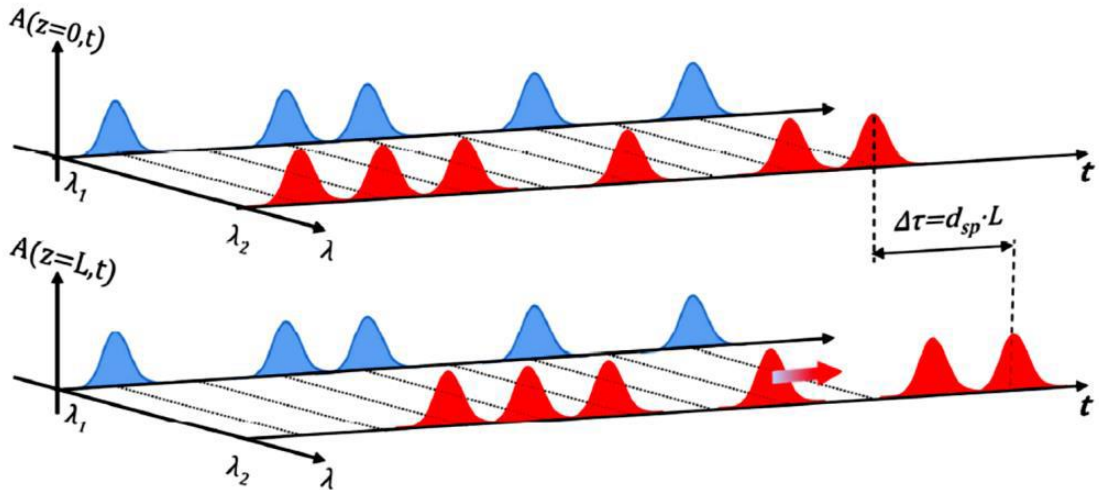
Figure (1.5): Walk-off between two waves at wavelength λ_1 and λ_2 after propagation over the distance L [16].

1.3.2.3 Four-Wave Mixing

This nonlinear effect comes from the nonlinear response of material bound electrons to the electromagnetic fields. The nonlinear effect is classified as a second order parametric process if the second-order susceptibility $\chi^{(2)}$ is responsible for this effect. While the effect that depends on the third-order susceptibility $\chi^{(3)}$ is classified as third-order parametric

process. In isotropic medium such as silica optical fiber, $\chi^{(2)}$ is almost vanished. Thus, the effects of the second-order processes can be ignored in silica fibers. FWM is a third-order parametric processes that occurs due to nonlinear interaction among three or four optical waves simultaneously forming a Non-Degenerate Four-Wave Mixing (NDFWM) where two pumps at frequency ω_{p1} and ω_{p2} ($\omega_{p1} \neq \omega_{p2}$) co-propagate with the signal at frequency ω_s in nonlinear medium; an idler wave at frequency $\omega_i = \omega_{p1} + \omega_{p2} - \omega_s$ is generated (see Figure 1.6) [19].
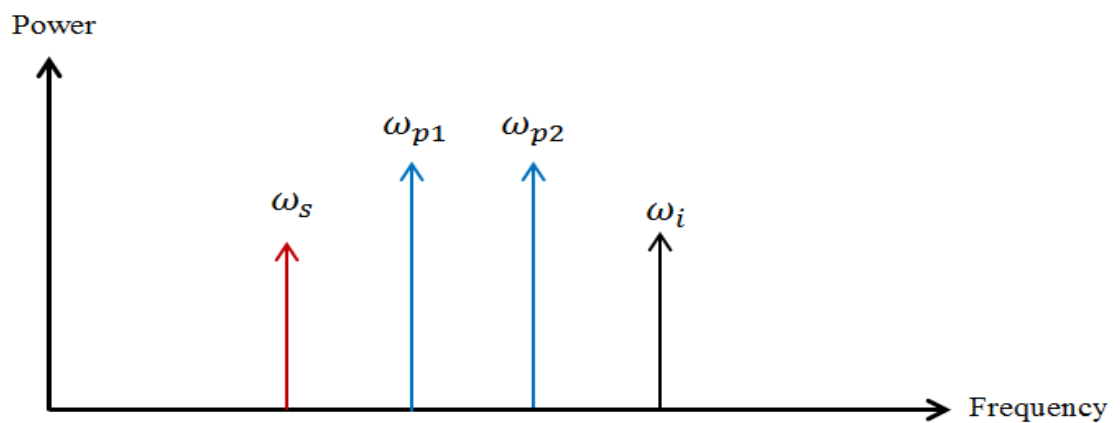
Figure (1.6): Waveforms of non-degenerated four-wave mixing.

If an intense pump at frequency ω_p and a signal at frequency ω_s are injected into the nonlinear medium together, an idler wave at frequency $\omega_i = 2\omega_p - \omega_s$ will be generated efficiently if the phase-matched condition is satisfied (see Figure (1.7)). This nonlinear process is called Degenerate FWM (DFWM), [19].
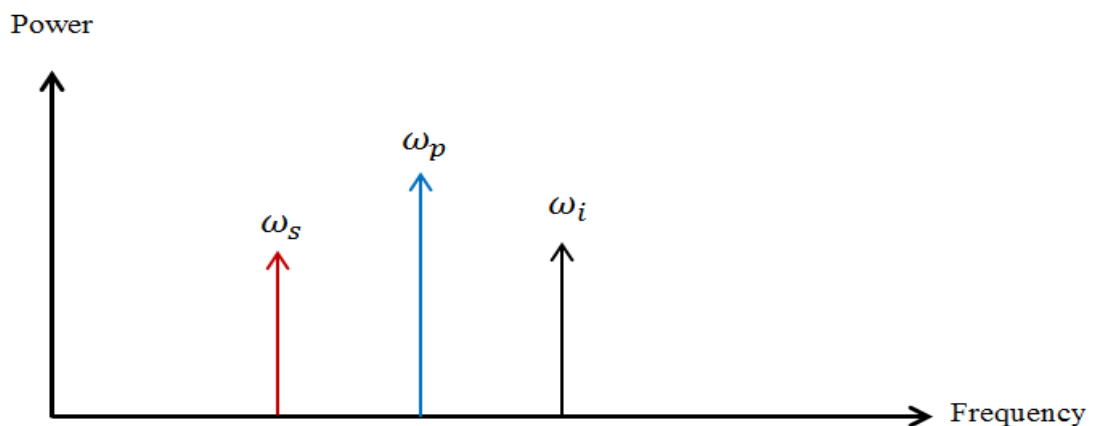
Figure (1.7): Waveforms of degenerated four-wave mixing.

The phase mismatch plays an important role in FWM process; if the phase mismatch is almost zero, significant FWM can be achieved. This condition is satisfied only by matching the frequencies of all the interacting waves, as well as the wave vectors [14]. The phase-matching condition required for this process is $\Delta k = 0$ where

$$\Delta k = \beta_s + \beta_i - \beta_{P1} - \beta_{P2} = (n_s \omega_s + n_i \omega_i - n_{P1} \omega_{P1} - n_{P2} \omega_{P2})/c \qquad (1.20)$$

Here $n_{P1.P2.s.\&i}$ are the effective mode indices at the frequencies $\omega_{P1.P2.s.\&i}$.

1.4 Nonlinearity Compensation Techniques in Fiber-optic communication Systems

Fiber-optic communication technology has been growing rapidly during recent decades to meet the increase of data capacity to be transmitted over the optical link. The broad development of fiber-optic communication has started from 1980s after the use of optical equipment that enhance the performance of optical systems such as low-loss SSMF, EDFA, and the use of various multiplexing techniques. Besides that, advanced modulation formats in coherent transmission systems enable high-speed, large-capacity, and long-haul transmission system. Currently, the transmission capacity of fiber-optic communication systems is mainly limited by the dispersion and fiber nonlinearity caused by Kerr effect. At low levels of signal power, transmission performance is limited by Amplified Spontaneous Emission (ASE) noise, so the capacity can be enhanced by increasing signal power to increase OSNR. However, with high signal power, fiber nonlinear effects dominate and make it impossible to enhance transmission performance by simply increasing signal power. Different optical and digital electronic compensation techniques have

been proposed in the literature to partially or completely compensate for fiber chromatic dispersion and nonlinearities [20].

1.4.1 Digital Back-Propagation Algorithm

The Digital Back-Propagation (DBP) algorithm is done by digitally inverting the distortions due to the chromatic dispersion and fiber nonlinearities. This process is done by the re-propagating of the received signal into a designed virtual link. This virtual link is characterized by inverse dispersion and nonlinear coefficients with respect to the original fiber link (see Fig. (1.8)). DBP is an effective compensation technique for dispersion and Kerr nonlinearities especially for single channel transmission systems [21]. However, due to the complexity of design and manufacturing, DBP compensation method is not suitable to be used in the WDM systems in long-haul transmission link [22].
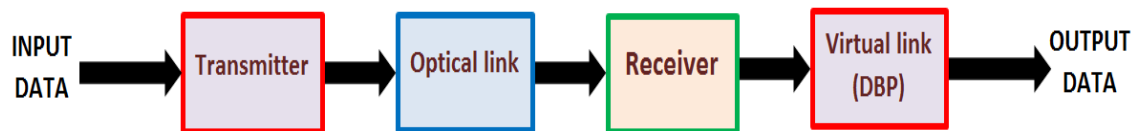
Figure (1.8): Schematic diagram of the fiber nonlinearity compensation system using digital back-propagation technique.

1.4.2 Frequency-Referenced Transmission

In this method, the canceling of the nonlinear distortions due to Kerr effect is achieved with the help of the optical carrier stability. If the optical carriers have a sufficient degree of mutual coherence, the nonlinear wave interaction in optical fiber can be substantially reverted. By this approach, all transmitted carriers are generated from a stable optical frequency

comb, in order to conserve a locked frequency separation. Such strategy is proved to benefit multi-channel nonlinearity compensation performed at the transmitter, with the use of nonlinear pre-distortion [23].

1.4.3 Phase-Conjugated Twin-Waves

Compensation of fiber nonlinearity can be achieved using a method of Phase Conjugated Twin Waves (PCTWs). In this method, the nonlinear distortions caused by Kerr effect of a pair of phase conjugated twin waves are anti-correlated and as a result, nonlinear distortions due to signal-signal nonlinear interactions are canceled by coherent superposition of the conjugated twin waves (see Fig. (1.9)). Experimentally, two orthogonal polarizations are used as twin waves and the data modulated on one polarization is the conjugation copy of that of the other polarization [24].
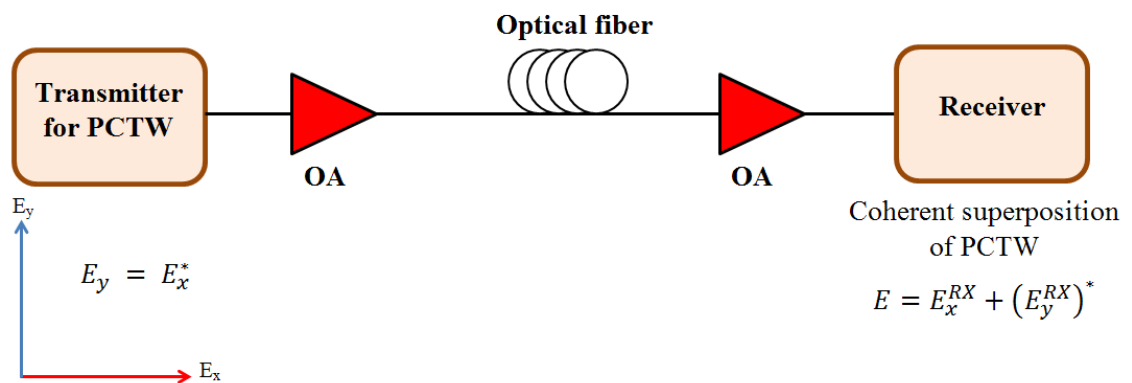
Figure (1.9): Illustration of nonlinearity cancellation based on phase-conjugated twin waves.

1.4.4 Optical Back-Propagation

Optical Back Propagation (OBP) has been proposed for the compensation of chromatic dispersion and fiber nonlinearity by placing an OBP device at the fiber output. The OBP module usually consists of Highly Dispersion Fiber (HDFs) and nonlinearity compensators (see Fig. (1.10)). These optical elements used to undo fiber distortions by reversing signal propagation. The nonlinearity compensator makes a phase shift that is equal in magnitude to the nonlinear phase shift caused by fiber propagation, but of course, opposite in sign. The effective negative nonlinear coefficient of the nonlinearity compensator is realized using two segments of HNLFs. This OBP scheme shows good transmission performance, however, it requires very good alignment in polarization between pumps and signal, and hence, the complexity of the receiver is significantly increased [25].
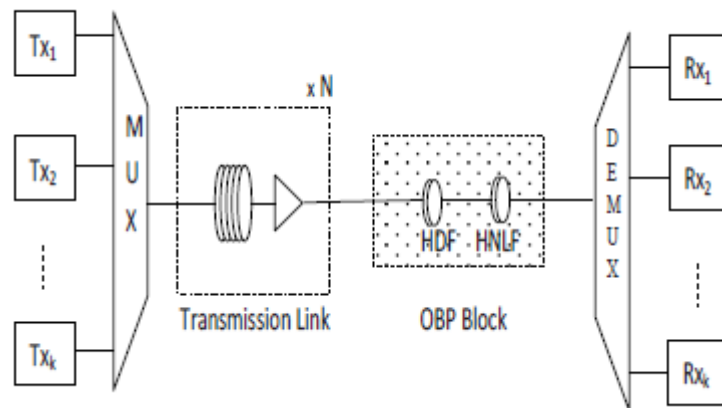
Figure (1.10): Optical pack-propagation module in WDM system [25].

1.4.5 Mid-Span Optical Phase Conjugation

Another interesting technique to mitigate fiber nonlinearity is by using OPC fixed in the middle of the optical link, a scheme known as Mid-Span Spectral Inversion (MSSI) [22,26]. This method firstly used for channel dispersion compensation, lately extended to show that OPC at the mid-point

of the link can also compensate nonlinear distortions. In a MSSI link, the phase of the signals is conjugated and the spectrum is inverted at the mid-point of the optical link. The signal phase distortion that accumulated from the first part of the link due to fiber dispersion and Kerr effect now has opposite phase in the second part of the link. Consequently, the effects in the second part of the optical link after the OPC cancel out the impairments of the first part. To achieve full nonlinearity mitigation, the mid-way OPC must be located exactly at the mid-point of the optical link, which can reduce the flexibility of optically routed networks because the 'mid-way' point is difficult to identify. Moreover, the mid-point of the link can be changed with time. In addition, in the mid-span OPC compensation scheme, the wavelength of the phase-conjugated signal is different compared to the original transmitted signal and this required extra complexity in the receiver design.

In this thesis, a dispersion and fiber nonlinearity mitigation using multiple OPCs placed in the optical link is introduced. In this method, the phase of the signal is conjugated after every certain length of the fiber and the phase conjugation is repeated after another equal length fiber. Therefore, the dispersion and fiber nonlinearities can be compensated along the optical link, not only at fiber end. This compensation scheme allows dynamic routing of the signals. Another advantage of using this scheme is that the signal wavelength can be conserved at the receiver using even number of OPC devices. This reduces the complexity of the receiver. Using multiple-OPC compensation scheme, a large capacity, high speed, and long-haul fiber-optic communication systems with high performance can be designed. Furthermore, the multiple-OPC compensation scheme is transparent to the modulation formats and suitable to single channel transmission as well as to WDM systems.

1.5 Literature Survey

This section reviews some of the works related the use of OPC technique in advanced fiber-optic communication systems which is the research area of this thesis.

In 2006, Jansen et al. [27] employed OPC for the mitigation of fiber dispersion and nonlinearity due to Kerr effect. In this work, 16×42.7 Gb/s NRZ is transmitted over an 800 km straight line of SSMF. An OPC device was used to get difference frequency generation in a periodically poled lithium-niobate waveguide, in order to achieve high conversion efficiency and transparent WDM operation. The principle of the use of OPC as a polarization-independent OPC subsystem was discussed. Then, the use of OPC for fiber dispersion and nonlinearity compensation in WDM long-haul transmission system was investigated. The results reveal that the transmission reach can be increased by 50% when the OPC is inserted in the transmission link with the help of DCF. The results show an improvement in the Q factor up to 4 dB due to the nonlinearity compensation resulting from the nonlinear phase noise. Then, the performance of an ultra-long haul WDM transmission system of 22×20 Gb/s Return-to-Zero Differential Quadrature Phase Shift keying (RZ-DQPSK) over same link was discussed. The results show that the use of OPC can completely compensate the fiber dispersion and nonlinear impairments. Comparing the results with those of a system using a DCF for fiber dispersion compensation shows a 44% increase in transmission reach when OPC is employed.

In 2007, Kaewplung and Kikuchi [28] proposed the use of MS-OPC with DRA for simultaneous mitigation of fiber attenuation, chromatic dispersion, and fiber nonlinearity caused by Kerr effect in ultra-long haul transmission link. DRA helps to provide symmetrical power profile along the link and the power becomes identical with respect to the midpoint of the

system where the OPC device is fixed. Then, the fiber dispersion and the nonlinear distortions caused by the Kerr effect are almost completely mitigated by the OPC. Numerical simulation results demonstrate that, by employing the flat power maps with a span of 40 km, a single-wavelength signal whose data rate is 160 Gb/s can be successfully transmitted over 5000 km at Q-factor 7 dB, and the Kerr effect is sufficiently suppressed near limitation due to the nonlinear accumulation of noise.

In 2012, Morshed et al. [29] reported through the simulation that OPC based on FWM for MSSI can be improved by splitting HNLF into two parts separated by an optical filter to suppress the XPM around the pump. Simulation results show an improvement of the maximum signal quality, Q-factor, by 1 dB in a 10×80 km 4QAM 224 Gb/s CO-OFDM system with MSSI. The simulation results of the proposed OPC was compared with the system in which a conventional OPC is used and showed an improvement in terms of Q factor.

In 2014, Ros et al. [30] investigated experimentally the use of a dual-pump Fiber Optic Parametric Amplifier (FOPA)-based optical phase conjugation to achieve MSSI in order to mitigate the fiber nonlinearity for a signal consisting of five channels each of 112 Gb/s per polarization (WDM-PDM 16-QAM signal) over 800 km dispersion-compensated optical link. The polarization insensitive operation of the designed OPC device using a dual-pump FOPA was demonstrated. The results show an improvement in the value of the maximum Q-factor provided by the compensation scheme for different dispersion-managed transmission lengths with clear improvement reported for all the lengths considered. In the nonlinear regime, the nonlinearity compensation provided by OPC enables improvements of the Q-factor of 0.56 dB, 0.71 dB and 0.9 dB, for 480 km, 640 km and 800 km, respectively, provided only 1 dB higher power per channel is launched in the spans. The OPC operation allows reaching BERs below the HD-FEC

threshold (3.85×10^{-3}) for 800 km transmission and the results show better performance when compared with a direct transmission link.

In 2014, Sackey et al. [31] presented experimental and numerical extension for their work reported in [30]. They used a particular link of 4×100 km SSMF spans employing backward pumping DRA. The transmitter and receiver configuration are the same as in the previous work. A dual-pump polarization-independent FOPA was used as a mid-link OPC. In single channel transmission, an improvement of 1.1 dB in Q-factor was achieved. While the Q-factor improvement of the five-channel WDM system is 0.8 dB. The experimental results are in good agreement with numerical simulations ones. Maximum transmission reach of 2400 km was obtained through simulation for a WDM system using mid-link OPC.

In 2014, Hu et al. [32] proposed multiple-OPC on an 8-channel WDM PDM quadrature phase-shift keying (QPSK) 1Tb/s data signal enabling a 6000 km transmission reach. Best performance is obtained for 600 km OPC span length and the results were compared experimentally with the case of MS-OPC and the direct link. The proposed method shows better performance than with MS-OPC and without OPC. The results show that the optimum launched power is still at -7 dBm when the FOPA without OPC is used, but the Q-factor is reduced by 1.4 dB compared to the case of a direct link (without FOPA). After 3600 km transmission, for the case of FOPA with MS-OPC, the optimum launch power is increased by 3 dB, but the optimized Q-factor is still 0.4 dB lower than without FOPA. For the case of FOPA with multiple- OPC, the optimum launch power is increased by about 5 dB, resulting in Q-factor improvement of 0.5 dB higher than the case without FOPA and 0.9 dB higher than the case of FOPA with MS-OPC.

In 2014, Sackey et al. [33] demonstrated experimentally a polarization-independent FOPA-based OPC with different values of the On-Off gain to transmit a test signal of 112 Gb/s PDM 16-QAM signals in a 5 channel 50-GHz spacing WDM system. Investigation of signal and generated idler shows OSNR penalties below 1 dB for single channel and a 5 channel WDM cases at 5 dB On-Off gain and at a BER of 10^{-4}. The maximum polarization dependent gain was also measured to be below 0.5 dB across a wavelength range from 1542.5 nm to 1565 nm. The proposed scheme is very useful for in-line OPC applications at 5 dB gain for gain-transparent operation with minimal penalty from the FOPA.

In 2015, Ros et al. [34] demonstrated a fiber nonlinearity compensation scheme by OPC in a WDM PDM 16-QAM system. Improved received signal quality was reported for both dispersion-compensated and dispersion-uncompensated transmission and a comparison with DBP scheme was investigated. The received Q-factor for the center channel is shown as a function of the power launched into each span for the two scenarios. In both cases application of the OPC device increases the optimum transmission power as well as the maximum received Q-factor with improvements of around 0.9 dB over 800 km transmission and 1.1 dB over 400 km transmission for the two link configurations. For the dispersion-compensated link, the use of OPC for 800 km transmission results in the same performance as 640 km straight transmission, increasing the reach by 25%.

In 2016, Yoshima et al. [35] demonstrated experimentally fiber nonlinearity compensation for two 10 Gbaud (60 Gb/s) 64-QAM signals using MS-OPC in a 400 km EDFA-amplified transmission link. The system was tested in a WDM environment using a single OPC to simultaneously conjugate two WDM signal bands. This provides twice the usable bandwidth when compared to conventional schemes. Q-factor improvement of more

than 1.7 dB was achieved for channels in the two bands when OPC was in place.

Also in 2016, Hu et al. [36] demonstrated multiple optical phase conjugation of an 8-channel WDM PDM 16-QAM signal achieving total bit rate of 2.048 Tb/s in a 900 km SSMF transmission experiment. In both single-channel and WDM cases, by using repeated OPC, the system performance was demonstrated to be improved over both the case of MS-OPC and the case of no OPC. The system performance was evaluated by the Q-factor (calculated from BER) measured with various launched powers.

In 2017, Hu et al. [26] investigated experimentally the use of multiple-OPC to fiber nonlinearity compensation in single-channel and WDM transmission systems. They used two signals with different modulation formats, the first is 8×32-Gbaud PDM QPSK signal, and the second is 8×32-Gbaud PDM 16-QAM signal. The total bit rates of 1.024 Tb/s and 2.048 Tb/s for the first and second signals, respectively. They compared their results with the scheme of single MS-OPC and with direct transmission link. The proposed method shows improved performance in terms of a best achievable Q factor after transmission and the nonlinear threshold. In addition, the signal wavelength can be preserved at the receiver using even number of OPCs. The results prove that the proposed technique is transparent to the modulation formats and effective for different optical transmission links. The WDM PDM QPSK signal band is transmitted over a long-haul DRA by employing multiple-OPC. In this system, 5 dB and 2 dB increasing in the nonlinear threshold were obtained compared to the case of no OPC and MS-OPC, respectively. While in WDM PDM 16-QAM signal transmission, the nonlinear thresholds are increased by 7 dB and 1 dB compared to the case of no OPC and MS-OPC, respectively.

It is clear from this survey that OPC can be adapted as an effective technique to compensate the combined effect of fiber chromatic dispersion and nonlinearities. Most of the researchers focus on using MS-OPC for this purpose from cost point of view. The benefits gained by using multiple-OPC technique have been addressed by few researchers in this field. Their results are deduced mainly on experimental investigation without considerable attention to SOPs of the associated pumps and signal as the main issue. In this thesis, this issue is addressed theoretically and by simulation using commercial software packages, namely Optisystem v. 14.1. The theoretical results are found to be in good agreement with experimental data reported in reference [29]. The theoretical modeling and simulation results can be used to design multi-span HNLF-OPC devices which can offer flat spectral conversion efficiency with less sensitivity to signal polarization. These devices are suitable for mitigation of linear and linear phase distortions associated with transmitted signals in high-bit rate and long-haul WDM systems incorporating high-order modulation formats.

1.6 Thesis Outlines

This thesis consists of four chapters; the rest three chapters are organized as follows

Chapter 2 introduces background information of optical pulse propagation starting with Maxwell's equations until reaching the complete NLSE which well describes the pulse propagation through optical fiber. Furthermore, coherent fiber-optic communication systems, multiplexing techniques, and advanced modulation formats are presented.

Chapter 3 investigates analytically the performance of dual-pump HNLF-OPC in the presence of SOP misalignment hence the signal and the

two pumps expressions are derived to characterize the fiber-optic communication system incorporating HNLF-OPC device for mitigating the effects of fiber dispersion and nonlinearities that is caused by Kerr effect. FWM parametric gain and conversion efficiency as a function of signal and pumps SOPs in both MS-OPC and multiple-OPC configurations are considered here.

Chapter 4 present and discuss the simulation results of proposed compensation systems and compare the obtained results with published experimental ones. Finally, discussion of the future steps that can be taken to improve this work will be provided.

Chapter Two

Theoretical Background

Chapter Two

Theoretical Background

2.1 Introduction

This chapter presents the basic theory for a propagation of electromagnetic wave in nonlinear dispersive optical fiber. Basic concepts of the optical pulses propagation into single mode fibers starting from Maxwell's equations are given. Maxwell's equations are used as the mathematical framework to introduce the NLSE which well describes the principles of optical pulse propagation in dispersive nonlinear fiber. This chapter presents the principle of the operation of OPC based on FWM process in a HNLF. The techniques that enable long-haul, large-capacity, and high-speed fiber-optic communication systems are also briefly mentioned in this chapter.

2.2 Maxwell's Equations and Optical Wave Equation

Similar to all electromagnetic phenomena, optical pulse propagation in fibers, either in linear or nonlinear regimes, is governed by the basic Maxwell's equations [37]

$$\nabla \times \boldsymbol{E} = -\frac{\partial \boldsymbol{B}}{\partial t} \tag{2.1a}$$

$$\nabla \times \boldsymbol{H} = \boldsymbol{J} + \frac{\partial \boldsymbol{D}}{\partial t} \tag{2.1b}$$

$$\nabla . D = \rho \tag{2.1c}$$

$$\nabla . B = 0 \tag{2.1d}$$

where E and H are the electric and magnetic fields vectors, respectively, D and B are associated electric and magnetic flux densities, respectively, J is the current density, and ρ represents the electromagnetic field source. In optical fibers, which are dielectric transmission media, $J = 0$ and $\rho = 0$.

D and B are generated as a response of the medium to the propagating electric and magnetic fields E and H. respectively, [37]

$$D = \epsilon_0 E + P \tag{2.2a}$$

$$B = \mu_0 H + M \tag{2.2b}$$

where ϵ_0 and μ_0 are the permittivity and permeability in the vacuum, respectively, P is the induced electric polarization while M represents the induced magnetic polarization. Note that the value of the magnetic polarization is equal to zero for non-magnetic mediums as in optical fibers.

The propagation of optical pulses in optical fiber is controlled by Maxwell's equations and governed by the following wave equation [14]

$$\nabla \times \nabla \times E = -\frac{1}{c^2}\frac{\partial^2 E}{\partial t^2} - \mu_0 \frac{\partial^2 P}{\partial t^2} \tag{2.3}$$

where c is the light vacuum speed and the relation $\mu_0 \epsilon_0 = 1/c^2$ is used.

The induced polarization P at position r in the fiber consists of two parts

$$P_T(r.t) = P_L(r.t) + P_{NL}(r.t) \tag{2.4}$$

where $\boldsymbol{P}_L$ is the linear polarization and $\boldsymbol{P}_{NL}$ is the nonlinear polarization. The linear part $\boldsymbol{P}_L(r.t)$ is related to the electric field by the first order susceptibility $\chi^{(1)}$ [14]

$$\boldsymbol{P}_L(r.t) = \epsilon_0 \, \chi^{(1)} \, \boldsymbol{E} = \epsilon_0 \int_{-\infty}^{t} \chi^{(1)} \, (t - t').\, \boldsymbol{E}(r.t')dt' \qquad (2.5)$$

In optical fiber, the nonlinear polarization often comes from the third order susceptibility $\chi^{(3)}$ and hence [14]

$$\boldsymbol{P}_{NL}(r.t) = \epsilon_0 \, \chi^{(3)} \vdots \boldsymbol{EEE}$$

$$= \epsilon_0 \int_{-\infty}^{t} dt_1 \int_{-\infty}^{t} dt_2 \int_{-\infty}^{t} dt_3 \times \chi^{(3)}(t - t_1.t - t_2.t - t_3)$$

$$\vdots \boldsymbol{E}(r.t_1)\boldsymbol{E}(r.t_2)\boldsymbol{E}(r.t_3) \qquad (2.6)$$

where $\chi^{(3)}$ is a tenser of fourth rank which contains 81 terms. In isotropic media, like a silica fiber operating away from any resonance, the independent terms in $\chi^{(3)}$ is reduced to be only one [14].

Equations (2.4) to (2.6) can be used in the wave Eqn. (2.3) to obtain the propagation equation of the optical pulse in nonlinear dispersive fibers. Before that, some practical assumptions are to be considered to solve Eqn. (2.3) [37].

i) Nonlinear polarization is considered as a small perturbation of a linear polarization and the polarization remains constant along the fiber.

ii) The small refractive index difference between the fiber core and cladding is neglected and the spectral width of the wave is much less than the center frequency of the wave, considering a quasi-monochromatic assumption. This leads to the use of the approximation of slowly varying envelope in the time domain.

iii) The propagation constant is approximated by only few terms of the expansion of Taylor series around the carrier frequency, and hence the propagation constant can be expressed as [38]

$$\beta(\omega) = \beta_0 + (\omega - \omega_0)\beta_1 + \frac{1}{2}(\omega - \omega_0)^2\beta_2 + \frac{1}{6}(\omega - \omega_0)^3\beta_3 \qquad (2.7)$$

where $\beta_0 = \beta(\omega_0)$ and other parameters are given as

$$\beta_m = \left(\frac{d^m\beta}{d\omega^m}\right)_{\omega=\omega_0} . (m = 1. 2. 3. ... ...) \qquad (2.8)$$

The parameters β_1 and β_2 are given in Eqns. (1.3) and (1.4), respectively.

The third-order term and beyond in equation (2.7) can be ignored as long as the quasi-monochromatic assumption is assumed. However, when the center of the signal wavelength is at or near the zero-dispersion wavelength, the second-order term of the propagation constant β_2 is negligible and therefore the β_3 term should be taken into account [39].

2.3 Nonlinear Schrödinger Equation

If the propagating electric field $A(z.t)$ propagates toward $+z$ direction and it is linearly polarized toward x direction, Eqn. (1.9) that governs the evolution of the slow-varying complex envelope of the optical pulses along a SSMF can be written as follow [14,37]

$$\frac{\partial A(z.t)}{\partial z} + \frac{\alpha}{2}A(z.t) + \beta_1\frac{\partial A(z.t)}{\partial t} + \frac{j}{2}\beta_2\frac{\partial^2 A(z.t)}{\partial t^2} - \frac{1}{6}\beta_3\frac{\partial^3 A(z.t)}{\partial t^3}$$
$$= -j\gamma |A(z.t)|^2 A(z.t) \qquad (2.9)$$

where z is the spatial longitudinal coordinate.

Equation (2.9) is usually called generalized NLSE. This equation describes the optical pulse propagation in a SSMF. This equation is applicable for propagation of short optical pulses with width as low as (~50 fs). This is associated to a spectral width of (~20THz) [14].

If the optical pulse width is much less than 1ps, the effect of SRS and the self-steepening should be included in the NLSE, then equation (2.9) can be written as [14, 38]:

$$
\frac{\partial A(z.t)}{\partial z} + \frac{\alpha}{2} A(z.t) + \beta_1 \frac{\partial A(z.t)}{\partial t} + \frac{j}{2} \beta_2 \frac{\partial^2 A(z.t)}{\partial t^2} - \frac{1}{6} \beta_3 \frac{\partial^3 A(z.t)}{\partial t^3}
$$

$$
= -j\gamma |A(z.t)|^2 A(z.t) + j\gamma T_R \frac{\partial}{\partial t} |A(z.t)|^2 A(z.t)
$$

$$
- \frac{\gamma}{\omega_0} \frac{\partial}{\partial t} |A(z.t)|^2 A(z.t) \tag{2.10}
$$

where T_R is the Raman gain slope (~5 fs). However, at higher pulse width (wider than 1 ps), the SRS and the self-steepening effect terms can be ignored compared to the Kerr effect term.

2.4 FWM-Based OPC

FWM is an important nonlinear process occurs in optical fibers. It is useful in many applications such as phase conjugation and wavelength conversion [40, 41]. In the conventional NDFWM processes in a nonlinear medium, a two pumps and a weak signal are simultaneously injected into the medium. As a result of the nonlinear interaction among these waves, an idler or conjugate wave can be generated when the phase-matching condition is met (see Fig. (2.1)). Using FWM-based OPC, the restoration of temporal pulses in optical fibers can be achieved, and hence, the pulse shape can be restored after being affected by fiber dispersion and nonlinearity. This leads to a restoration of the shape of the propagated pulse in a fiber as the pulse

propagates through another fiber after conjugation of its phase, and hence, undoes the chromatic dispersion and fiber nonlinearity induced by the original pulse. As a result of these important properties, FWM-based OPC has received much attention in long-haul fiber-optic communication systems [27]. A phase conjugation with high efficiency becomes possible with fairly high input powers and this may lead to an optimum fiber length of maximum conversion efficiency.

Figure (2.1): Generation of a conjugated idler using four-wave mixing.

Consider non-degenerate FWM in a HNLF where all the four frequencies (two pumps, signal and idler) are different. In this process, two pump waves at frequencies (ω_{p1}) and (ω_{p2}), and signal wave (to be phase conjugated) at frequency (ω_s) are launched into a HNLF generating an idler wave with an optical frequency ($\omega_i = \omega_{p1} + \omega_{p2} - \omega_s$), the total electric field is expressed as [42]

$$E = \frac{1}{2}\, \dot{x} \sum_{n=1}^{4} \exp[j(\beta_n z - \omega_n t)] + c.c. \tag{2.11}$$

where c.c. stands for complex conjugate mirror.

The nonlinear polarization parameter $\boldsymbol{P}_{NL}$ can be expanded in the same form as $\boldsymbol{E}$

$$P_{NL} = \frac{1}{2} \dot{x} \sum_{n=1}^{4} P_n \exp[j(\beta_n z - \omega_n t)] + c.c. \tag{2.12}$$

Substituting Eqns. (2.11) and (2.12) into the wave equation together with a linear part of the polarization that has similar expression, and neglecting all the time dependence terms of field components, yields the following set of coupled NLSE$_S$ in terms of the complex amplitudes of these waves [19,37]

$$\frac{dA_{p1}(z)}{dz} = \frac{-\alpha}{2} A_{p1}(z)$$
$$+ j\gamma\big[\,|A_{p1}(z)|^2 + 2\,|A_{p2}(z)|^2 + 2\,|A_s(z)|^2 + 2\,|A_i(z)|^2\big]A_{p1}(z)$$
$$+ 2j\gamma A_{p2}^*(z)A_s(z)A_i(z)\exp(j\Delta kz) \tag{2.13a}$$

$$\frac{dA_{p2}(z)}{dz} = \frac{-\alpha}{2} A_{p2}(z)$$
$$+ j\gamma\big[2\,|A_{p1}(z)|^2 + |A_{p2}(z)|^2 + 2\,|A_s(z)|^2 + 2\,|A_i(z)|^2\big]A_{p2}(z)$$
$$+ 2j\gamma A_{p1}^*(z)A_s(z)A_i(z)\exp(j\Delta kz) \tag{2.13b}$$

$$\frac{dA_s(z)}{dz} = \frac{-\alpha}{2} A_s(z)$$
$$+ j\gamma\big[2\,|A_{p1}(z)|^2 + 2\,|A_{p2}(z)|^2 + |A_s(z)|^2 + 2\,|A_i(z)|^2\big]A_s(z)$$
$$+ 2j\gamma\, A_i^*(z)A_{p1}(z)A_{p2}(z)\exp(-j\Delta kz) \tag{2.13c}$$

$$\frac{dA_i(z)}{dz} = \frac{-\alpha}{2} A_i(z)$$
$$+ j\gamma\big[2\,|A_{p1}(z)|^2 + 2\,|A_{p2}(z)|^2 + 2\,|A_s(z)|^2 + |A_i(z)|^2\big]A_i(z)$$
$$+ 2j\gamma\, A_s^*(z)A_{p1}(z)A_{p2}(z)\exp(-j\Delta kz) \tag{2.13d}$$

where, $A_{p1}(z)$, $A_{p2}(z)$ $A_s(z)$, and $A_i(z)$ are the electric field of the pump1, pump2, signal, and idler waves, respectively. Further, z is the direction of propagation, and Δk is the wave-vector mismatch given in Eqn. (1.20).

2.5 Advanced Techniques in Long-Haul, High-Speed Fiber-optic communication Systems

This section covers some key technologies that enable long-haul, large-capacity fiber-optic communications beyond 1 Tb/s, such as high-order modulation formats, different multiplexing techniques, and optical amplifiers.

2.5.1 Optical Modulation Formats

Fiber-optic communication systems are forming the main infrastructure that enables a high performance, large-capacity and long-haul global data network. Modern advanced applications such as high definition video conferences, satellite television channels, and complex internet applications have become affordable with the help of the fiber-optic communication [43,44]. The need for higher data rate signals transportation, and at the same time, reduction of the construction cost, have led to use the optical networks with high spectral efficiencies. Advanced optical modulation formats have been playing a great rule to design the advanced fiber-optic communication systems [45].

In this subsection, some of the optical modulation formats are presented briefly which are suitable for optically routed WDM networks such as amplitude-shift keying (ASK), phase-shift keying (PSK), and quadrature-amplitude modulation (QAM).

a) Amplitude Shift keying

Optical Amplitude Shift Keying (ASK) is a type of amplitude modulation in which the digital data is represented by variations of

the amplitude of an optical carrier wave. In binary ASK system, the binary digit of the input signal is represented by transmitting a constant amplitude carrier wave with constant carrier frequency for time duration of T seconds per bit. In ASK, each symbol contains only one bit. Therefore, the symbol rate (number of transmitted symbol per second) is equal to the bit rate. The simplest and most common method to generate the ASK signal uses a switch. The presence of a carrier wave indicates a binary 1 and absence of the carrier wave to indicate a binary 0. This type of modulation is usually called On-Off Keying (OOK) [16]. Figure (2.1a) shows the OOK constellation diagram. From this diagram, it is clear that the choice of the threshold is critical to the performance of the receiver. OOK receiver needs an adaptable amplitude threshold, this can be achieved by an automatic gain control in order to ensure setting of the optimal threshold. Figure (2.1b) explains the ASK waveforms with simple on-off binary method to send a series of four bits '1001' [46].
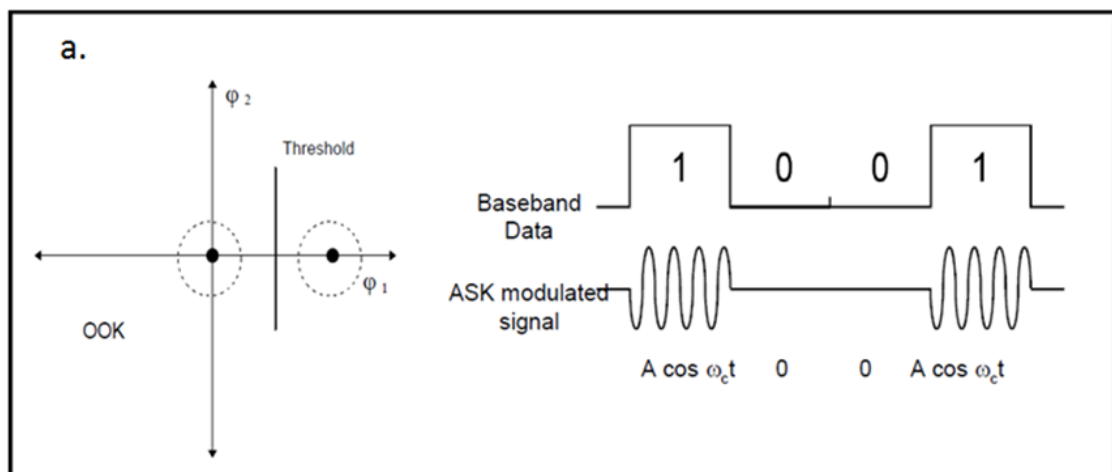
Figure (2.2): (a) OOK signal constellation diagram, and (b) is the modulated binary ASK signal corresponding to a baseband input data [46].

b) Phase Shift Keying

Phase Shift Keying (PSK) is a one of the most important digital modulation formats in fiber-optic communication systems. PSK modulation

process conveys data by modulating the phase of the optical carrier wave. PSK uses a specific number of phases, a symbol of an equal number of bits is encoded by each phase. The PSK demodulator is designed with high accuracy to deal with the phase of each received symbol and this phase must be defined by the modulator, and then maps it back to the bit stream of each symbol, thus recovering the original data. This is achieved if the receiver is able to compare the phases of the received symbols to a reference symbols, such system is well known to be called coherent detection system. PSK is classified into many types depending on number of bit per symbol [37].

i) **Binary Phase-Shift Keying (BPSK)** encodes one bit per symbol by modulating the carrier wave in two phase states (0 and π) as illustrated in Fig. (2.3) [16, 37] BPSK signal can be generated using a Mach-Zehnder Interferometer (MZI) which consists of two nested phase modulators. This phase modulator is used to manipulate the relative phase between the two branches and to achieve either constructive or destructive interference at the output. The MZI is driven in push-pull mode around its zero-transmission point, to achieve a relative phase of π radians [16]. The BPSK modulated signal can be given by the following two equations

$$S_1 = A\cos(\omega_c t) \qquad\qquad (2.14a)$$

$$S_0 = -A\cos(\omega_c t) \qquad\qquad (2.14b)$$

where S_1 and S_0 are the two input states (1 and 0), and ω_c is the angular carrier frequency.
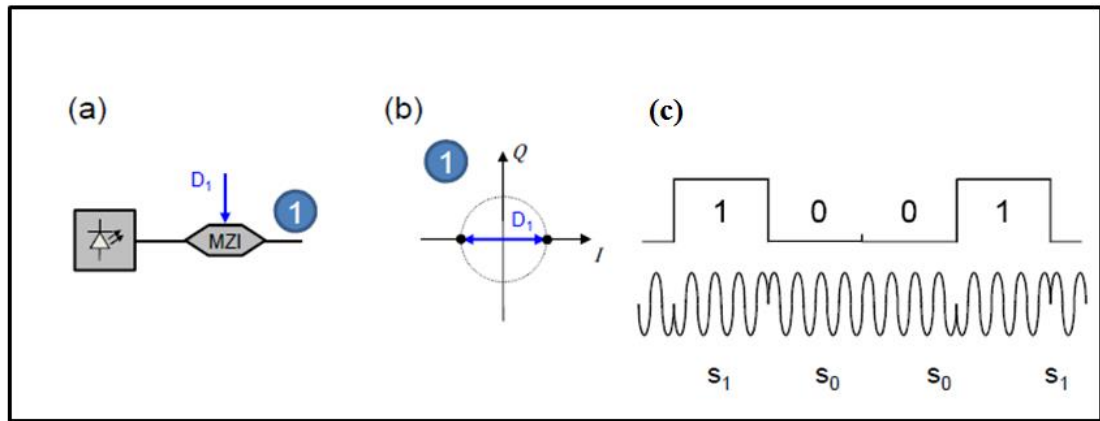
Figure (2.3): (a) Generation of BPSK signal using Mach-Zehnder interferometer, (b) constellation diagram of the BPSK signal, and (c) is the modulated BPSK signal corresponding to a baseband input data [37].

ii) **Quadrature phase-shift keying (QPSK)** contains 4 phase states separated by $\pi/2$ rad from each other (see Figure (2.4b)) [37, 46]. QPSK encodes 2 bits per symbol. QPSK can be represented effectively by two BPSK systems (I and Q), and hence achieve the same performance but twice the bandwidth efficiency. QPSK is often generated by two nested MZI. One of the optical outputs is then phase shifted by $\pi/2$ rad and combined with the other signal (see Figure (2.4)).

iii) **Eight phase-shift keying (8PSK)** encodes 3 bits per symbol with 8 phase-states [46], equally spaced with a phase difference of $\pi/4$ rad as depicted in Fig. (2.4). It can be generated by using a QPSK transmitter followed by a phase-modulator, which shifts the phase between 0 and $\pi/4$ rad. Note, that it is possible to encode 16 different phase states and obtain 16PSK if an 8PSK transmitter is preceded by an additional phase-modulator shifting the signals phase between 0 and $\pi/8$ rad.
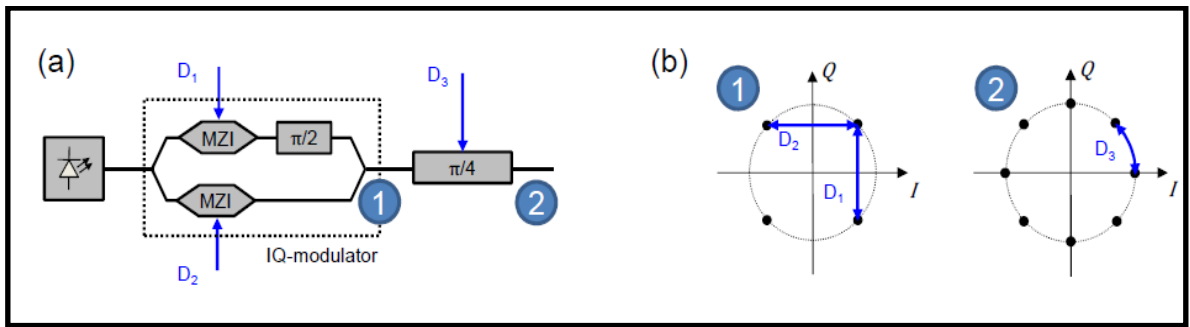
Figure (2.4): (a) Generation of QPSK and 8PSK signals, and (b) Constellation diagrams of QPSK and 8PSK signals, $D_1 – D_3$ are the binary data [46].

c) Quadrature Amplitude Modulation

QAM is an important type of modulation formats which is widely used for modulating data signals onto a carrier in fiber-optic communication systems. It provides number of advantages compared to the other modulation formats such as ASK and PSK. QAM is a signal with two carriers shifted in phase by 90°, they are modulated to produce an output that varies in both amplitude and phase. QAM is considered as a mixture of amplitude and phase modulation because of the presence of both amplitude and phase in the output signal. Many forms of QAM constellation are often used and some of the most common forms are 4QAM, 8QAM, 16QAM, 32 QAM, 64 QAM. Figure (2.5) explains the constellation diagram of some types of QAM signals depending on the number of points in each electrical constellation diagram [47].
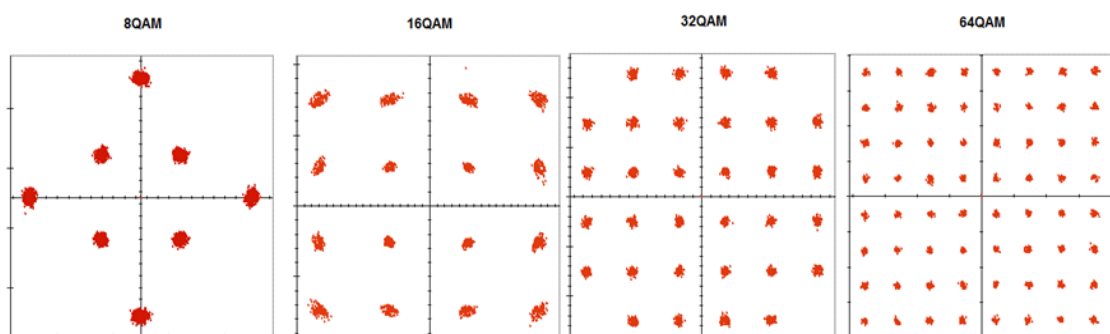
Figure (2.5): Constellation diagram of the 8QAM, 16QAM, 32QAM, and 64QAM.

QAM enables higher data rates with respect to the conventional amplitude and phase modulation schemes. When QAM is used, the points of the electrical constellation diagram are normally arranged either in a square grid with equal vertical and horizontal spacing or in star form. The higher order modulation formats utilizing more points on the constellation enables transmitting more than one bit per symbol, and hence, increases the data rate of the system. However, the electrical constellation points are relatively closer together and therefore more possibility to be affected by noise and data errors arises. Table (2.1) gives a summary for the symbol rates of different forms of QAM and PSK.

Table (2.1): Summary of symbol rate for different forms of modulation formats.

Modulation	Bit per symbol	Symbol rate
BPSK	1	Bit rate
QPSK	2	1/2 Bit rate
8PSK	3	1/3 Bit rate
16-QAM	4	1/4 Bit rate
32-QAM	5	1/5 Bit rate
64-QAM	6	1/6 Bit rate

Although QAM is used to increase the efficiency of different communication systems by utilizing both phase and amplitude variations, unfortunately it has many disadvantages [48]. For example, the states are closer together, therefore it is more affected by noise, and hence a lower level of noise is needed to drift the received symbol from the correct decision point. In phase or frequency modulation, the receivers are able to use amplifiers that are able to reduce the effect of amplitude noise, and results in improvement in the noise reliance. This property is not existent with QAM because of its dependence on the signal amplitude. Second, when a signal is phase or frequency modulated, there is no need to use linear amplifiers, while in QAM, that includes an amplitude component, amplification linearity must

be taken into account. But the linear amplifiers have many disadvantages such as, high power consumption and low amplification efficiency.

2.5.2 Wavelength Division Multiplexing

Multiplexing of signals at different wavelengths through the same optical fiber leads to multiplying transmission capacity. WDM (see Fig. ((2.6)) is one of the promising techniques used for increasing transmission capacity in fiber-optic communication systems. WDM is a technique that multiplex number of optical signals at different wavelengths, each signal is modulated independently by different electrical bit streams [2].
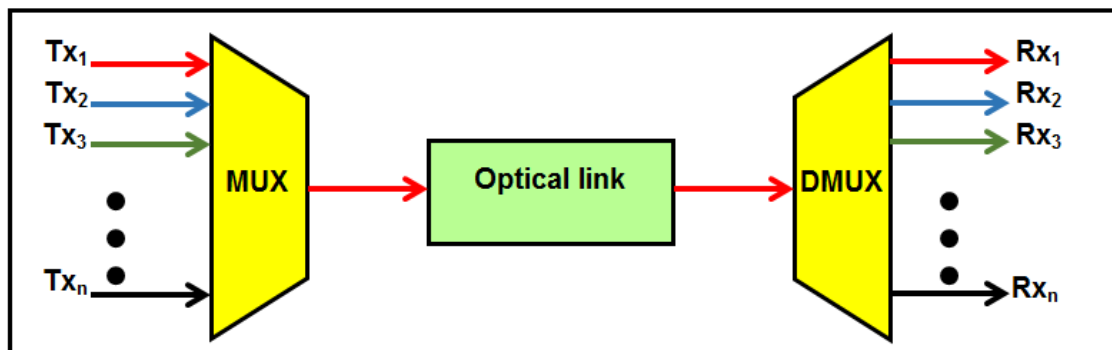
Figure (2.6): Simplified block diagram for wavelength division multiplexing system including MUX: Multiplexer, DMUX: Demultiplexer, and Tx (Rx): Single-channel optical transmitter (receiver).

This technique allows multiple optical signals to be transmitted at same the time through the same optical fiber, therefore, increases the capacity of the system transmission significantly. An optical multiplexer with suitable number of channels is used to combine the signals and an optical wavelength division demultiplexer is used to separate the signals at the receiving end. The separated optical signals at different wavelengths can be then distributed into different detectors.

2.5.3 Polarization Division Multiplexing

Optical PDM is based on independently transmitting two modulated signals over orthogonal polarizations of the same optical wavelength and therefore doubling the transmission capacity. In optics, the SOP is the shape of direction of propagation of the electric field vector of the optical signal in a constant plane. Figure (2.7) shows the linear, circular, and elliptical polarization states.

Linear polarization is obtained when the direction of the electric wave propagation is constant over a certain axis (the electric-field vectors along with E_x and E_y directions are in phase). When E_x and E_y are exactly ninety degree out of phase, one has a circular polarization. There are right-handed or left-handed circular/elliptical polarizations, depending on which direction the electric field vector rotates, that is, if the electric field vector is seen rotating clockwise or counterclockwise.
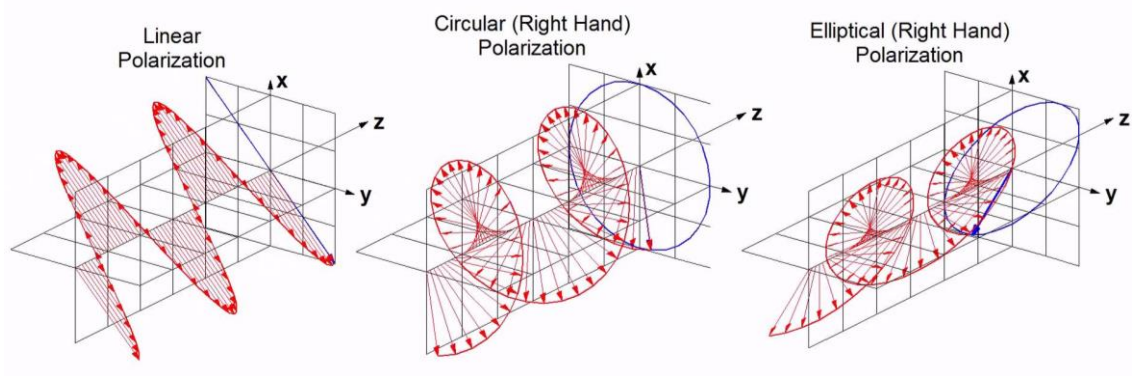
Figure (2.7): Examples of linear, circular, and elliptical polarization states [39].

2.5.4 Optical Amplifiers

Fiber attenuation that is caused by absorption loss, coupling loss, bending losses, and different types of scattering limits the transmission

distance. An Optical Amplifier (OA) such as EDFA can simply amplify the optical signal in optical domain by several orders of magnitude without converting the signal to electrical domain. In addition, optical amplification is transparent to the change of the signal bit rate and modulation format. OAs can compensate the fiber losses efficiently and therefore they are important in fiber-optic communication systems because they help to enable long-haul transmission. The most common approaches for loss compensation are to use either lumped amplification or distributed amplification [49].

a)   Lumped amplification

The most common type of lumped OAs is the EDFA which is inserted after each fiber span to compensate the fiber loss. For example, the transmission span consists of 50 km SSMF of 0.2 dB/km attenuation coefficient followed by a 6 km forward pumped EDFA of 10 dB gain. The model for this scheme looks as shown in Figure (2.8).
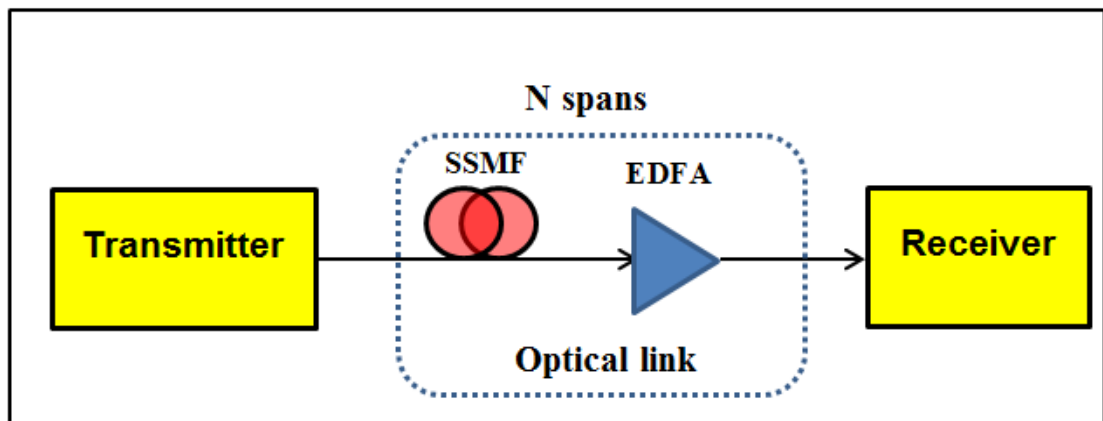
Figure (2.8): Model for lumped amplification using EDFA.

EDFA is considered as one of the most important inventions in fiber-optic communication technologies [50]. Before the appearance of EDFAs, the standard amplification method to compensate the fiber loss was

electronic signal regenerators fixed in the optical transmission link. The electronic regenerator consists of a photodetector, DSP, electrical amplifier, and an optical transmitter. The regenerator receives the optical signal and converts it into electrical signal, then amplifies it and performs the conversion from electrical to optical domains, and finally retransmission of the regenerated optical signal. However, electronic devices that used in regenerators will prevent exploitation of the huge bandwidth of the optical fiber. Moreover, if the system capacity is increased, all the electronic repeaters must be replaced because they would be designed to a specific bit rate and modulation format.

b)   **Distributed Amplification**

One of the most important types of distributed amplifiers is SRS-based OA which is called Distributed Raman Amplifier (DRA). Pump power and signal is injected into the fiber using pump coupler. Figures (2.9a) and (2.9b) illustrate the DRA with forward and backward Raman pumping, respectively. DRA has become a very attractive amplification principle in modern high-speed, long-haul, and broadband fiber-optic communication systems. Raman amplifier provides better performance in L band amplification and it also provides a flat gain profile compared to the other discrete amplifier types [51]. The accumulation of amplifier noise is reduced significantly if the DRA is used within the link because the level of the signal power is kept from decreasing to very low values, as it can occur when discrete EDFAs amplifiers are used. Therefore, the level of the maximum signal power can be reduced without accumulating significant amplifier noise. Reduction of the input signal power level also leads to reduce the effects of fiber nonlinearities [52].
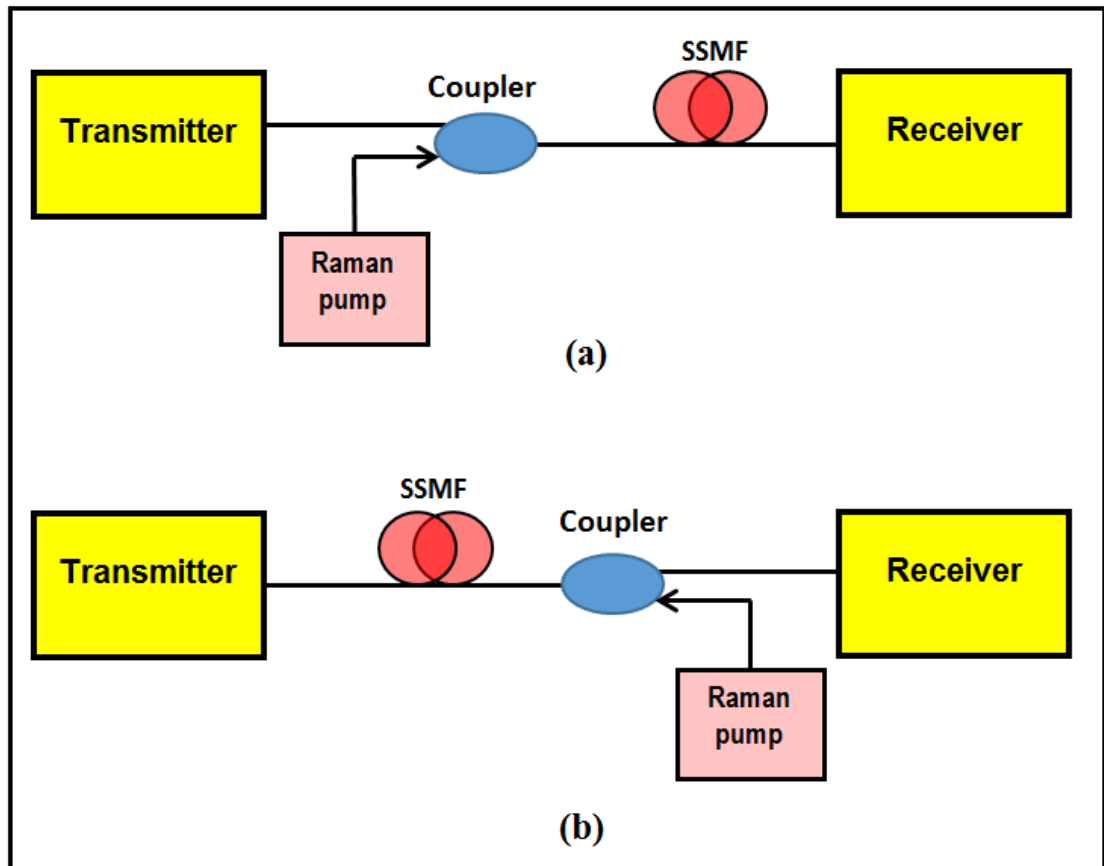
Figure (2.9): (a) Forward pumped-distributed Raman amplified link, and (b) Backward pumped-distributed Raman amplified link.

Raman amplification is a function to the frequency difference between the signal frequency and pump frequency. The basic theory of the Raman effect can be concluded by a transition of molecule from the ground state to the virtual state and finally to the vibrational excited state, a photon with energy $\hbar\omega_p$ is converted by a molecule to another photon at lower frequency with energy of $\hbar\omega_s$, when the molecule is transitioned to a new vibrational excited state (Fig. (2.10)) [14].
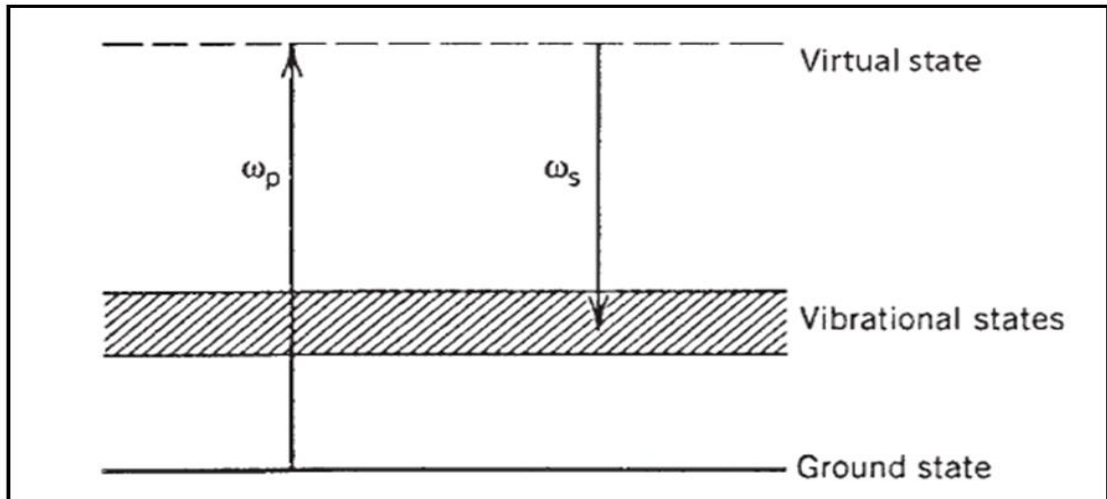
Figure (2.10): Schematic illustration of spontaneous Raman scattering [14].

From a practical view, energy can be transferred from a pump to the signal which has lower frequency; as a result, the signal (Stocks wave) is amplified. The following equation describes the primary growth of the Raman Stokes wave [14]

$$\frac{dI_s}{dz} = g_R I_p I_s \qquad (2.15)$$

where I_P and I_S are the Raman pump and Stokes intensities, respectively, g_R is the Raman-gain coefficient which is associated with the value of the cross section of spontaneous Raman scattering. g_R is a function to the frequency difference between the pump wave and the Stokes. It also depends significantly on the SOP of the pump and Stokes, it shows higher values if the pump and Stocks are co-polarized.

Figure (2.11) shows g_R variation with the frequency shift between Raman pump and the Stocks for an optical fiber made from silica [14].
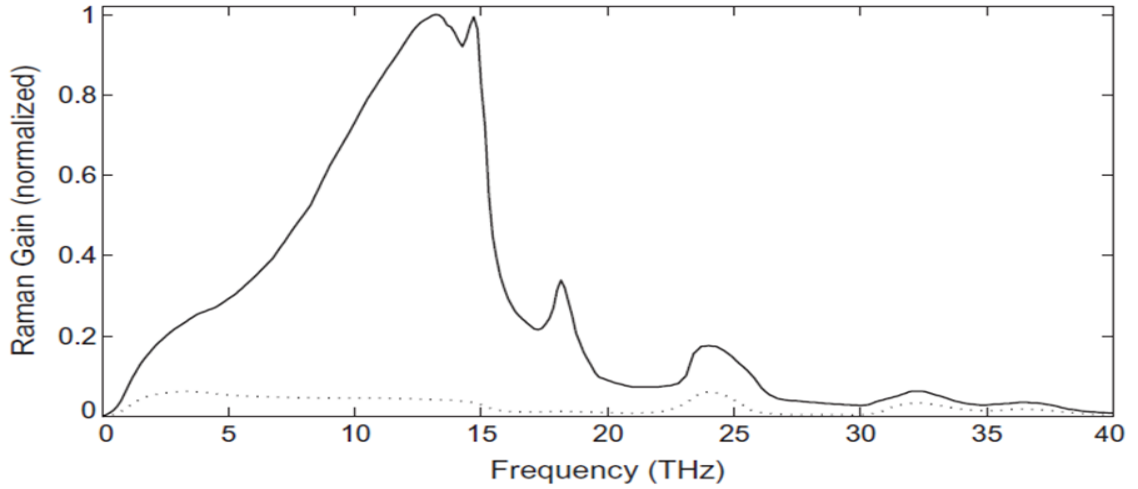
Figure (2.11): Normalized Raman gain for fused silica when the pump and Stokes waves are co-polarized (solid curve). The dotted curve shows the situation in which the pump and stokes waves are orthogonally polarized [14].

From Fig. (2.11), g_R is maximum when the frequency of the stokes wave is shifted from the pump frequency into lower frequency by about 13.2 THz, if the pump power is greater than the threshold Raman pump. Equations (2.16a) and (2.16b) provide the critical Raman pump power which is required to reach the value of the Raman threshold in the case of forward and backward pumping, respectively. The Raman-gain spectrum is assumed to have a Lorentzian shape here [14]

$$\frac{g_R P_0^{cr} L_{eff}}{A_{eff}} \approx 16 \qquad (forward\ pumping) \qquad (2.16a)$$

$$\frac{g_R P_0^{cr} L_{eff}}{A_{eff}} \approx 20 \qquad (backward\ pumping) \qquad (2.16b)$$

where P_0^{cr} is the critical Raman pump power, (it is the Raman pump power required to reach the threshold Raman effect), A_{eff} is the effective core area of the fiber and it can be given by $A_{eff} = \pi w^2$. The width parameter w depends on the V parameter of fiber , L_{eff} is the effective fiber length and it is given by

$$L_{eff} = [1 - \exp(-\alpha_p L)]/\alpha_p \qquad\qquad (2.17)$$

where α_p is the fiber loss at the Raman pump frequency. Equation (2.17) depicted that the fiber effective length is reduced from L_{eff} to L due to the fiber loss.

Chapter Three

Analysis of HNLF-Based Optical Phase Conjugation

Chapter Three

Analysis of HNLF-Based Optical Phase Conjugation

3.1 Introduction

A comprehensive analysis was performed in this chapter to address the effect of SOPs of associated waveforms on the performance of dual-pump HNLF-OPC. The analysis starts with set of coupled NLSEs for each of the two orthogonal SOPs. Approximate analytical solutions were developed under the assumption that the pump powers control the fiber nonlinearity (i.e., relatively high pump powers compared with signal power and hence the power of the generated idler). For comparison purposes, results related to linearly-polarized case are given. Section 3.2 gives some basic concepts that are related to the principle of operation of the HNLF-OPC. The performance of single- and dual-pump FWM in optical fibers is well addressed in the literature under the assumption of polarization alignment. A summary of the results related to single-polarization HNLF-OPC is given in section 3.3, (for more detailed analysis, refer to Appendix A). The effect of SOPs associated with the two pumps, signal, and idler is given in section 3.4. The output equations of signal wave, conjugated idler, and conversion efficiency are presented in section 3.5. In section 3.6, the expressions of the signal and idler waves at the end of the HNLF, as well as, the conversion efficiency are presented. And finally some results related to the HNLF-OPC conversion efficiency are given in section 3.7.

3.2 Basic Concepts of HNLF-Based Optical Phase Conjugation

OPC generates one or more idler waves during the process of FWM in a nonlinear medium such as HNLF. Since each idler is a phase-conjugated replica of the correspondinng signal, the idler contains all the information of the signal and thus it can be used for signal phase conjugation. Optical signal propagation in a nonlinear, dispersive, and lossy medium can be well described by the NLSE given in Eqn. (2.9) assuming a slowly varying envelope approximation. The complex conjugate of Eqn. (2.9, p.p. 36) can be expressed as

$$\frac{\partial \boldsymbol{A}^*(z.t)}{\partial z} + \frac{\alpha}{2} \boldsymbol{A}^*(z.t) + \beta_1 \frac{\partial \boldsymbol{A}^*(z.t)}{\partial t} - \frac{j}{2} \beta_2 \frac{\partial^2 \boldsymbol{A}^*(z.t)}{\partial t^2}$$

$$- \frac{1}{6} \beta_3 \frac{\partial^3 \boldsymbol{A}^*(z.t)}{\partial t^3} = j\gamma \, |\boldsymbol{A}^*(z.t)|^2 \, \boldsymbol{A}^*(z.t) \qquad (3.1)$$

where * denotes the complex conjugate operation. From Eqn. (3.1), it can be observed that the sign of both chromatic dispersion term β_2 and the Kerr effect term γ are reversed. Therefore, the GVD induced chirp and nonlinear distortion due to Kerr effect that occur after OPC will cancel the GVD induced chirp and nonlinear distortion due to Kerr effect occuring before OPC. Thus, in a transmission link with a fully symmetric fiber before and after the OPC, full GVD and nonliniarity compensation can be acheived by placing the OPC in the midlink.

Figure (3.1) represtnts a schematic diagram of the dual-pump HNLF-OPC. The setup consists of two CW pump sources whose outputs are seperatly amplified by two optical EDFAs. The ASE noise is suppressed using two Optical Band-Pass Filters (OBPFs). The SOPs of the pumps are controlled via two polarization controllers (PCs) placed after the OBPFs. The two pumps are multiplexed together using WDM coupler, this coupler is used here because it helps to reduce the insertion loss compared with the other types of couplers. The signal and the two pumps are combined together and the resultant signal then launched into the HNLF. The conjugated idlers

will be generated via process of FWM. The wavelength selective switch (WSS) then chooses either the signal or the conjugated idler.
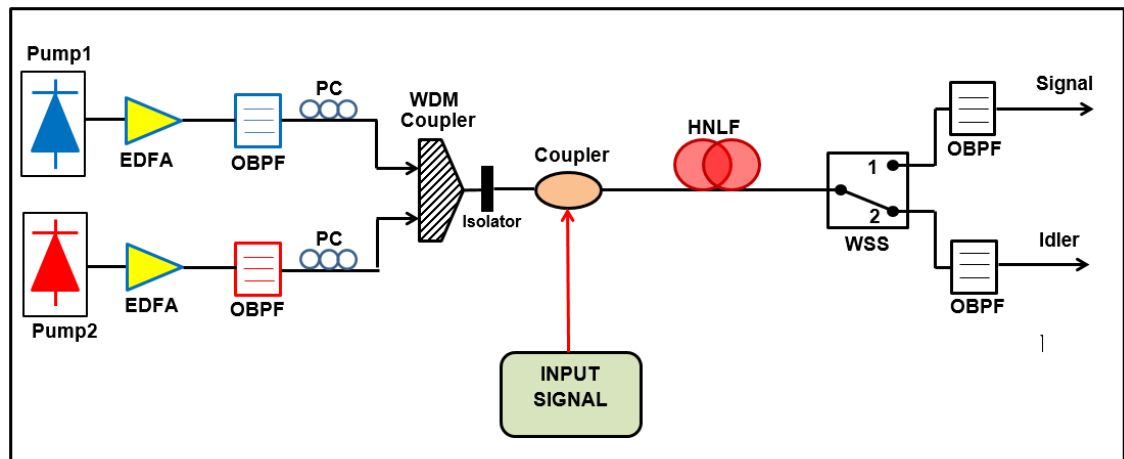
Figure (3.1): Schematic diagram of the optical phase conjugation device including erbium-doped fiber amplifier (EDFAs), optical band-pass filter (OBPF), polarization controller (PC), highly nonlinear fiber (HNLF), and wavelength selective switch (WSS).

The four waves (pump1, pump2, signal, and conjugated idler) that interact in the OPC system of Fig. (3.1) can be described by four coupled NLSEs described by Eqns. (2.13a-d, p.p. 39). Figure (3.2) shows the optical spectrum of all the four waves at the output of the HNLF. The amplified signal exits across one port of the WSS while the conjugated idler exits from the other port of the WSS.
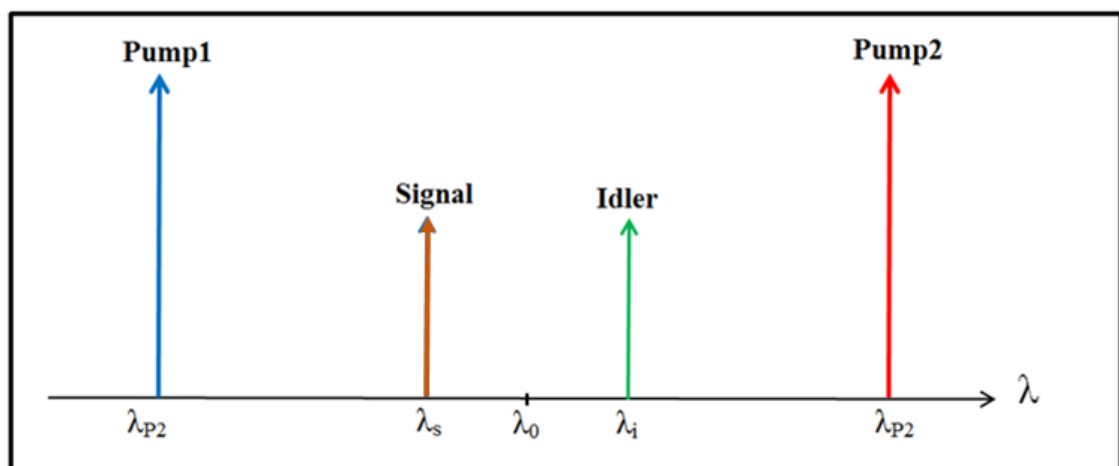
Figure (3.2): Schematic diagram of the optical spectrum at the HNLF output, λ_0 denotes, zero dispersion wavelength.

3.3 Analysis of Dual-Pump Polarization-Aligned HNLF-OPC

A dual-pump HNLF-OPC employing NDFWM process has several advantages over a single-pump counterpart which is based on degenerate FWM. The most important advantage is that the dual-pump HNLF-OPC can provide relatively high and flat gain when it is used as parametric amplifier. Further, it provides high and flat conversion efficiency over a much wider bandwidth than what is possible with a single-pump HNLF-OPC and thus it can be used efficiently as an OPC device with the WDM systems.

In this section, the analysis of NDFWM-based OPC in HNLF using dual-pump configuration is summarized in the absence of polarization effect and the result will be used in the next sections for comparison purposes. The final aim is to find an expression describing the conversion efficiency of the OPC device. The model is based on a set of NLSEs (Eqns. (2.13a-d)) describing the propagation of the pumps, signal and conjugated idler waveforms through the HNLF. Exact analytical solution of these coupled equations is very complex. Therefore, to solve the coupled equations exactly, a numerical approach is required. However, some assumptions are introduced to provide an approximate analytical solution. The results of the approximate analytical solution are verified with a numerical solution using Matlab software.

3.3.1 Approximate Analytical Analysis

The analysis given in this subsection stands heavily on the results reported in references [14, 18, 20] which address FWM in SSMF. To develop an approximate analytical model for the NDFWM, some considerable assumptions should be taken into account. Firstly, a scalar case is considered with all four fields that are linearly co-polarized along the propagation axis of a birefringent fiber (+z direction) such that they maintain their SOPs during propagation. Secondly, the four waves are oscillating at

frequencies ω_{p1}, ω_{p2}, ω_s, and ω_i, these four waves are linearly polarized along x axis. Thirdly, the pump waves are much more intense than the other waves and remain undepleted during the FWM process. Fourthly, the small frequency difference among the four waves is neglected when the nonlinear coefficient is calculated, so that, $\gamma_{p1} \approx \gamma_{p2} \approx \gamma_s \approx \gamma_i \approx \gamma$. Finally, the effective fiber attenuation is neglected, this is satisfied when the OAs compensate the fiber losses. Under these assumptions, Eqns. (2.13a, p.p. 39) and (2.13b, p.p. 39) can be simplified to

$$\frac{d\boldsymbol{A}_{p1}(z)}{dz} = j\gamma\big[P_{p1} + 2P_{p2}\big]\boldsymbol{A}_{p1}(z) \tag{3.2a}$$

$$\frac{d\boldsymbol{A}_{p2}(z)}{dz} = j\gamma\big[2P_{p1} + P_{p2}\big]\boldsymbol{A}_{p2}(z) \tag{3.2b}$$

where $P_{p1} = \big|\boldsymbol{A}_{p1}(0)\big|^2$ and $P_{p2} = \big|\boldsymbol{A}_{p2}(0)\big|^2$ are the incident pump powers at the HNLF input $z = 0$. The approximate analytical solution of Eqns. (3.2a) and (3.2b) can be expressed as (see Appendix A)

$$\boldsymbol{A}_{p1}(z) = \boldsymbol{A}_{p1}(0)\, exp\big(j\gamma\big[P_{p1} + 2P_{p2}\big]z\big) \tag{3.3a}$$

$$\boldsymbol{A}_{p2}(z) = \boldsymbol{A}_{p2}(0)\, exp\big(j\gamma\big[2P_{p1} + P_{p2}\big]z\big) \tag{3.3a}$$

Now, to find the signal amplitude $\boldsymbol{A}_s(z)$ and idler amplitude $\boldsymbol{A}_i(z)$, Eqns. (2.13c, pp. 39) and (2.13d, pp. 39) can be written under same previous assumptions as

$$\frac{d\boldsymbol{A}_s(z)}{dz} = 2j\gamma\big(\big[P_{p1} + P_{p2}\big]\boldsymbol{A}_s(z) + \boldsymbol{A}_i^*(z)\boldsymbol{A}_{p1}(z)\boldsymbol{A}_{p2}(z)\ exp(-j\Delta kz)\big) \tag{3.4a}$$

$$\frac{d\boldsymbol{A}_i^*(z)}{dz} = -2j\gamma\big(\big[P_{p1} + P_{p2}\big]\boldsymbol{A}_i^*(z) + \boldsymbol{A}_s(z)\boldsymbol{A}_{p1}^*(z)\boldsymbol{A}_{p2}^*(z)\ exp(j\Delta kz)\big) \tag{3.4b}$$

Solution of Eqns. (3.4a) and (3.4b) with the help of Eqns. (3.3a) and (3.3b) can be written as (see Appendix A)

$$A_s(z) = A_s(0)\left(\cosh(gz) + \frac{jk}{2g}\sinh(gz)\right)$$

$$\times \exp\left(j\,\frac{3\gamma(P_{p1} + P_{p2}) - \Delta k}{2}z\right) \tag{3.5a}$$

$$A_i^*(z) = A_s(0)\left(\frac{-j2\gamma\,A_{p1}^*(0)\,A_{p2}^*(0)}{g}\right)\sinh(gz)$$

$$\times \exp\left(-j\,\frac{3\gamma(P_{p1} + P_{p2}) - \Delta k}{2}z\right) \tag{3.5b}$$

where g is the parametric gain coefficient and it can be given by

$$g = \sqrt{4\gamma^2 P_{p1} P_{p2} - (k/2)^2} \tag{3.6}$$

Further, k is the total phase mismatch and it is given by

$$k = \Delta k + \gamma(P_{p1} + P_{p2}) \tag{3.7}$$

where Δk represents the linear phase mismatch and is defined in Eqn. (1.20).

From Eqn. (3.5a), the optical signal power can be expressed as

$$P_s(z) = P_s(0)\left[\cosh^2(gz) + \frac{k^2}{4g^2}\sinh^2(gz)\right] \tag{3.8}$$

Using the hyperbolic functions property $\left(\cosh^2(x) = 1 + \sinh^2(x)\right)$. Eqn. (3.9) at the end of the fiber where $z = L$ can be written as

$$P_s(L) = P_s(0)\left[1 + \left(1 + \frac{k^2}{4g^2}\right)\sinh^2(gL)\right] \tag{3.9}$$

The signal and the idler in the HNLF are amplified together during the process of FWM, and hence, it can be concluded that the difference between the signal power and the idler power is only the signal launched power at $z = 0$. Therefore, the idler power can be given by $P_i(z) = P_s(z) - P_s(0)$. Thus, from Eqn. (3.5b), the optical idler power at the end of the fiber can be obtained from the following equation

$$P_i(L) = P_s(0) \left[\left(1 + \frac{k^2}{4g^2} \right) \sinh^2(gL) \right] \qquad (3.10)$$

From Eqn. (3.10), the power of the idler wave depends on the signal launched power and it is directly generated after applying the input signal to the fiber. The pump sources feed the signal and idler waves with some energy and hence amplify the signal and generated idler as well. The idler power is proportional directly to the square of the fiber length when $gL \ll 1$. When a product of gL becomes more than 1, both the original signal and the converted idler grow exponentially with fiber length and parametric gain. In this case, the idler amplitude becomes almost equal to the signal amplitude at the HNLF output because they are amplified together along the fiber length. The idler wave carries the phase-converted data which is similar to the original signal data.

The conversion efficiency η_c of the HNLF-OPC (defined as the ratio of the converted idler power at the fiber output $z = L$ to the signal power at the HNLF input $z = 0$) can be calculated from Eqn. (3.10) as follow

$$\eta_c \equiv \frac{P_i(L)}{P_s(0)} = \left(1 + \frac{k^2}{4g^2} \right) \sinh^2(gL) \qquad (3.11)$$

The same analysis can be performed in the case of a single-pump configuration to evaluate the performance of the HNLF-OPC operation. The conversion efficiency in this case can be obtained also from Eqn. (3.11), with a single pump power P_p, but the phase mismatch is $k = \Delta k + 2\gamma P_p$, and the parametric gain is $g = \sqrt{\left(2\gamma P_p \right)^2 - (k/2)^2}$.

3.3.2 Numerical Solution

To validate the analytical approximate solution of the set of four NLSEs given in Eqns. (2.13a-d), comparisons were made versus the results

based on numerical solution using MATLAB code. The results reveal that the numerical solution is in excellent agreement with the analytical approximate solution in both single-pump and dual-pump configurations, and hence serves to validate the use of Eqn. (3.11). This conclusion is verified for two sets of dual-pump HNLF-OPC parameter values (see Tables (3.1)), which will be used later in chapter four.

Table (3.1): Parameters values of single-pump HNLF-OPC and dual-pump HNLF-OPC1 and HNLF-OPC2

Parameter	Single pump	Dual pump	
		HNLF-OPC1	HNLF-OPC2
Power of pump1 (W)	0.5	0.5	0.3
Power of pump2 (W)	-	0.5	0.3
Pump1 wavelength (nm)	1550.106	1502.6	1567.06
Pump2 wavelength (nm)	-	1600.6	1589.74
Length of the HNLF (km)	2.5	0.5	0.5
Attenuation coefficient of the HNLF (dB/km)	0.5	0.5	0.5
Nonlinear coefficient of the HNLF ($W^{-1}.km^{-1}$)	2	10	20
Nonlinear refractive index (m^2/W)	26×10^{-21}	26×10^{-21}	26×10^{-21}
Effective core area of the HNLF (μm^2)	52.7	10	5.7
Group velocity dispersion of the HNLF (ps/nm/km)	16.75	16.75	16.75
Dispersion slope of the HNLF ($ps/nm^2/km$)	0.1	0.1	0.1
Zero-dispersion wavelength of the HNLF (nm)	1550	1550	1578.3

Figure (3.3a) shows the conversion efficiency for a single-pump HNLF-OPC. The HNLF that used in this configuration is of 2.5 km length with a zero-dispersion wavelength of 1550 nm. The pump has 0.5 W power and 1550.106 nm wavelength. The pump wavelength is chosen near zero-dispersion wavelength to decrease the effect of phase mismatch. A flat conversion efficiency of about 15 dB is obtained in two wavelength regions extending from 1515 to 1530 nm and from 1570 to 1585 nm. In Fig. (3.3b), in order to increase the conversion efficiency of the single-pump HNLF-OPC, the pump power is increased from 0.5 to 1W. In this case, the maximum conversion efficiency increased to 33.2 dB but the flat region of the conversion efficiency is narrowed.
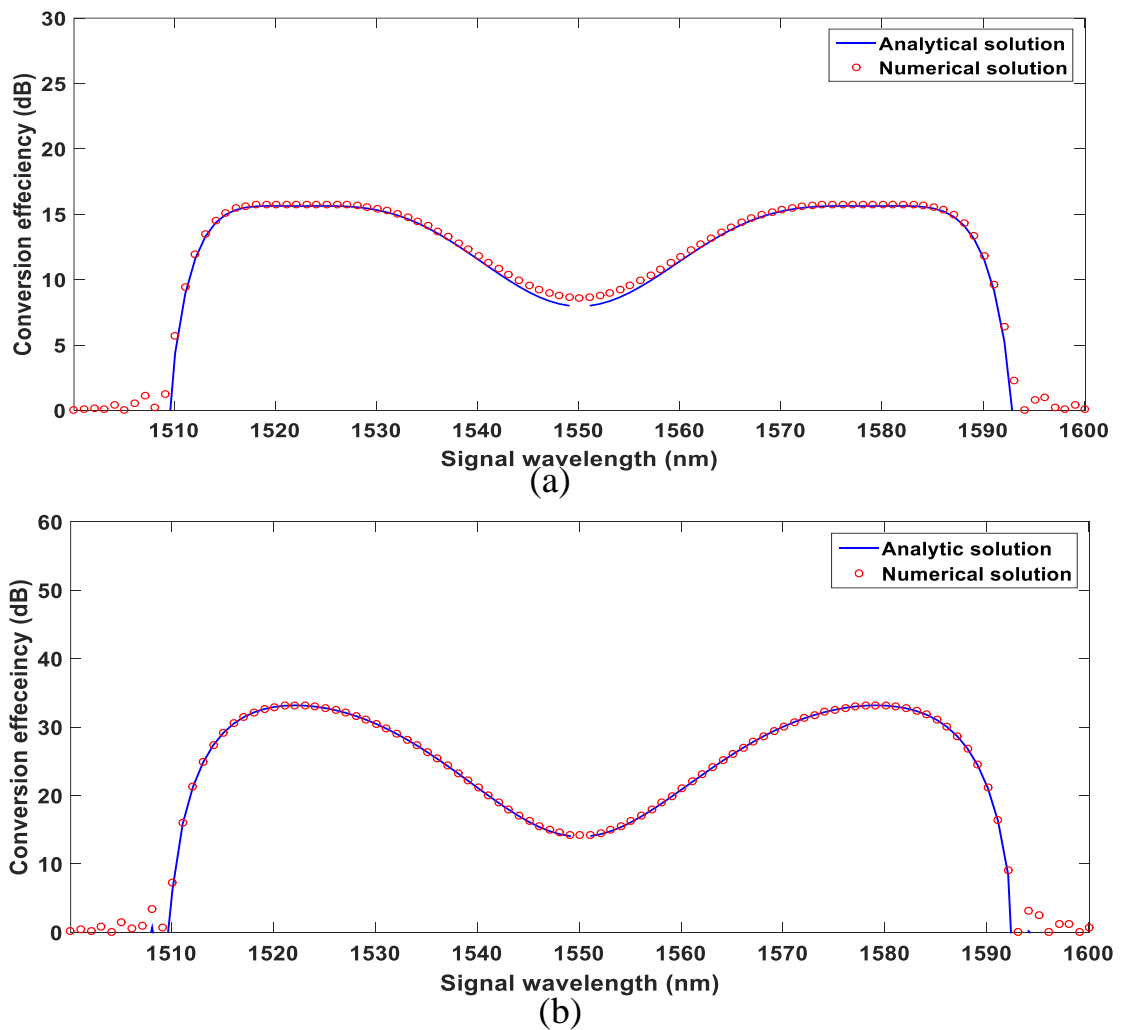
Figure (3.3): Analytical and numerical conversion efficiencies of the single-pump HNLF-OPC with (a) 0.5 W pump power, and (b) 1 W pump power.

The dual-pump HNLF-OPC configuration provides higher conversion efficiency over a wider wavelength region compared to the single-pump configuration. Figure (3.4a) compares the conversion efficiency of the dual-pump HNLF-OPC1, calculated analytically and numerically. The HNLF has 1550 nm zero-dispersion wavelength and 0.5 km length. Other HNLF-OPC1 parameters used in this example are given in Table (3.1). In this figure, a constant conversion efficiency of about 37 dB is obtained over a wide-wavelength region extending from 1510 to 1590 nm.

Recall that the analytical solution is conducted under the assumption that the pump powers remain undepleted over the fiber. However, the HNLF length can be increased to obtain higher values of conversion efficiency. In this case, the depletion of pump may take place and the conversion efficiency will show a difference between the analytical and numerical solutions. For example, in Fig. (3.4b), the length of the HNLF is increased from 0.5 to 0.8 km. The calculated numerical and analytical conversion efficiencies are 55 and 65 dB, respectively.
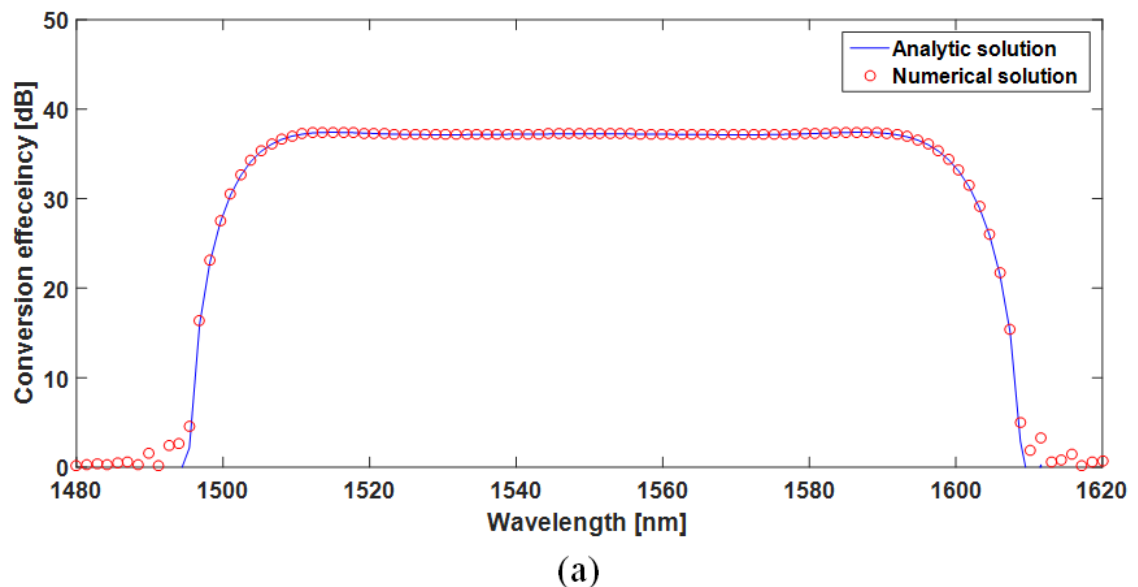
Figure (3.4): Analytical and numerical conversion efficiencies of HNLF-OPC1 with the parameters values listed in Table (3.1) when the length of the HNLF is (a) 0.5 km, and (b) 0.8 km.
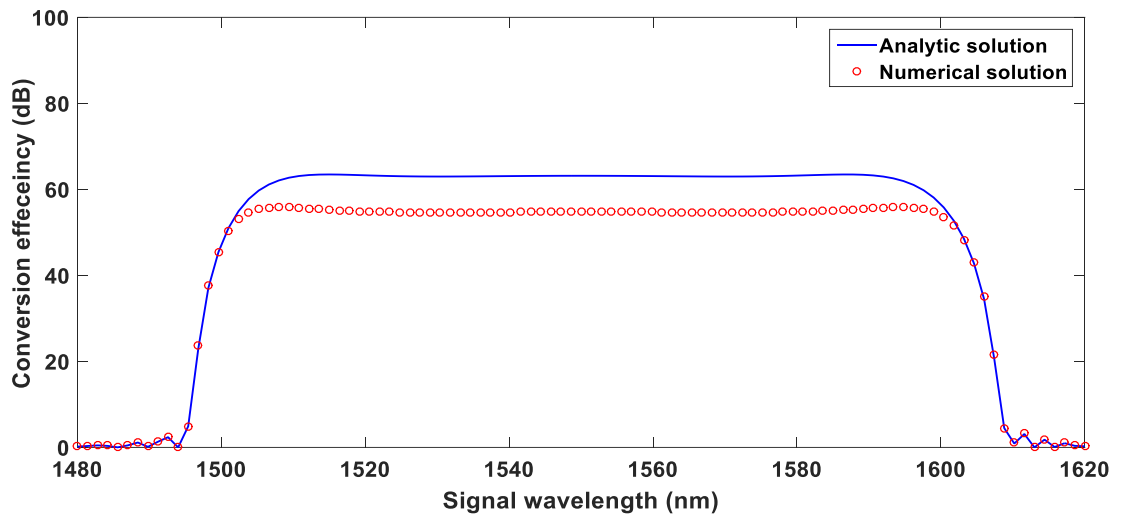
(b)

Figure (3.4): Continued

The performance of HNLF-OPC2 which works at different wavelength region is also investigated and the results are given in Fig. (3.5). Again, the results show very good agreement between the analytical and the numerical solutions.
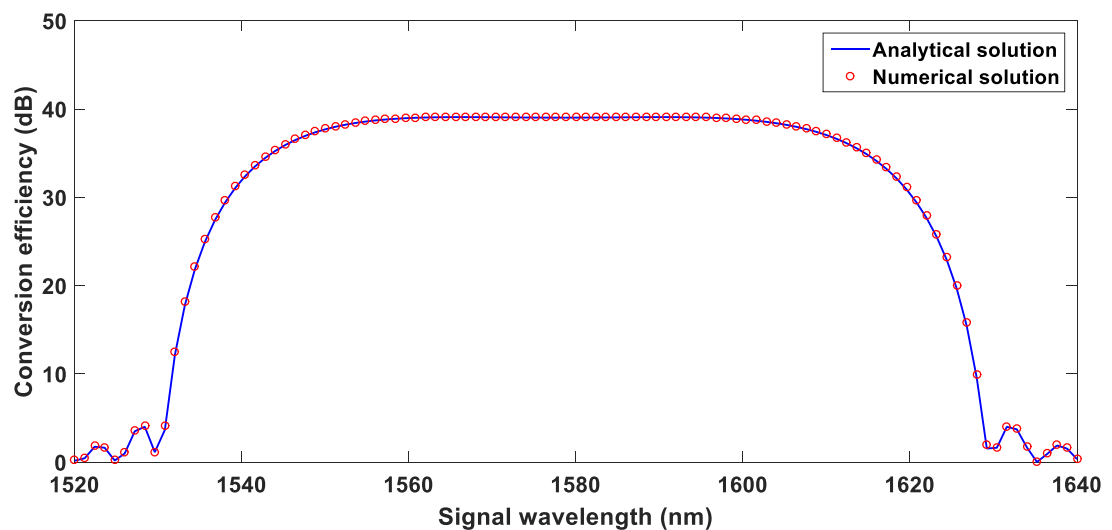
Figure (3.5): Analytical and numerical conversion efficiencies of HNLF-OPC2 with the parameters values listed in Table (3.1).

3.4 Effect of Polarization on the FWM Process in HNLF-OPC

In the previous section, the theory assumes that the all propagating waves are aligned linear polarization states along the fiber length. However, this condition is difficult to be satisfied. The SOP of propagating light randomly changes along the fiber length due to external perturbations, such as fiber bending and asymmetrical fiber cross section. In this section, the performance of FWM operating under general polarization states is investigated due to its importance in fiber-optic communications.

3.4.1 Mathematical Framework

Consider the general case where the incident two pumps and signal have the polarization angles θ_{P1}, θ_{P2} and θ_s, respectively, measured against the TE-axis (see Fig. (3.6)). Each of these waves can be decomposed into Transvers Electric (TE) and Transvers Magnetic (TM) modes.
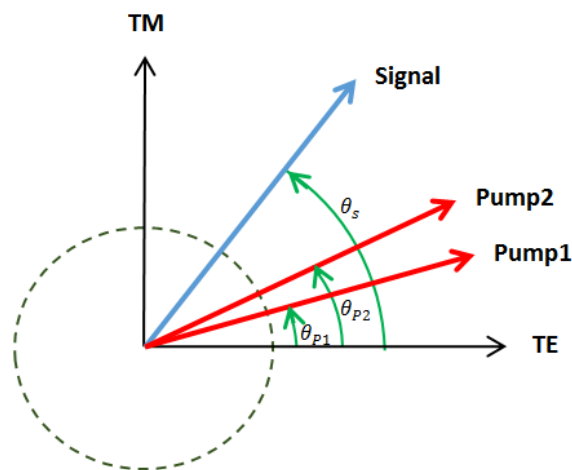
Figure (3.6): Schematic diagram to analyze the effect of polarization on FWM in highly nonlinear fiber.

The FWM occurs only among waves with the same polarization mode. In this case, (Eqns. (2.13a-d)) can be rewritten for each polarization mode leading to a set of eight coupled equations.

$$\frac{dA_{p1TE}(z)}{dz} = \frac{-\alpha_{p1TE}}{2} A_{p1TE}(z)$$
$$+ j\gamma_{p1TE}\left[\left|A_{p1TE}(z)\right|^2 + 2\left|A_{p2TE}(z)\right|^2 + 2\left|A_{STE}(z)\right|^2\right.$$
$$+ 2\left|A_{iTE}(z)\right|^2\right]A_{p1TE}(z)$$
$$+ 2j\gamma A_{p2TE}^*(z)A_{STE}(z)A_{iTE}(z)\exp(j\Delta k_{TE}z) \qquad (3.12a)$$

$$\frac{dA_{p1TM}(z)}{dz} = \frac{-\alpha_{p1TM}}{2} A_{p1TM}(z)$$
$$+ j\gamma_{p1TM}\left[\left|A_{p1TM}(z)\right|^2 + 2\left|A_{p2TM}(z)\right|^2 + 2\left|A_{STM}(z)\right|^2\right.$$
$$+ 2\left|A_{iTM}(z)\right|^2\right]A_{p1TM}(z)$$
$$+ 2j\gamma A_{p2TM}^*(z)A_{STM}(z)A_{iTM}(z)\exp(j\Delta k_{TM}z) \qquad (3.12b)$$

$$\frac{dA_{p2TE}(z)}{dz} = \frac{-\alpha_{p2TE}}{2} A_{p2TE}(z)$$
$$+ j\gamma_{p2TE}\left[2\left|A_{p1TE}(z)\right|^2 + \left|A_{p2TE}(z)\right|^2 + 2\left|A_{STE}(z)\right|^2\right.$$
$$+ 2\left|A_{iTE}(z)\right|^2\right]A_{p2TE}(z)$$
$$+ 2j\gamma A_{p1TE}^*(z)A_{STE}(z)A_{iTE}(z)\exp(j\Delta k_{TE}z) \qquad (3.12c)$$

$$\frac{dA_{p2TM}(z)}{dz} = \frac{-\alpha_{p2TM}}{2} A_{p2TM}(z)$$
$$+ j\gamma_{p2TM}\left[2\left|A_{p1TM}(z)\right|^2 + \left|A_{p2TM}(z)\right|^2 + 2\left|A_{STM}(z)\right|^2\right.$$
$$+ 2\left|A_{iTM}(z)\right|^2\right]A_{p2TM}(z)$$
$$+ 2j\gamma A_{p1TM}^*(z)A_{STM}(z)A_{iTM}(z)\exp(j\Delta k_{TM}z) \qquad (3.12d)$$

$$\frac{dA_{STE}(z)}{dz} = \frac{-\alpha_{STE}}{2} A_{STE}(z)$$
$$+ j\gamma_{STE}\left[2\left|A_{p1TE}(z)\right|^2 + 2\left|A_{p2TE}(z)\right|^2 + \left|A_{STE}(z)\right|^2\right.$$
$$+ 2\left|A_{iTE}(z)\right|^2\right]A_{STE}(z)$$
$$+ 2j\gamma A_{iTE}^*(z)A_{p1TE}(z)A_{p2TE}(z)\exp(-j\Delta k_{TE}z) \qquad (3.12e)$$

$$\frac{dA_{sTM}(z)}{dz} = \frac{-\alpha_{sTM}}{2} A_{sTM}(z)$$

$$+ j\gamma_{sTM}\big[2\,|A_{p1TM}(z)|^2 + 2\,|A_{p2TM}(z)|^2 + |A_{sTM}(z)|^2$$

$$+ 2\,|A_{iTM}(z)|^2\big]A_{sTM}(z)$$

$$+ 2j\gamma\, A_{iTM}^*(z)A_{p1TM}(z)A_{p2TM}(z)\ \exp(-j\Delta k_{TM}z) \qquad (3.12f)$$

$$\frac{dA_{iTE}(z)}{dz} = \frac{-\alpha_{iTE}}{2} A_{iTE}(z)$$

$$+ j\gamma_{iTE}\big[2\,|A_{p1TE}(z)|^2 + 2\,|A_{p2TE}(z)|^2 + 2\,|A_{sTE}(z)|^2$$

$$+ |A_{iTE}(z)|^2\big]A_{iTE}(z)$$

$$+ 2j\gamma\, A_{sTE}^*(z)A_{p1TE}(z)A_{p2TE}(z)\ \exp(-j\Delta k_{TE}z) \qquad (3.12g)$$

$$\frac{dA_{iTM}(z)}{dz} = \frac{-\alpha_{iTM}}{2} A_{iTM}(z)$$

$$+ j\gamma_{iTM}\big[2\,|A_{p1TM}(z)|^2 + 2\,|A_{p2TM}(z)|^2 + 2\,|A_{sTM}(z)|^2$$

$$+ |A_{iTM}(z)|^2\big]A_{iTM}(z)$$

$$+ 2j\gamma\, A_{sTM}^*(z)A_{p1TM}(z)A_{p2TM}(z)\ \exp(-j\Delta k_{TM}z) \qquad (3.12h)$$

In Eqns. (3.12a-h), the subscript TE (TM) denotes TE (TM) wave component. The TE and TM wave components of the two pumps and signal powers coupled to the HNLF can be expressed as

$$P_{P1TE}(0) = C_{TE}\, P_{P10}\, cos^2(\theta_{P1}) \qquad\qquad (3.13a)$$

$$P_{P1TM}(0) = C_{TM}\, P_{P10}\, sin^2(\theta_{P1}) \qquad\qquad (3.13b)$$

$$P_{P2TE}(0) = C_{TE}\, P_{P20}\, cos^2(\theta_{P2}) \qquad\qquad (3.13c)$$

$$P_{P2TM}(0) = C_{TM}\, P_{P20}\, sin^2(\theta_{P2}) \qquad\qquad (3.13d)$$

$$P_{sTE}(0) = C_{TE}\, P_{s0}\, cos^2(\theta_s) \qquad\qquad (3.13e)$$

$$P_{sTM}(0) = C_{TM}\, P_{s0}\, sin^2(\theta_s) \qquad\qquad (3.13f)$$

where C_{TE} (C_{TM}) is the relative coupling efficiency for TE (TM) mode, and the linear phase mismatch for TE (TM) wave components are given by

$$\Delta k_{TE} = \beta_{STE} + \beta_{cTE} - \beta_{P1TE} - \beta_{P2TE} \tag{3.14a}$$

$$\Delta k_{TM} = \beta_{STM} + \beta_{cTM} - \beta_{P1TM} - \beta_{P2TM} \tag{3.14b}$$

It can be considered that all the propagating waves are in the same wavelength region. Therefore, the linear-loss coefficients of all the waves are almost equal ($\alpha_{p1TE} = \alpha_{p1TM} = \alpha_{p2TE} = \alpha_{p2TM} = \alpha_{STE} = \alpha_{STM} = \alpha_{iTE} = \alpha_{iTM} = \alpha$). Further, the nonlinear parameters can be assumed equal for all the waves too ($\gamma_{p1TE} = \gamma_{p1TM} = \gamma_{p2TE} = \gamma_{p2TM} = \gamma_{STE} = \gamma_{STM} = \gamma_{iTE} = \gamma_{iTM} = \gamma$).

3.4.2 Applying Practical Assumptions

Exact analytical solution of Eqns. (3.12a-h) is very difficult because of their complexity. However, some practical assumptions must be taken into account to get the approximate analytical solution

i)   The effects of SPM and XPM are negligible.

ii)   The optical power of the two pump waves control the fiber nonlinearity

iii)   The pump powers remain undepleted during the FWM process.

iv)   The effective attenuation coefficient α is negligible.

Under these assumptions, Eqns. (3.12a-d) can be simplified to

$$\frac{dA_{p1TE}(z)}{dz} = j\gamma[P_{P1TE} + 2P_{P2TE}]\,A_{p1TE}(z) \tag{3.15a}$$

$$\frac{dA_{p1TM}(z)}{dz} = j\gamma[P_{P1TM} + 2P_{P2TM}]A_{p1TM}(z) \tag{3.15b}$$

$$\frac{dA_{p2TE}(z)}{dz} = j\gamma[2P_{P1TE} + P_{P2TE}]A_{p2TE}(z) \tag{3.15c}$$

$$\frac{dA_{p2TM}(z)}{dz} = j\gamma[2P_{P1TM} + P_{P2TM}]A_{p2TM}(z) \tag{3.15d}$$

where $\left| A_{pjk}(z) \right|^2 = P_{Pjk}$, $(j = 1.2 \; and \; k = TE. \; TM)$ are the pump powers of the corresponding components. Integrating both sides of Eqns. (3.15a-d) yields

$$\int \frac{1}{A_{p1TE}(z)} dA_{p1TE}(z) = \int j\gamma [P_{P1TE} + 2P_{P2TE}] \, dz \tag{3.16a}$$

$$\int \frac{1}{A_{p1TM}(z)} dA_{p1TM}(z) = \int j\gamma [P_{P1TM} + 2P_{P2TM}] \, dz \tag{3.16b}$$

$$\int \frac{1}{A_{p2TE}(z)} dA_{p2TE}(z) = \int j\gamma [2P_{P1TE} + P_{P2TE}] \, dz \tag{3.16c}$$

$$\int \frac{1}{A_{p2TM}(z)} dA_{p2TM}(z) = \int j\gamma [2P_{P1TM} + P_{P2TM}] \, dz \tag{3.16d}$$

Equations (3.16a-d) can be solved as follow

$$ln\left(A_{p1TE}(z)\right) = j\gamma [P_{P1TE} + 2P_{P2TE}] \, z + C_{10} \tag{3.17a}$$

$$ln\left(A_{p1TM}(z)\right) = j\gamma [P_{P1TM} + 2P_{P2TM}] \, z + C_{20} \tag{3.17b}$$

$$ln\left(A_{p2TE}(z)\right) = j\gamma [2P_{P1TE} + P_{P2TE}] \, z + C_{30} \tag{3.17c}$$

$$ln\left(A_{p2TM}(z)\right) = j\gamma [2P_{P1TM} + P_{P2TM}] \, z + C_{40} \tag{3.17d}$$

where $C_{j0}. (j = 1 - 4)$ are the integration constants. Let $C_{j1} = \exp(C_{j0})$, then by taking exponential for both sides to Eqns. (3.17a-d) yields

$$A_{p1TE}(z) = C_{11} \, exp(j\gamma [P_{P1TE} + 2P_{P2TE}] \, z) \tag{3.18a}$$

$$A_{p1TM}(z) = C_{12} \, exp(j\gamma [P_{P1TM} + 2P_{P2TM}] \, z) \tag{3.18b}$$

$$A_{p2TE}(z) = C_{13} \, exp(j\gamma [2P_{P1TE} + P_{P2TE}] \, z) \tag{3.18c}$$

$$A_{p2TM}(z) = C_{14} \, exp(j\gamma [2P_{P1TM} + P_{P2TM}] \, z) \tag{3.18d}$$

where $C_{11} = A_{p1TE}(0)$, $C_{12} = A_{p1TM}(0)$, $C_{13} = A_{p2TE}(0)$, and $C_{14} = A_{p2TM}(0)$ are the integration constants obtained from the initial conditions

when $z = 0$ is applied to Eqns. (3.18a-d). Then, inserting these values into Eqns. (3.18a-d) produces

$$A_{p1TE}(z) = A_{p1TE}(0) \, exp(j\gamma[P_{P1TE} + 2P_{P2TE}] \, z) \tag{3.19a}$$

$$A_{p1TM}(z) = A_{p1TM}(0) \, exp(j\gamma[P_{P1TM} + 2P_{P2TM}] \, z) \tag{3.19b}$$

$$A_{p2TE}(z) = A_{p2TE}(0) \, exp(j\gamma[2P_{P1TE} + P_{P2TE}] \, z) \tag{3.19c}$$

$$A_{p2TM}(z) = A_{p2TM}(0) \, exp(j\gamma[2P_{P1TM} + P_{P2TM}] \, z) \tag{3.19d}$$

The complex conjugations of Eqns. (3.19a-d) can be written as

$$A_{p1TE}^*(z) = A_{p1TE}^*(0) \, exp(-j\gamma[P_{P1TE} + 2P_{P2TE}] \, z) \tag{3.20a}$$

$$A_{p1TM}^*(z) = A_{p1TM}^*(0) \, exp(-j\gamma[P_{P1TM} + 2P_{P2TM}] \, z) \tag{3.20b}$$

$$A_{p2TE}^*(z) = A_{p2TE}^*(0) \, exp(-j\gamma[2P_{P1TE} + P_{P2TE}] \, z) \tag{3.20c}$$

$$A_{p2TM}^*(z) = A_{p2TM}^*(0) \, exp(-j\gamma[2P_{P1TM} + P_{P2TM}] \, z) \tag{3.20d}$$

Now, to solve Eqns. (3.12e-h), the same previous assumptions are applied and these equations can be written in the following forms

$$\frac{dA_{sTE}(z)}{dz} = 2j\gamma\Big([P_{P1TE} + P_{P2TE}]A_{sTE}(z)$$
$$+ \; A_{iTE}^*(z)A_{p1TE}(z)A_{p2TE}(z) \; exp(-j\Delta k_{TE}z)\Big) \tag{3.21a}$$

$$\frac{dA_{sTM}(z)}{dz} = 2j\gamma\Big([P_{P1TM} + P_{P2TM}]A_{sTM}(z)$$
$$+ \; A_{iTM}^*(z)A_{p1TM}(z)A_{p2TM}(z) \; exp(-j\Delta k_{TM}z)\Big) \tag{3.21b}$$

$$\frac{dA_{iTE}^*(z)}{dz} = -2j\gamma\Big([P_{P1TE} + P_{P2TE}]A_{iTE}(z)$$
$$+ \; A_{sTE}(z) \, A_{p1TE}^*(z) \, A_{p2TE}^*(z) \; exp(j\Delta k_{TE}z)\Big) \tag{3.21c}$$

$$\frac{dA_{iTM}^*(z)}{dz} = -2j\gamma\Big([P_{P1TM} + P_{P2TM}]A_{iTM}(z)$$
$$+ \; A_{sTM}(z) \, A_{p1TM}^*(z) \, A_{p2TM}^*(z) \; exp(j\Delta k_{TM}z)\Big) \tag{3.21d}$$

Substituting Eqns. (3.19a and 3.19c) into Eqn. (3.21a), Eqns. (3.19b and 3.19d) into Eqn. (3.19b), Eqns. (3.20a and 3.20c) into Eqn. (3.21c), and Eqns. (3.20b and 3.20d) into Eqn. (3.21d) yields

$$\frac{dA_{sTE}(z)}{dz} = 2j\gamma\big([P_{P1TE} + P_{P2TE}]A_{sTE}(z) + A_{iTE}^*(z)A_{p1TE}(0)\,exp(j\gamma[P_{P1TE} +$$

$$2P_{P2TE}]\,z)A_{p2TE}(0)\,exp(j\gamma[2P_{P1TE} + P_{P2TE}]\,z)\,\exp(-j\Delta k_{TE}z)\big) \qquad (3.22a)$$

$$\frac{dA_{sTM}(z)}{dz} = 2j\gamma\big([P_{P1TM} + P_{P2TM}]A_{sTM}(z) + A_{iTM}^*(z)A_{p1TM}(0)\,exp(j\gamma[P_{P1TM} +$$

$$2P_{P2TM}]\,z)A_{p2TM}(0)\,exp(j\gamma[2P_{P1TM} + P_{P2TM}]\,z)\,\exp(-j\Delta k_{TM}z)\big) \qquad (3.22b)$$

$$\frac{dA_{iTE}^*(z)}{dz} = -2j\gamma\big([P_{P1TE} + P_{P2TE}]A_{iTE}(z) + A_{sTE}(z)\,A_{p1TE}^*(0)\,exp(-j\gamma[P_{P1TE} +$$

$$2P_{P2TE}]\,z)\,A_{p2TE}^*(0)\,exp(-j\gamma[2P_{P1TE} +$$

$$P_{P2TE}]\,z)\exp(j\Delta k_{TE}z)\big) \qquad (3.22c)$$

$$\frac{dA_{iTM}^*(z)}{dz} = -2j\gamma\big([P_{P1TM} + P_{P2TM}]A_{iTM}(z) + A_{sTM}(z)A_{p1TM}^*(0)exp(-j\gamma[P_{P1TM} +$$

$$2P_{P2TM}]\,z)\,A_{p2TM}^*(0)exp(-j\gamma[2P_{P1TM} + P_{P2TM}]\,z)\,exp(j\Delta k_{TM}z)\big) \qquad (3.22d)$$

Simplifying Eqns. (3.22a-d) mathematically yields

$$\frac{dA_{sTE}(z)}{dz} = 2j\gamma\big([P_{P1TE} + P_{P2TE}]A_{sTE}(z)$$
$$+ A_{iTE}^*(z)A_{p1TE}(0)\,A_{p2TE}(0)\;\exp(-jR_{TE}z)\big) \qquad (3.23a)$$

$$\frac{dA_{sTM}(z)}{dz} = 2j\gamma\big([P_{P1TM} + P_{P2TM}]A_{sTM}(z)$$
$$+ A_{iTM}^*(z)A_{p1TM}(0)\,A_{p2TM}(0)\;\exp(-jR_{TM}z)\big) \qquad (3.23b)$$

$$\frac{dA_{iTE}^*(z)}{dz} = -2j\gamma\big([P_{P1TE} + P_{P2TE}]A_{iTE}(z)$$
$$+ A_{sTE}(z)\,A_{p1TE}^*(0)\,A_{p2TE}^*(0)\;\exp(jR_{TE}z)\big) \qquad (3.23c)$$

$$\frac{dA_{iTM}^*(z)}{dz} = -2j\gamma\big([P_{P1TM} + P_{P2TM}]A_{iTM}(z)$$
$$+ A_{sTM}(z)\,A_{p1TM}^*(0)\,A_{p2TM}^*(0)\;\exp(jR_{TM}z)\big) \qquad (3.23d)$$

where

$$R_{TE} = \Delta k_{TE} - 3\gamma(P_{P1TE} + P_{P2TE}) \tag{3.24a}$$

$$R_{TM} = \Delta k_{TM} - 3\gamma(P_{P1TM} + P_{P2TM}) \tag{3.24b}$$

3.4.3 Variation of Signal and Idler Waveforms Along the Fiber

To solve Eqns. (3.23a-d), the following equations are introduced

$$\boldsymbol{B}_{sTE}(z) = \boldsymbol{A}_{sTE}(z)\, exp(-2j\gamma[P_{P1TE} + P_{P2TE}]z) \tag{3.25a}$$

$$\boldsymbol{B}_{sTM}(z) = \boldsymbol{A}_{sTM}(z)\, exp(-2j\gamma[P_{P1TM} + P_{P2TM}]z) \tag{3.25b}$$

$$\boldsymbol{B}_{iTE}^{*}(z) = \boldsymbol{A}_{iTE}^{*}(z)\, exp(2j\gamma[P_{P1TE} + P_{P2TE}]z) \tag{3.25c}$$

$$\boldsymbol{B}_{iTM}^{*}(z) = \boldsymbol{A}_{iTM}^{*}(z)\, exp(2j\gamma[P_{P1TM} + P_{P2TM}]z) \tag{3.25d}$$

Differentiating Eqns. (3.25a-d) with respect to z gives

$$\frac{d\boldsymbol{B}_{sTE}(z)}{dz} = \boldsymbol{A}_{sTE}(z)\,(-2j\gamma[P_{P1TE} + P_{P2TE}])\, exp(-2j\gamma[P_{P1TE} + P_{P2TE}]z)$$
$$+ \frac{d\boldsymbol{A}_{sTE}(z)}{dz}\, exp(-2j\gamma[P_{P1TE} + P_{P2TE}]z) \tag{3.26a}$$

$$\frac{d\boldsymbol{B}_{sTM}(z)}{dz} = \boldsymbol{A}_{sTM}(z)\,(-2j\gamma[P_{P1TM} + P_{P2TM}])\, exp(-2j\gamma[P_{P1TM} + P_{P2TM}]z)$$
$$+ \frac{d\boldsymbol{A}_{sTM}(z)}{dz}\, exp(-2j\gamma[P_{P1TM} + P_{P2TM}]z) \tag{3.26b}$$

$$\frac{d\boldsymbol{B}_{iTE}^{*}(z)}{dz} = \boldsymbol{A}_{iTE}^{*}(z)\,(2j\gamma[P_{P1TE} + P_{P2TE}])\, exp(2j\gamma[P_{P1TE} + P_{P2TE}]z)$$
$$+ \frac{d\boldsymbol{A}_{iTE}^{*}(z)}{dz}\, exp(2j\gamma[P_{P1TE} + P_{P2TE}]z) \tag{3.26c}$$

$$\frac{d\boldsymbol{B}_{iTM}^{*}(z)}{dz} = \boldsymbol{A}_{iTM}^{*}(z)\,(2j\gamma[P_{P1TM} + P_{P2TM}])\, exp(2j\gamma[P_{P1TM} + P_{P2TM}]z)$$
$$+ \frac{d\boldsymbol{A}_{iTM}^{*}(z)}{dz}\, exp(2j\gamma[P_{P1TM} + P_{P2TM}]z) \tag{3.26d}$$

Substituting Eqns. (3.23a-d) into Eqns. (3.26a-d) yields

$$\frac{d\boldsymbol{B}_{sTE}(z)}{dz} = \boldsymbol{A}_{sTE}(z)\,(-2j\gamma[P_{P1TE} + P_{P2TE}])\,exp(-2j\gamma[P_{P1TE} + P_{P2TE}]z)$$

$$+\ 2j\gamma\big([P_{P1TE} + P_{P2TE}]\boldsymbol{A}_{sTE}(z)\,exp(-2j\gamma[P_{P1TE} + P_{P2TE}]z)\big)$$

$$+\ 2j\gamma\,\boldsymbol{A}_{iTE}^{*}(z)\boldsymbol{A}_{p1TE}(0)\boldsymbol{A}_{p2TE}(0)\exp(-j\theta_{TE}z)\,exp(-2j\gamma[P_{P1TE}$$

$$+\ P_{P2TE}]z) \tag{3.27a}$$

$$\frac{d\boldsymbol{B}_{sTM}(z)}{dz} = \boldsymbol{A}_{sTM}(z)\,(-2j\gamma[P_{P1TM} + P_{P2TM}])\,exp(-2j\gamma[P_{P1TM} + P_{P2TM}]z)$$

$$+\ 2j\gamma\big([P_{P1TM} + P_{P2TM}]\boldsymbol{A}_{sTM}(z)\,exp(-2j\gamma[P_{P1TM} + P_{P2TM}]z)\big)$$

$$+\ 2j\gamma\,\boldsymbol{A}_{iTM}^{*}(z)\boldsymbol{A}_{p1TM}(0)\boldsymbol{A}_{p2TM}(0)\exp(-j\theta_{TM}z)\,exp(-2j\gamma[P_{P1TM}$$

$$+\ P_{P2TM}]z) \tag{3.27b}$$

$$\frac{d\boldsymbol{B}_{iTE}^{*}(z)}{dz} = \boldsymbol{A}_{iTE}^{*}(z)\,(2j\gamma[P_{P1TE} + P_{P2TE}])\,exp(2j\gamma[P_{P1TE} + P_{P2TE}]z)$$

$$-\ 2j\gamma[P_{P1TE} + P_{P2TE}]\boldsymbol{A}_{iTE}^{*}(z)\,exp(2j\gamma[P_{P1TE} + P_{P2TE}]z)$$

$$-\ 2j\gamma\boldsymbol{A}_{sTE}(z)\,\boldsymbol{A}_{p1TE}^{*}(0)\,\boldsymbol{A}_{p2TE}^{*}(0)\ \exp(j\theta_{TE}z)\,exp(2j\gamma[P_{P1TE}$$

$$+\ P_{P2TE}]z) \tag{3.27c}$$

$$\frac{d\boldsymbol{B}_{iTM}^{*}(z)}{dz} = \boldsymbol{A}_{iTM}^{*}(z)\,(2j\gamma[P_{P1TM} + P_{P2TM}])\,exp(2j\gamma[P_{P1TM} + P_{P2TM}]z)$$

$$-\ 2j\gamma\ [P_{P1TM} + P_{P2TM}]\boldsymbol{A}_{iTM}^{*}(z)\,exp(2j\gamma[P_{P1TM} + P_{P2TM}]z)$$

$$-\ 2j\gamma\boldsymbol{A}_{sTM}(z)\,\boldsymbol{A}_{p1TM}^{*}(0)\ \boldsymbol{A}_{p2TM}^{*}(0)\ \exp(j\theta_{TM}z)exp(2j\gamma[P_{P1TM}$$

$$+\ P_{P2TM}]z) \tag{3.27d}$$

Simplifying Eqns. (3.27a-d) produces

$$\frac{d\boldsymbol{B}_{sTE}(z)}{dz} = 2j\gamma\,\boldsymbol{A}_{iTE}^{*}(z)\boldsymbol{A}_{p1TE}(0)\boldsymbol{A}_{p2TE}(0)\exp(-jR_{TE}z)\,exp(-2j\gamma[P_{P1TE}$$

$$+\ P_{P2TE}]z) \tag{3.28a}$$

$$\frac{d\boldsymbol{B}_{sTM}(z)}{dz} = 2j\gamma\,\boldsymbol{A}_{iTM}^{*}(z)\boldsymbol{A}_{p1TM}(0)\boldsymbol{A}_{p2TM}(0)\exp(-jR_{TM}z)\,exp(-2j\gamma[P_{P1TM}$$

$$+\ P_{P2TM}]z) \tag{3.28b}$$

$$\frac{d\boldsymbol{B}_{iTE}^*(z)}{dz} = -2j\gamma \boldsymbol{A}_{sTE}(z)\, \boldsymbol{A}_{p1TE}^*(0)\, \boldsymbol{A}_{p2TE}^*(0)\ \exp(jR_{TE}z)\, exp(2j\gamma[P_{P1TE}$$

$$+ P_{P2TE}]z) \tag{3.28c}$$

$$\frac{d\boldsymbol{B}_{iTM}^*(z)}{dz} = -2j\gamma \boldsymbol{A}_{sTM}(z)\, \boldsymbol{A}_{p1TM}^*(0)\, \boldsymbol{A}_{p2TM}^*(0)\ \exp(jR_{TM}z)exp(2j\gamma[P_{P1TM}$$

$$+ P_{P2TM}]z) \tag{3.28d}$$

From Eqns. (3.25a-d), $\boldsymbol{A}_{sTE}(z).\boldsymbol{A}_{sTM}(z).\boldsymbol{A}_{iTE}^*(z).$ and $\boldsymbol{A}_{iTM}^*(z)$ can be written as

$$\boldsymbol{A}_{sTE}(z) = \boldsymbol{B}_{sTE}(z)\, exp(2j\gamma[P_{P1TE} + P_{P2TE}]z) \tag{3.29a}$$

$$\boldsymbol{A}_{sTM}(z) = \boldsymbol{B}_{sTM}(z)exp(2j\gamma[P_{P1TM} + P_{P2TM}]z) \tag{3.29b}$$

$$\boldsymbol{A}_{iTE}^*(z) = \boldsymbol{B}_{iTE}^*(z)\, exp(-2j\gamma[P_{P1TE} + P_{P2TE}]z) \tag{3.29c}$$

$$\boldsymbol{A}_{iTM}^*(z) = \boldsymbol{B}_{iTM}^*(z)exp(-2j\gamma[P_{P1TM} + P_{P2TM}]z) \tag{3.29d}$$

Substituting Eqns. (3.29a-d) into Eqns. (3.28a-d) yields

$$\frac{d\boldsymbol{B}_{sTE}(z)}{dz} = 2j\gamma\, \boldsymbol{B}_{iTE}^*(z)\, \boldsymbol{A}_{p1TE}(0)\boldsymbol{A}_{p2TE}(0)\, exp(-jk_{TE}z) \tag{3.30a}$$

$$\frac{d\boldsymbol{B}_{sTM}(z)}{dz} = 2j\gamma\, \boldsymbol{B}_{iTM}^*(z)\, \boldsymbol{A}_{p1TM}(0)\boldsymbol{A}_{p2TM}(0)\, \exp(-jk_{TM}z) \tag{3.30b}$$

$$\frac{d\boldsymbol{B}_{iTE}^*(z)}{dz} = -2j\gamma\boldsymbol{B}_{sTE}(z)\, \boldsymbol{A}_{p1TE}^*(0)\, \boldsymbol{A}_{p2TE}^*(0)\ \exp(jk_{TE}z) \tag{3.30c}$$

$$\frac{d\boldsymbol{B}_{iTM}^*(z)}{dz} = -2j\gamma\boldsymbol{B}_{sTM}(z)\, \boldsymbol{A}_{p1TM}^*(0)\, \boldsymbol{A}_{p2TM}^*(0)\ \exp(jk_{TM}z) \tag{3.30d}$$

where $k_{TE}\ and\ k_{TM}$ is the effective phase mismatch for the $k_{TE}\ and\ k_{TM}$ wave components and they are given by

$$k_{TE} = \Delta k_{TE} + \gamma(P_{P1TE} + P_{P2TE}) \tag{3.31a}$$

$$k_{TM} = \Delta k_{TM} + \gamma(P_{P1TM} + P_{P2TM}) \tag{3.31b}$$

The effective phase mismatch plays an important role in the process of FWM and hence in its applications such as parametric amplifier and phase conjugation. The linear phase mismatch $\Delta k_{TE(TM)}$ depends directly on the

interacting waves frequencies. The second part of Eqns. (3.31a) and (3.31b) represent the nonlinear phase mismatch terms, which depend on the pumps intensity. Better FWM performance is achieved when the effective phase mismatch vanishes or becomes near to zero.

3.5 FWM Parametric Gain

The effective phase mismatch and the parametric gain (g) are the two parameters that can evaluate the performance of the FWM process. The effective phase mismatch is given in the previous subsection. However, to derive the formula of the parametric gain and to study its effect in corporation with the effective phase mismatch on the FWM process, the previous analytical analysis is continued. Taking the second derivative of Eqns. (3.30a-d) with respect to z yields

$$\frac{d^2 \boldsymbol{B}_{sTE}(z)}{dz^2} = 2j\gamma \; \boldsymbol{A}_{p1TE}(0)\boldsymbol{A}_{p2TE}(0) \left[\boldsymbol{B}_{iTE}^*(z) \, (-jk_{TE})exp(-jk_{TE}z) \right.$$
$$\left. + \frac{d\boldsymbol{B}_{iTE}^*(z)}{dz} \; exp(-jk_{TE}z) \right] \qquad (3.32a)$$

$$\frac{d^2 \boldsymbol{B}_{sTM}(z)}{dz^2} = 2j\gamma \; \boldsymbol{A}_{p1TM}(0)\boldsymbol{A}_{p2TM}(0) \left[\boldsymbol{B}_{iTM}^*(z) \, (-jk_{TM})exp(-jk_{TM}z) \right.$$
$$\left. + \frac{dB_{iTM}^*(z)}{dz} \; exp(-jk_{TM}z) \right] \qquad (3.32b)$$

$$\frac{d^2 \boldsymbol{B}_{iTE}^*(z)}{dz^2} = -2j\gamma \; \boldsymbol{A}_{p1TE}^*(0) \, \boldsymbol{A}_{p2TE}^*(0) \left[\boldsymbol{B}_{sTE}(z) \, (jk_{TE}) \, exp(jk_{TE}z) \right.$$
$$\left. + \frac{d\boldsymbol{B}_{sTE}(z)}{dz} \; exp(jk_{TE}z) \right] \qquad (3.32c)$$

$$\frac{d^2 \boldsymbol{B}_{iTM}^*(z)}{dz^2} = -2j\gamma \; \boldsymbol{A}_{p1TM}^*(0) \, \boldsymbol{A}_{p2TM}^*(0) \left[\boldsymbol{B}_{sTM}(z) \, (jk_{TM}) \, exp(jk_{TM}z) \right.$$
$$\left. + \frac{d\boldsymbol{B}_{sTM}(z)}{dz} \; exp(jk_{TM}z) \right] \qquad (3.32d)$$

From Eqns. (3.30a-d), one can get the following expressions

$$\boldsymbol{B}^*_{iTE}(z) = \frac{1}{2j\gamma \ \boldsymbol{A}_{p1TE}(0)\boldsymbol{A}_{p2TE}(0) \ exp(-jk_{TE}z)} \frac{d\boldsymbol{B}_{sTE}(z)}{dz} \qquad (3.33a)$$

$$\boldsymbol{B}^*_{iTM}(z) = \frac{1}{2j\gamma \ \boldsymbol{A}_{p1TM}(0)\boldsymbol{A}_{p2TM}(0) \ exp(-jk_{TM}z)} \frac{d\boldsymbol{B}_{sTM}(z)}{dz} \qquad (3.33b)$$

$$\boldsymbol{B}_{sTE}(z) = \frac{-1}{2j\gamma \ \boldsymbol{A}^*_{p1TE}(0) \ \boldsymbol{A}^*_{p2TE}(0) \ exp(jk_{TE}z)} \frac{d\boldsymbol{B}^*_{iTE}(z)}{dz} \qquad (3.33c)$$

$$\boldsymbol{B}_{sTM}(z) = \frac{-1}{2j\gamma \ \boldsymbol{A}^*_{p1TM}(0) \ \boldsymbol{A}^*_{p2TM}(0) \ exp(jk_{TM}z)} \frac{d\boldsymbol{B}^*_{iTM}(z)}{dz} \qquad (3.33d)$$

Substituting Eqns. (3.33a) and (3.30c) into Eqn. (3.32a), Eqns. (3.33b) and (3.30d) into Eqn. (3.32b), Eqns. (3.33c) and (3.30a) into Eqn. (3.32c), and Eqns. (3.33d) and (3.30b) into Eqn. (3.32d) yields

$$\frac{d^2\boldsymbol{B}_{sTE}(z)}{dz^2} + jk_{TE}\frac{d\boldsymbol{B}_{sTE}(z)}{dz} - 4\gamma^2 P_{P1TE} \ P_{P2TE} \ \boldsymbol{B}_{sTE}(z) = 0 \qquad (3.34a)$$

$$\frac{d^2\boldsymbol{B}_{sTM}(z)}{dz^2} + jk_{TE}\frac{d\boldsymbol{B}_{sTM}(z)}{dz} - 4\gamma^2 P_{P1TM} \ P_{P2TM} \ \boldsymbol{B}_{sTM}(z) = 0 \qquad (3.34b)$$

$$\frac{d^2\boldsymbol{B}^*_{iTE}(z)}{dz^2} - jk_{TE}\frac{d\boldsymbol{B}^*_{iTE}(z)}{dz} - 4\gamma^2 P_{P1TE} \ P_{P2TE} \ \boldsymbol{B}^*_{iTE}(z) = 0 \qquad (3.34c)$$

$$\frac{d^2\boldsymbol{B}^*_{iTM}(z)}{dz^2} - jk_{TE}\frac{d\boldsymbol{B}^*_{iTM}(z)}{dz} - 4\gamma^2 P_{P1TM} \ P_{P2TM} \ \boldsymbol{B}^*_{iTM}(z) = 0 \qquad (3.34d)$$

The general solutions of Eqns. (3.34a-d) are given as

$$\boldsymbol{B}_{sTE}(z) = [C_1 \exp(g_{TE} \ z) + C_2 \exp(-g_{TE} \ z) \ ] \exp\left(-j\frac{k_{TE}}{2} \ z\right) \qquad (3.35a)$$

$$\boldsymbol{B}_{sTM}(z) = [C_3 \exp(g_{TM} \ z) + C_4 \exp(-g_{TM} \ z) \ ] \exp\left(-j\frac{k_{TM}}{2} \ z\right) \qquad (3.35b)$$

$$\boldsymbol{B}^*_{iTE}(z) = [C_5 \exp(g_{TE} \ z) + C_6 \exp(-g_{TE} \ z) \ ] \exp\left(j\frac{k_{TE}}{2} \ z\right) \qquad (3.35c)$$

$$\boldsymbol{B}^*_{iTM}(z) = [C_7 \exp(g_{TM} \ z) + C_8 \exp(-g_{TM} \ z) \ ] \exp\left(j\frac{k_{TM}}{2} \ z\right) \qquad (3.35d)$$

where $C_j. (j = 1 - 8)$ are constants determined from the boundary conditions and g_{TE} and g_{TM} is the parametric gain of the TE and TM wave components, respectively, and they are given by

$$g_{TE} = \sqrt{\left(2\gamma\sqrt{P_{P1TE}\ P_{P2TE}}\right)^2 - \left(\frac{k_{TE}}{2}\right)^2} \qquad (3.36a)$$

$$g_{TM} = \sqrt{\left(2\gamma\sqrt{P_{P1TM}\ P_{P2TM}}\right)^2 - \left(\frac{k_{TM}}{2}\right)^2} \qquad (3.36b)$$

It is logically that the maximum parametric gain is obtained when the phase mismatch decays to zero. This condition reduces Eqns. (3.36a) and (3.36b) to

$$(g_{TE})_{MAX} = 2\gamma\sqrt{P_{P1TE}\ P_{P2TE}} \qquad (3.37a)$$
$$(g_{TM})_{MAX} = 2\gamma\sqrt{P_{P1TM}\ P_{P2TM}} \qquad (3.37b)$$

One assumes that the two pumps have the same power and SOP, then $P_{P1TE} = P_{P2TE} = P_{TE}$ and $P_{P1TM} = P_{P2TM} = P_{TM}$.   Under   these   two assumptions, $(g_{TE})_{MAX}$ and $(g_{TM})_{MAX}$ can be given by

$$(g_{TE})_{MAX} = 2\gamma P_{TE} \qquad (3.38a)$$
$$(g_{TM})_{MAX} = 2\gamma P_{TM} \qquad (3.38b)$$

Figures (3.7a) and (3.7b) show the variation of the parametric gain coefficient with the linear phase mismatch for different values of γP_{TE} and γP_{TM}. Note that the peak of the parametric gain in both figures are shifted from $\Delta k = 0$, due to the effects of fiber nonlinearities.
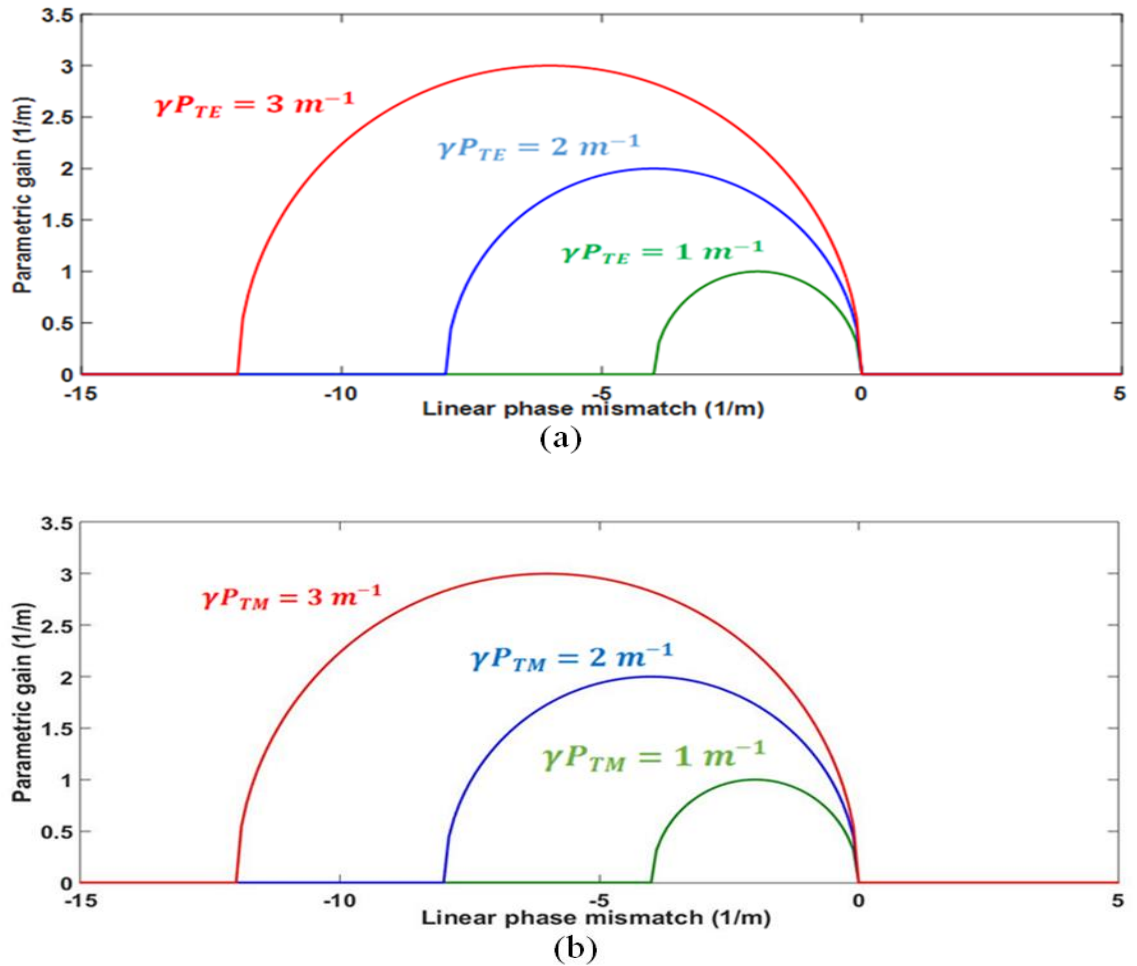
Figure (3.7): (a) Variation of the parametric gain of the TE component with different values of γP_{TE} product, and (b) Variation of the parametric gain of the TM component with different values of γP_{TM} product.

3.6 Conversion Efficiency

In this section, derivation of the conversion efficiency in dual-pump HNLF-OPC is addressed. The conversion efficiency is a parameter that evaluates the performance of the OPC device. This parameter with linearly polarized waves is well studied in literature. However, the effect of polarization is taken into account in this section to calculate the HNLF-OPC conversion efficiency. Applying $z = 0$ to Eqns. (3.35a-d) produces

$$B_{sTE}(0) = C_1 + C_2 \tag{3.39a}$$

$$B_{sTM}(0) = C_3 + C_4 \tag{3.39b}$$

$$C_5 + C_6 = 0 \tag{3.39c}$$

$$C_7 + C_8 = 0 \tag{3.39d}$$

Note that only the signal and the two pumps are launched to the HNLF at $z = 0$, and hence, $\boldsymbol{B}^*_{iTE}(0) = \boldsymbol{B}^*_{iTM}(0) = 0$. Taking the derivative of Eqns. (3.35a-d) with respect to z yields

$$\frac{d\boldsymbol{B}_{sTE}(z)}{dz} = [C_1 \exp(g_{TE}\,z) + C_2 \exp(-g_{TE}\,z)]\left(-j\frac{k_{TE}}{2}\right)\exp\left(-j\frac{k_{TE}}{2}\,z\right)$$
$$+ [g_{TE}C_1 \exp(g_{TE}\,z)$$
$$- g_{TE}\,C_2\exp(-g_{TE}\,z)]\,\exp\left(-j\frac{k_{TE}}{2}\,z\right) \tag{3.40a}$$

$$\frac{d\boldsymbol{B}_{sTM}(z)}{dz} = [C_3 \exp(g_{TM}\,z) + C_4 \exp(-g_{TM}\,z)]\left(-j\frac{k_{TM}}{2}\right)\exp\left(-j\frac{k_{TM}}{2}\,z\right)$$
$$+ [g_{TM}C_3 \exp(g_{TM}\,z)$$
$$- g_{TM}\,C_4\exp(-g_{TM}\,z)]\,\exp\left(-j\frac{k_{TM}}{2}\,z\right) \tag{3.40b}$$

$$\frac{d\boldsymbol{B}^*_{iTE}(z)}{dz} = [C_5 \exp(g_{TE}\,z) + C_6 \exp(-g_{TE}\,z)]\left(j\frac{k_{TE}}{2}\right)\exp\left(j\frac{k_{TE}}{2}\,z\right)$$
$$+ [g_{TE}C_5 \exp(g_{TE}\,z)$$
$$- g_{TE}C_6 \exp(-g_{TE}\,z)]\,\exp\left(j\frac{k_{TE}}{2}\,z\right) \tag{3.40c}$$

$$\frac{d\boldsymbol{B}^*_{iTM}(z)}{dz} = [C_7 \exp(g_{TM}\,z) + C_8 \exp(-g_{TM}\,z)]\left(j\frac{k_{TM}}{2}\right)\exp\left(j\frac{k_{TM}}{2}\,z\right)$$
$$+ [g_{TM}\,C_7 \exp(g_{TM}\,z)$$
$$- g_{TM}C_8 \exp(-g_{TM}\,z)]\,\exp\left(j\frac{k_{TM}}{2}\,z\right) \tag{3.40d}$$

Equating Eqns. (3.40a-d) with Eqns. (3.30a-d) and applying the primary conditions at $z = 0$, (i.e. $\boldsymbol{B}^*_{iTE}(0) = 0$. and $\boldsymbol{B}^*_{iTM}(0) = 0$) yields

$$(C_1 + C_2)\left(-j\frac{k_{TE}}{2}\right) + g_{TE}(C_1 - C_2) = 0 \tag{3.41a}$$

$$(C_1 + C_2)\left(-j\frac{k_{TM}}{2}\right) + g_{TM}(C_1 - C_2) = 0 \tag{3.41b}$$

$$-2j\gamma \boldsymbol{B}_{sTE}(0)\, \boldsymbol{A}_{p1TE}^*(0)\, \boldsymbol{A}_{p2TE}^*(0) = (C_5 + C_6)\left(j\frac{k_{TE}}{2}\right) + g_{TE}(C_5 - C_6) \quad (3.41c)$$

$$-2j\gamma \boldsymbol{B}_{sTM}(0)\boldsymbol{A}_{p1TM}^*(0)\, \boldsymbol{A}_{p2TM}^*(0) = (C_7 + C_8)\left(j\frac{k_{TM}}{2}\right) + g_{TM}(C_7 - C_8) \quad (3.41d)$$

Solving Eqns. (3.39a-d) and Eqns. (3.41a-d) produces

$$C_1 = \frac{1}{2}\left(1 + \frac{jk_{TE}}{2g_{TE}}\right) \boldsymbol{B}_{sTE}(0) \tag{3.42a}$$

$$C_2 = \frac{1}{2}\left(1 - \frac{jk_{TE}}{2g_{TE}}\right) \boldsymbol{B}_{sTE}(0) \tag{3.42b}$$

$$C_3 = \frac{1}{2}\left(1 + \frac{jk_{TM}}{2g_{TM}}\right) \boldsymbol{B}_{sTM}(0) \tag{3.42c}$$

$$C_4 = \frac{1}{2}\left(1 - \frac{jk_{TM}}{2g_{TM}}\right) \boldsymbol{B}_{sTM}(0) \tag{3.42d}$$

$$C_5 = \frac{-j\gamma \boldsymbol{B}_{sTE}(0)\, \boldsymbol{A}_{p1TE}^*(0)\, \boldsymbol{A}_{p2TE}^*(0)}{g_{TE}} \tag{3.42e}$$

$$C_6 = \frac{j\gamma \boldsymbol{B}_{sTE}(0)\, \boldsymbol{A}_{p1TE}^*(0)\, \boldsymbol{A}_{p2TE}^*(0)}{g_{TE}} \tag{3.42f}$$

$$C_7 = \frac{-j\gamma \boldsymbol{B}_{sTM}(0)\, \boldsymbol{A}_{p1TM}^*(0)\, \boldsymbol{A}_{p2TM}^*(0)}{g_{TM}} \tag{3.42g}$$

$$C_8 = \frac{j\gamma \boldsymbol{B}_{sTM}(0)\, \boldsymbol{A}_{p1TM}^*(0)\, \boldsymbol{A}_{p2TM}^*(0)}{g_{TM}} \tag{3.42h}$$

Substituting $C_1\ and\ C_2$ into Eqn. (3.35a), $C_3\ and\ C_4$ into Eqn. (3.35b), $C_5\ and\ C_6$ into Eqn. (3.35c), and $C_7\ and\ C_8$ into Eqn. (3.35d), yields after simplification

$$\boldsymbol{B}_{sTE}(z) = \left[\boldsymbol{B}_{sTE}(0)\left(\cosh(g_{TE}z) + \frac{jk_{TE}}{2g_{TE}}\sinh(g_{TE}z)\right)\right]$$

$$* \exp\left(-j\frac{k_{TE}}{2}z\right) \tag{3.43a}$$

$$B_{sTM}(z) = \left[B_{sTM}(0)\left(\cosh(g_{TM}z) + \frac{jk_{TM}}{2g_{TM}}\sinh(g_{TM}z)\right)\right]$$

$$* \exp\left(-j\frac{k_{TM}}{2}z\right) \qquad (3.43b)$$

$$B_{iTE}^{*}(z) = \left[\frac{-2j\gamma B_{sTE}(0)\,A_{p1TE}^{*}(0)\,A_{p2TE}^{*}(0)}{g_{TE}}\sinh(g_{TE}z)\right]$$

$$* \exp\left(j\frac{k_{TE}}{2}z\right) \qquad (3.43c)$$

$$B_{iTM}^{*}(z) = \left[\frac{-2j\gamma B_{sTM}(0)\,A_{p1TM}^{*}(0)\,A_{p2TM}^{*}(0)}{g_{TM}}\sinh(g_{TM}z)\right]$$

$$* \exp\left(j\frac{k_{TM}}{2}z\right) \qquad (3.43d)$$

where the following hyperbolic function properties are used

$$\cosh(x) = \frac{exp\left(g_{TE(TM)}z\right) + exp\left(-g_{TE(TM)}z\right)}{2}$$

$$\sinh(x) = \frac{exp\left(g_{TE(TM)}z\right) - exp\left(-g_{TE(TM)}z\right)}{2}$$

Return back to Eqns. (3.26a-d) to find expressions describing $A_{sTE}(z)$. $A_{sTM}(z)$. $A_{iTE}^{*}(z)$. and $A_{iTM}^{*}(z)$

$$A_{sTE}(z) = B_{sTE}(z)\,exp(2j\gamma[P_{P1TE} + P_{P2TE}]z) \qquad (3.44a)$$

$$A_{sTM}(z) = B_{sTM}(z)\,exp(2j\gamma[P_{P1TM} + P_{P2TM}]z) \qquad (3.44b)$$

$$A_{iTE}^{*}(z) = B_{iTE}^{*}(z)\,exp(-2j\gamma[P_{P1TE} + P_{P2TE}]z) \qquad (3.44a)$$

$$A_{iTM}^{*}(z) = B_{iTM}^{*}(z)\,exp(-2j\gamma[P_{P1TM} + P_{P2TM}]z) \qquad (3.44a)$$

Substituting Eqns. (3.43a-d) into Eqns. (3.44a-d) yields

$$A_{sTE}(z) = \left[A_{sTE}(0)\left(\cosh(g_{TE}z) + \frac{jk_{TE}}{2g_{TE}}\sinh(g_{TE}z)\right)\right]$$

$$* \exp\left[-j\left(\frac{k_{TE}}{2} - 2\gamma(P_{P1TE} + P_{P2TE})\right)z\right] \qquad (3.45a)$$

$$A_{sTM}(z) = \left[A_{sTM}(0) \left(\cosh(g_{TM}z) + \frac{jk_{TM}}{2g_{TM}} \sinh(g_{TM}z) \right) \right]$$

$$* \exp \left[-j \left(\frac{k_{TM}}{2} - 2\gamma(P_{P1TM} + P_{P2TM}) \right) z \right] \qquad (3.45b)$$

$$A_{iTE}^*(z) = \left[\frac{-2j\gamma \boldsymbol{B}_{sTE}(0) \, \boldsymbol{A}_{p1TE}^*(0) \, \boldsymbol{A}_{p2TE}^*(0)}{g_{TE}} \sinh(g_{TE}z) \right]$$

$$\times \exp \left[j \left(\frac{k_{TE}}{2} - 2\gamma(P_{P1TE} + P_{P2TE}) \right) z \right] \qquad (3.45c)$$

$$A_{iTM}^*(z) = \left[\frac{-2j\gamma \boldsymbol{B}_{sTM}(0) \, \boldsymbol{A}_{p1TM}^*(0) \, \boldsymbol{A}_{p2TM}^*(0)}{g_{TM}} \sinh(g_{TM}z) \right]$$

$$\times \exp \left[j \left(\frac{k_{TM}}{2} - 2\gamma(P_{P1TM} + P_{P2TM}) \right) z \right] \qquad (3.45d)$$

3.6.1 Signal and Idler Wave Equations

At the HNLF output, there are two waves expected to be seen, the amplified signal wave and the conjugated idler wave. From Eqns. (3.45a) and (3.45b), the power of the signal of the TE and TM component at the HNLF output can be expressed as

$$P_{sTE}(z) = \left[P_{sTE}(0) \left(\cosh^2(g_{TE}z) + \frac{k_{TE}^2}{4g_{TE}^2} \sinh^2(g_{TE}z) \right) \right] \qquad (3.46a)$$

$$P_{sTM}(z) = \left[P_{sTM}(0) \left(\cosh^2(g_{TM}z) + \frac{k_{TM}^2}{4g_{TM}^2} \sinh^2(g_{TM}z) \right) \right] \qquad (3.46b)$$

Using the hyperbolic functions property $\cosh^2 \left(g_{TE(TM)}z \right) = 1 + \sinh^2 \left(g_{TE(TM)}z \right)$. Eqns. (3.46a) and (3.46b) can be written at the end of the fiber (z = L) as

$$P_{sTE}(L) = \left[P_{sTE}(0) \left(\cosh^2(g_{TE}L) + \frac{k_{TE}^2}{4g_{TE}^2} \sinh^2(g_{TE}L) \right) \right] \qquad (3.47a)$$

$$P_{sTM}(L) = \left[P_{sTM}(0)\left(\cosh^2(g_{TM}L) + \frac{k_{TM}^2}{4g_{TM}^2}\sinh^2(g_{TM}L)\right)\right] \tag{3.47b}$$

The signal and the idler waves are equally amplified during the FWM process in the HNLF, but the difference between them is only the signal launched power, and hence, the idler power for TE and TM components can be calculated at any point of z as

$$P_{iTE}(z) = P_{sTE}(z) - P_{sTE}(0)$$

$$P_{iTE}(z) = P_{sTE}(z) - P_{sTE}(0)$$

Therefore, from Eqns. (3.47a) and (3.47b), the optical power of the orthogonal components of the idler wave can be calculated at the end of the fiber (z = L) and the result is

$$P_{iTE}(L) = \left[P_{sTE}(0)\left(\left(1 + \frac{k_{TE}^2}{4g_{TE}^2}\right)\sinh^2(g_{TE}L)\right)\right] \tag{3.48a}$$

$$P_{iTM}(L) = \left[P_{sTM}(0)\left(\left(1 + \frac{k_{TM}^2}{4g_{TM}^2}\right)\sinh^2(g_{TM}L)\right)\right] \tag{3.48b}$$

3.6.2 Expression of the Conversion Efficiency

From Eqns. (3.48a) and (3.48b), it can be concluded that the idler wave components $P_{iTE}(L)$ and $P_{iTM}(L)$ are generated when the signal power is launched into the fiber. The idler components powers increase with the square of the fiber length L^2 when $g_{TE(M)}L \ll 1$. When the distance is increased to satisfy $g_{TE(M)}L > 1$, both signal and idler waves would be growing exponentially. At the HNLF output, the signal and the idler waves may be at same level because they are all amplified together along the fiber.

The total signal and idler powers for TE and TM components at the HNLF output can be expressed as

$$P_s(L) = |A_{sTE}(L)|^2 + |A_{sTM}(L)|^2 = P_{sTE}(L) + P_{sTM}(L) \tag{3.49a}$$

$$P_i(L) = |A_{iTE}(L)|^2 + |A_{iTM}(L)|^2 = P_{iTE}(L) + P_{iTM}(L) \tag{3.49b}$$

Substituting Eqns. (3.47a-b), (3.48a-b), and (3.13e-f) into Eqns. (3.49a-b) yields

$$P_i(L) = \left[C_{TE} \, P_{s0} \, cos^2(\theta_s) \left(\left(1 + \frac{k_{TE}^2}{4g_{TE}^2} \right) \sinh^2(g_{TE}L) \right) \right]$$
$$+ \left[C_{TM} \, P_{s0} \, sin^2(\theta_s) \left(\left(1 + \frac{k_{TM}^2}{4g_{TM}^2} \right) \sinh^2(g_{TM}L) \right) \right] \tag{3.50a}$$

$$P_s(L) = \left[C_{TE} \, P_{s0} \, cos^2(\theta_s) \left(1 + \left(1 + \frac{k_{TE}^2}{4g_{TE}^2} \right) \sinh^2(g_{TE}L) \right) \right]$$
$$+ \left[C_{TM} \, P_{s0} \, sin^2(\theta_s) \left(1 + \left(1 + \frac{k_{TM}^2}{4g_{TM}^2} \right) \sinh^2(g_{TM}L) \right) \right] \tag{3.50b}$$

The total launched signal power is given by

$$P_s(0) = [C_{TE} \, P_{s0} \, cos^2(\theta_s)] + [C_{TM} \, P_{s0} \, sin^2(\theta_s)] \tag{3.51}$$

The conversion efficiency at the HNLF output is the then given by

$$\eta_c \equiv \frac{P_i(L)}{P_s(0)} = \left[C_{TE} \, cos^2(\theta_s) \left(\left(1 + \frac{k_{TE}^2}{4g_{TE}^2} \right) \sinh^2(g_{TE}L) \right) \right.$$
$$+ C_{TM} \, sin^2(\theta_s) \left(\left(1 + \frac{k_{TM}^2}{4g_{TM}^2} \right) \sinh^2(g_{TM}L) \right) \right]$$
$$/[C_{TE} \, cos^2(\theta_s) + C_{TM} \, sin^2(\theta_s)] \tag{3.52}$$

3.7 Calculated Results Related to HNLF-OPC Conversion Efficiency

The obtained conversion efficiency expression defined in Eqn. (3.52) is well evaluating the performance of the HNLF-OPC devices when the effect of SOPs of the pumps and signal waves is included in the study. The following figures show the conversion efficiency in the wavelength region around the zero-dispersion wavelength for different system parameters.

Firstly, the signal and both pumps are assumed linearly co-polarized, in this case, the HNLF-OPC provides maximum conversion efficiency. Figures (3.8a) and (3.8b) show the conversion efficiency spectra for the

HNLF-OPC1 and HNLF-OPC2, respectively, when the signal and both pumps are linearly copolarized along TE axis. In Fig. (3.8a), HNLF-OPC1 shows a flat maximum conversion of about 37.4 dB for a wide wavelength region extending from 1510 to 1590 nm. In Fig. (3.8b), the HNLF-OPC2 offers a flat conversion efficiency of about 39 dB extending from 1550 to 1610 nm.
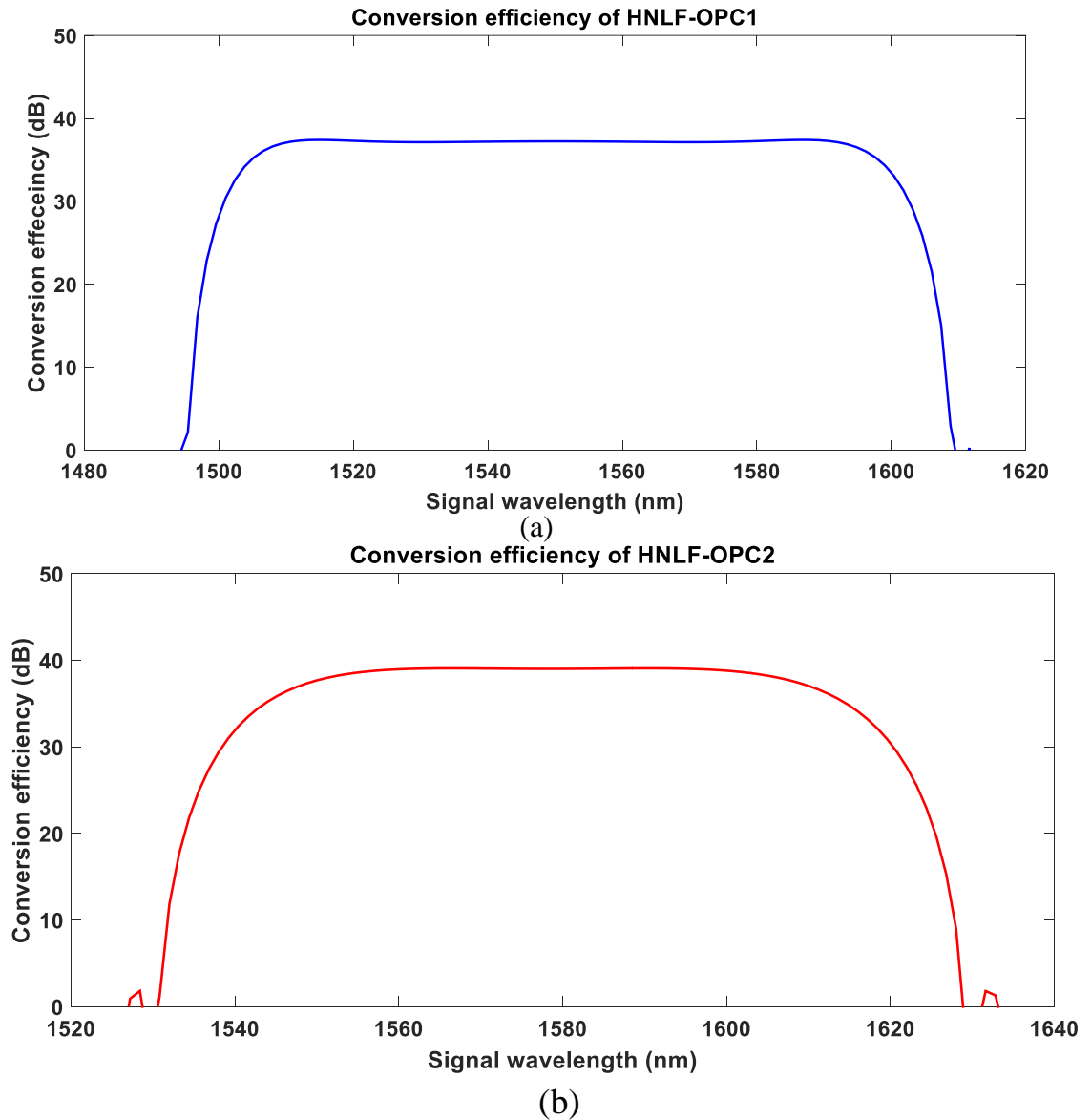

(a)

(b)

Figure (3.8): Conversion efficiency as a function of signal wavelength when the signal and both pumps are linearly copolarized along TE axis for (a) HNLF-OPC1, and (b) HNLF-OPC2.

The conversion efficiencies in Figs. (3.8a) and (3.8b) are obtained based on the assumption that the signal and the two pumps are linearly

copolarized initially and maintain their SOPs during propagation inside the HNLF. However, the FWM process is highly polarization-dependent because it requires conservation of angular momenta among the four interacting waves.

In practice, the SOPs of the input pumps can be chosen, but the SOP of the input signal is often arbitrary. Furthermore, in PDM signals, two orthogonally polarized signals are sent simultaneously in same fiber. However, to investigate this issue, Figs (3.9a) and (3.9b) illustrate the variation of the maximum conversion efficiencies for HNLF-OPC1 and HNLF-OPC2, respectively, as a function of the signal polarization angle. In these figures, the two pumps are linearly copolarized along the TE axis.
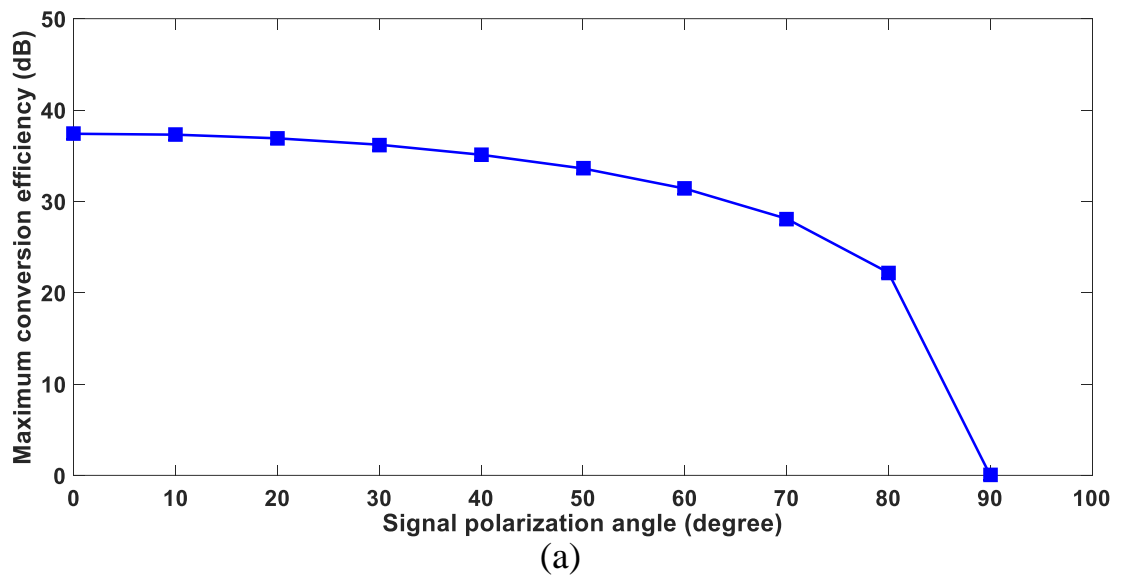

(a)

Figure (3.9): Variation of the maximum conversion efficiency as a function of signal polarization angle when the two pumps are linearly copolarized along the TE axis for (a) HNLF-OPC1, and (b) HNLF-OPC2.
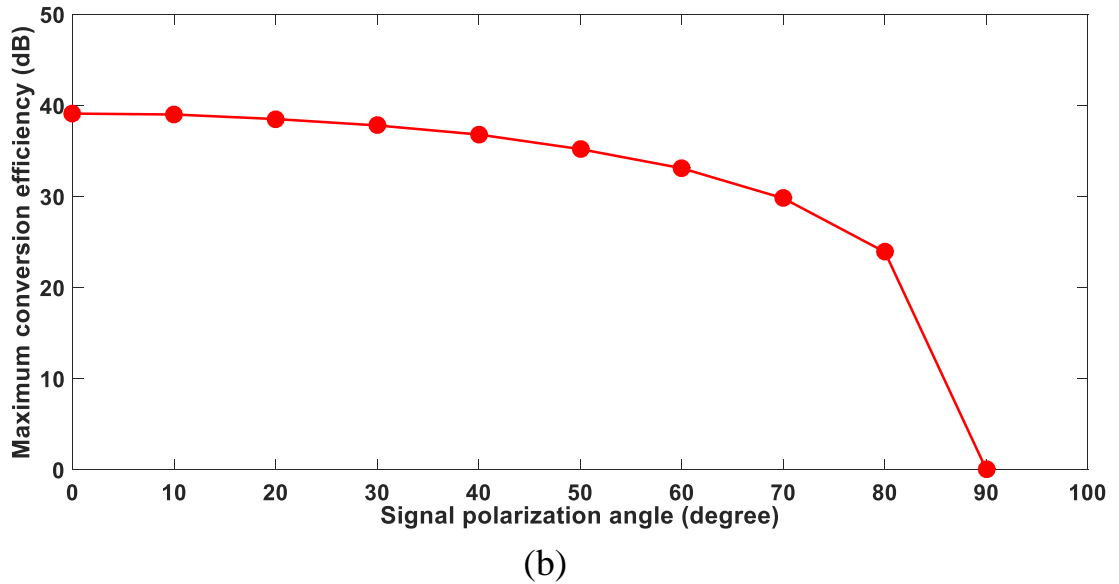
(b)

Figure (3.9): continued.

Figures (3.10a) and (3.10b) show the variation of the maximum conversion efficiencies for HNLF-OPC1 and HNLF-OPC2 as a function to the signal polarization angle, respectively when the two pumps are linearly copolarized along the TM axis.
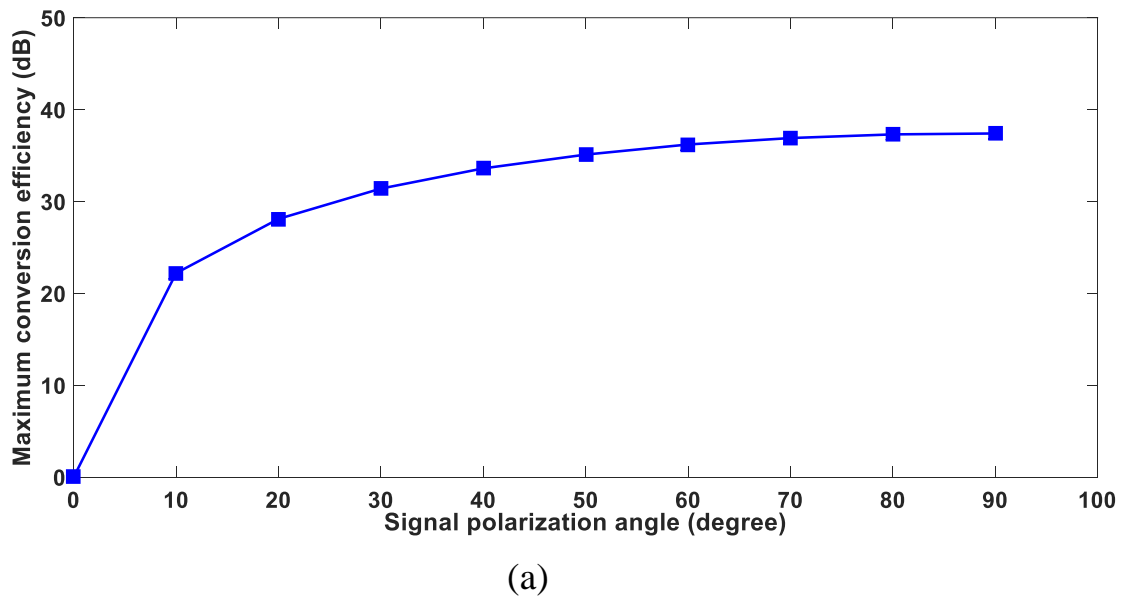

(a)

Figure (3.10): Variation of the maximum conversion efficiency as a function of signal polarization angle when the two pumps are linearly copolarized along TM axis for (a) HNLF-OPC1, and (b) HNLF-OPC2.
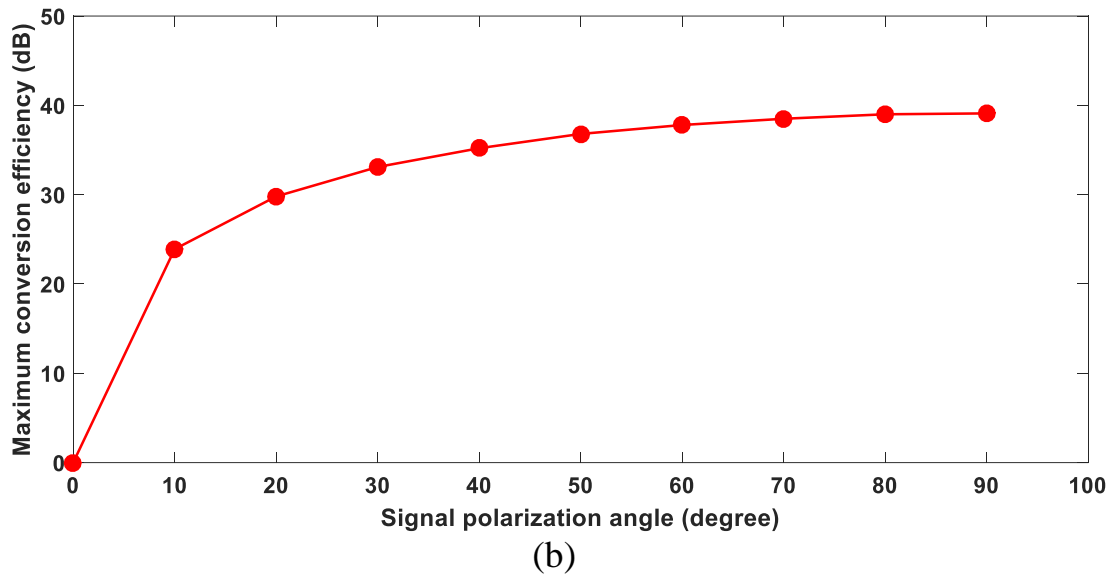
(b)

Figure (3.10): continued.

Figures (3.9) and (3.10) show that the conversion efficiency is strongly polarization dependent because of an intrinsic angular-momentum conservation requirement. This polarization sensitivity is an obstacle to the practical implementation of OPC devices in fiber-optic communication systems. To solve this problem, polarization-independent HNLF-OPC device is investigated here using linearly orthogonal polarized pumps. Unfortunately, the conversion efficiency is reduced dramatically when linearly orthogonal polarized pumps are used due to the nonlinear coupling efficiency. However, the reduction in the conversion efficiency can be compensated using higher pump powers.

Figures (3.11a) and (3.11b) show the conversion efficiencies spectra as a function signal wavelength for HNLF-OPC1 and HNLF-OPC2, respectively, when pumps are orthogonally polarized. In Fig. (3.11a), the maximum conversion efficiency of the HNLF-OPC1 is reduced by 58.3% compared to the case when the signal and the two pumps are linearly copolarized. In Fig. (3.11b), the maximum conversion efficiency of the HNLF-OPC2 is also reduced by 56.3% compared with the case when the signal and the two pumps are linearly copolarized.
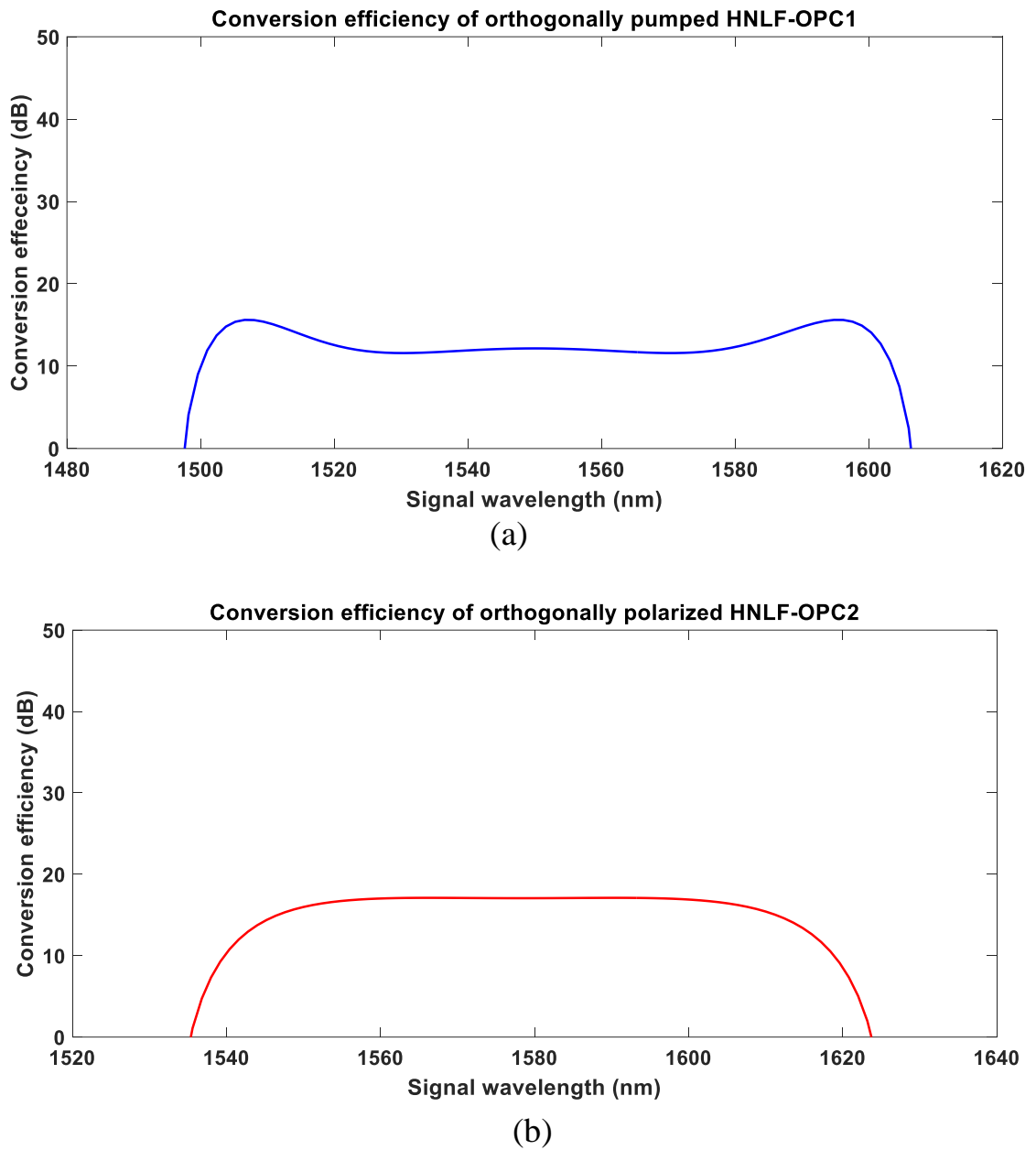
Conversion efficiency of orthogonally pumped HNLF-OPC1

(a)

Conversion efficiency of orthogonally polarized HNLF-OPC2

(b)

Figure (3.11): Conversion efficiencies as a function of signal wavelength with orthogonally polarized pumps for (a) HNLF-OPC1, and (b) HNLF-OPC2.

To compensate the reduction of the conversion efficiencies associated with orthogonally polarized pumps, the pump powers should be increased. In Fig. (3.12a), HNLF-OPC1 gives maximum conversion efficiencies of 15.6, 26.5, and 37.4 dB when both pump powers are 0.5, 0.75, and 1 W, respectively. Figure (3.12b) shows that the maximum conversion efficincy increases from 17.7 dB to 32.8 dB in HNLF-OPC2 when each of the pump powers is increased 0.2 W. Morever, a maximum conversion efficiency of

47.8 dB is obtained when each power of the orthogonally polarized pump powers increase by 0.4 W.
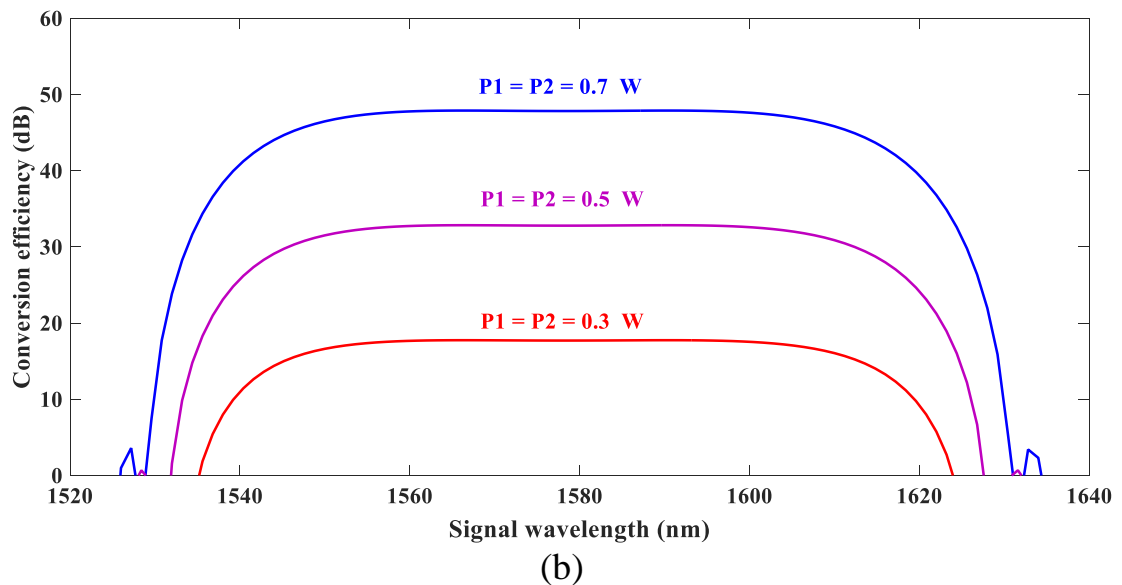
Figure (3.12): Variation of conversion efficiencies as a function of signal wavelength with different associated values of orthogonally polarized pump powers for (a) HNLF-OPC1, and (b) HNLF-OPC2.

Figures (3.13a) and (3.13b) show the conversion efficiencies as a function of signal polarization angle for HNLF-OPC1 and HNLF-OPC2, respectively. The results are obtained for different values of orthogonally polarized pump powers.
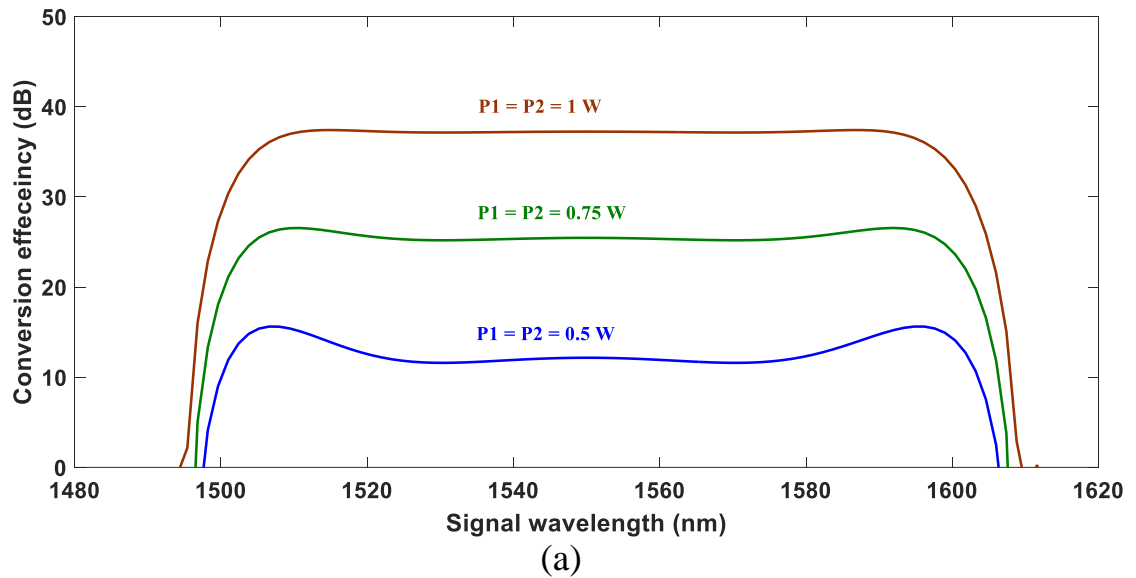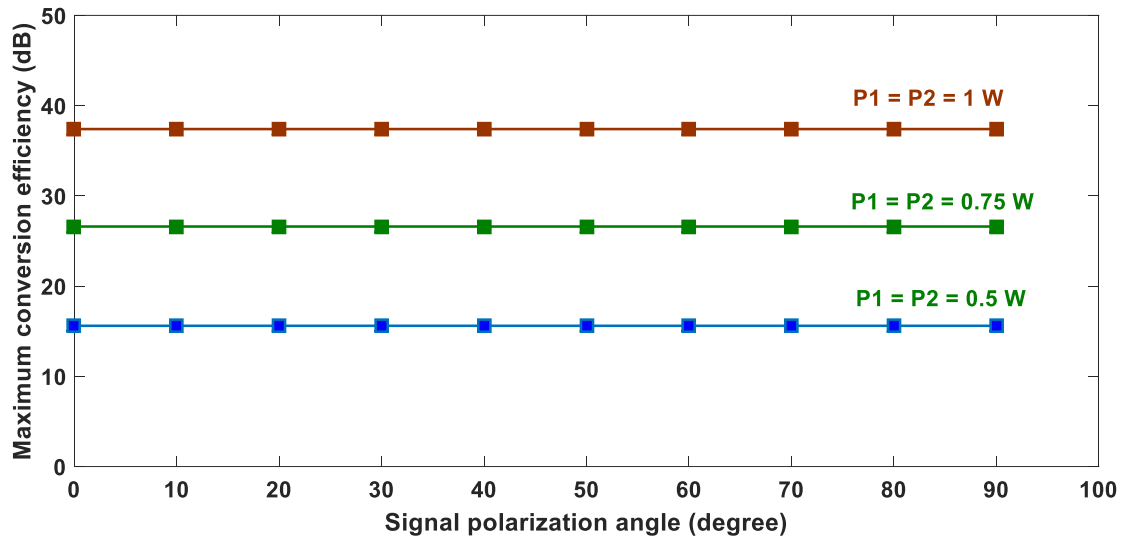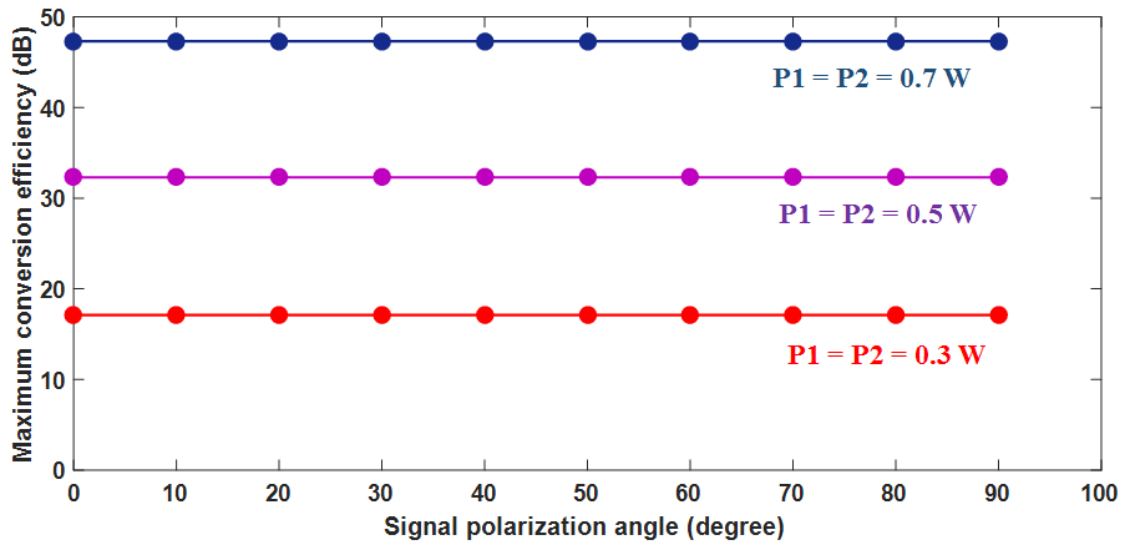
(a)

(b)

Figure (3.13): Conversion efficiency as a function of signal polarization angle for (a) HNLF-OPC1 and (b) HNLF-OPC2, with orthogonal polarization pumps.

Note that the conversion efficiency are almost independent of signal polarization angle. It is clear that the HNLF-OPC device becomes polarization independent for any two orthogonally polarized pumps.

It is worth to discuss the dependence of conversion efficiency of a dual-pump HNLF-OPC driven by two orthogonal pumps (i.e., $\theta_{P1}-\theta_{P2}=90°$) on signal polarization. The pumps components along the signal polarization

vector are given by $P_{P1}\cos^2(\theta_{P1}-\theta_S)$ and $P_{P2}\cos^2(\theta_{P2}-\theta_S) = P_{P2}\sin^2(\theta_{P1}-\theta_S)$. Thus, one can treat the OPC as driven by an equivalent single pump of power $(P_P)_{eq} = P_{P1}\cos^2(\theta_{P1}-\theta_S) + P_{P2}\sin^2(\theta_{P1}-\theta_S)$ whose polarization is aligned with the signal polarization. For equal pump powers $P_{P1} = P_{P2}$, the equivalent pump power $(P_P)_{eq} = P_{P1} = P_{P2}$. This condition makes the OPC to behave as a polarization-independent device. This conclusion is illustrated in Figs. (3.13a) and (3.13b) where the conversion efficiency of HNLF-OPC is depicted as a function of signal polarization angle.

Chapter Four

Simulation Results, Discussion, Conclusions, and Suggestions for future works

Chapter Four

Simulation Results, Discussion, Conclusions, and Suggestions for future works

4.1 Introduction

In the previous chapters, the effects of OPC-based mitigation of dispersion and Kerr effect nonlinearities have been discussed. This chapter presents the simulation results of the fiber-optic communication system employing OPC with different high order-modulation formats. First, the system parameters and simulation setup are given. Section 4.2 introduces the usage of MS-OPC and multiple-OPC compensation schemes. Sections 4.3 presents the simulation results of fiber-optic communication systems with NRZ-OOK, and 16-QAM modulation formats. The main conclusions drawn from this study and some suggestion for future work are given in sections 4.4 and 4.5, respectively. The results are obtained using Optisystem v.14.1 software and compared with experimental data reported in the literature.

4.2 Mitigation of Fiber Dispersion and Nonlinearity using HNLF-based OPC

Fiber dispersion and nonlinearity caused by Kerr effect are considered to be the major obstacles in the development of long-haul and large-capacity fiber-optic communication systems. OPC is the most promising way to address this problem. This section explores the effect of OPC on the performance of the fiber-optic communication systems employing different

modulation formats. The results of multiple-OPC compensation scheme are compared with those of MS-OPC counterpart.

4.2.1 Mid-Span OPC Compensation Scheme

MS-OPC is a technique which can compensate distortion due to fiber dispersion and nonlinearities. MS-OPC, which is sometimes called mid-span spectral inversion, can be used for simultaneous multi-channel dispersion and nonlinearity compensation. In MS-OPC compensation scheme, the optical link is divided into two equal parts and the OPC device is placed at the midpoint of the optical link (see Figs. (4.1a) and (4.1b)). Therefore, the accumulated phase shift due to dispersion and nonlinearities in the first half of the fiber is inverted by the OPC, and subsequently compensated through the second half of the fiber path. Nonlinearity compensation based on MS-OPC is implemented by FWM process in HNLF.

The MS-OPC is investigated in two different fiber-optic communication systems employing different modulation formats, NRZ-On-Off Keying, and 16-QAM, for both, single-channel and multi-channel transmission systems. Figure (4.1a) illustrates a single-channel transmission system with a MS-OPC compensation scheme. The signal is generated by an optical transmitter and amplified by an EDFA before launching to the first part of the optical link. The optical link consists of n spans of SSMF forming the first half, the OPC device, another n spans of SSMF forming the second half of the link, and coherent optical receiver. Each span of the SSMF is backward pumped with a Raman pump to achieve a symmetric power profile along the fiber spans.

An 8-channel WDM transmission system with MS-OPC is depicted in Fig. (4.1b). The WDM channels are combined using an optical WDM

multiplexer and, after amplification with an EDFA, the multiplexed signal is launched into the optical first part of the optical link. At the receiver end, the WDM channels are demultiplexed using an optical demultiplexer.

4.2.2 Multiple-OPC Compensation Scheme

In a MS-OPC system, the OPC device must be fixed exactly at the middle of the link to accomplish complete dispersion and nonlinearity compensation. However, the mid-link point may change over time. Furthermore, the similarity of the two parts of the optical link is sometimes difficult to achieve.

In contrast, multiple-OPC scheme allows phase conjugation of the transmitted signal after every certain distance of transmission and conjugating the phase again after another transmission with the same length. Therefore, the fiber nonlinearity can be compensated along the optical link, instead of just at the end of the transmission, which helps to maintain the signal from degradation along the optical link. Another advantage of using the multiple-OPC scheme is that the signal wavelength can be maintained unchanged if an even number of OPCs is used which leads to a reduction in the complexity of the receiver device.

Figure (4.1c) depicts a single-channel transmission system with multiple-OPC compensation scheme. The multiple-OPC configuration uses the same transmitter and receiver that are used in the MS-OPC compensation scheme. However, the optical link now consists of more than two parts separated by a suitable number of OPC devices.

The first and the last part of the optical link consist of n×L km SSMF, while the middle part consists of 2n×L km SSMF. Each SSMF span is backward pumped with a Raman pump to achieve a symmetric power profile

along the fiber spans. The accumulated phase shift due to dispersion and nonlinearities in the first part of the fiber is inverted by the first OPC device. This phase shift is compensated at the midpoint of the second part of the fiber path. Therefore, full fiber dispersion and nonlinearity compensation can be achieved at the end of the optical link.

An fiber-optic communication system with 8-channel WDM transmission system using multiple-OPC compensation scheme is explained in Fig. (4.1d). The WDM channels are combined using an optical WDM multiplexer and, after amplification with an EDFA, the WDM signal is launched into the first part of the optical link. At the receiver end, the WDM channels are demultiplexed using an optical demultiplexer.

As both MS-OPC and multiple-OPC are promising compensation techniques, a direct comparison between the two schemes for higher order modulation format is of high interest.

In next subsections, an investigation of Kerr nonlinearity mitigation using multiple-OPC compensation scheme is performed with a comparison of the results with MS-OPC compensation scheme for up to 912 km transmission in a dispersion-unmanaged DRA link.
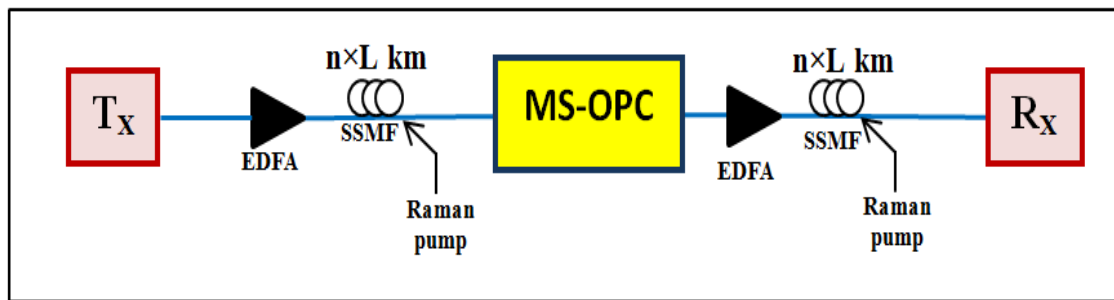
(a)
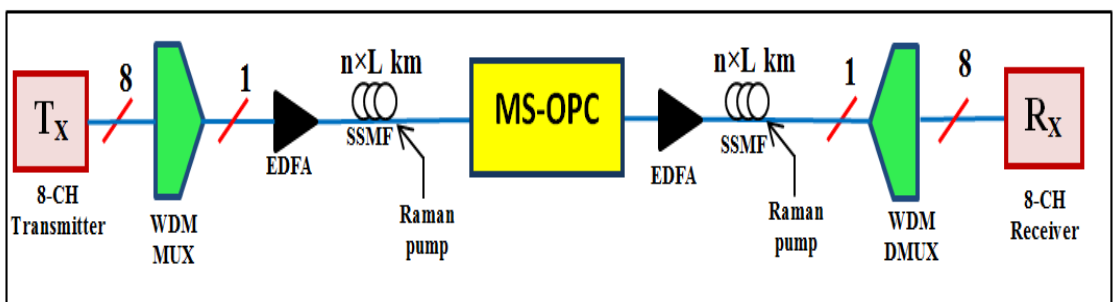
(b)
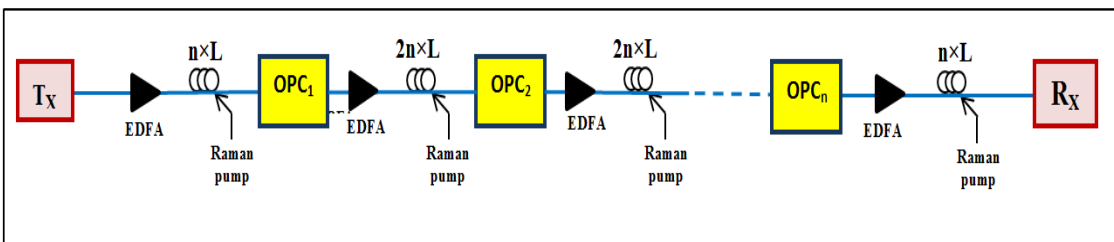
(c)

(d)

Figure (4.1): (a) Single channel transmission system with MS-OPC configuration, (b) 8-channel WDM transmission system with MS-OPC configuration, (c) Single channel transmission system with multiple-OPC configuration, and (d) 8-channel WDM transmission system with multiple-OPC configuration.

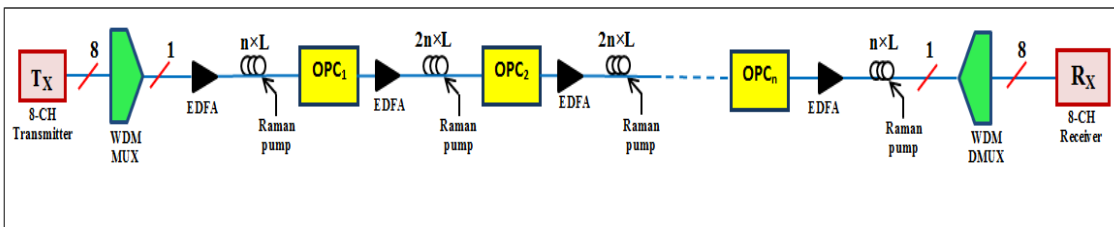## 4.3 Dispersion and Nonlinearity Compensation using HNLF-OPC

The performance of dispersion and nonlinearity compensation are investigated using the multiple-OPC with a single-channel and multi-channel systems over a transmission link of 912 km length. The results are compared with that based on using MS-OPC and also with experimental data reported in the literature. Simulation results are presented for NRZ-OOK and 16-QAM fiber-optic communication systems. Some of the parameters values used in the simulation are selected to match those used in the published experimental work [26].

4.3.1 NRZ-OOK Signaling

Initially, the multiple-OPC compensation scheme is investigated in 40 Gb/s NRZ-OOK single-channel operating at 190.2 THz (center channel in the WDM system). The transmission length is 912 km and consists of three spans before OPC_1 and after OPC_2, and 6 spans in the middle part of the link. The results are compared with that of the MS-OPC compensation scheme. Figure (4.2) illustrates the construction of the NRZ-OOK transmitter. The Bit-Sequence Generator (BSG) generates the binary data to be transmitted while the NRZ pulse generator forms each bit as a NRZ pulse. Then the sequence of pulses is modulated with optical CW carrier using Mach-Zehnder Modulator (MZM). Both polarization signal components are combined together using polarization combiner (PC). Then the signal is amplified and filtered before it is launched to the fiber span. In WDM system, eight channels with a frequency starting from 190 to 190.35 THz with 50 GHz frequency spacing are multiplexed together using WDM multiplexer.
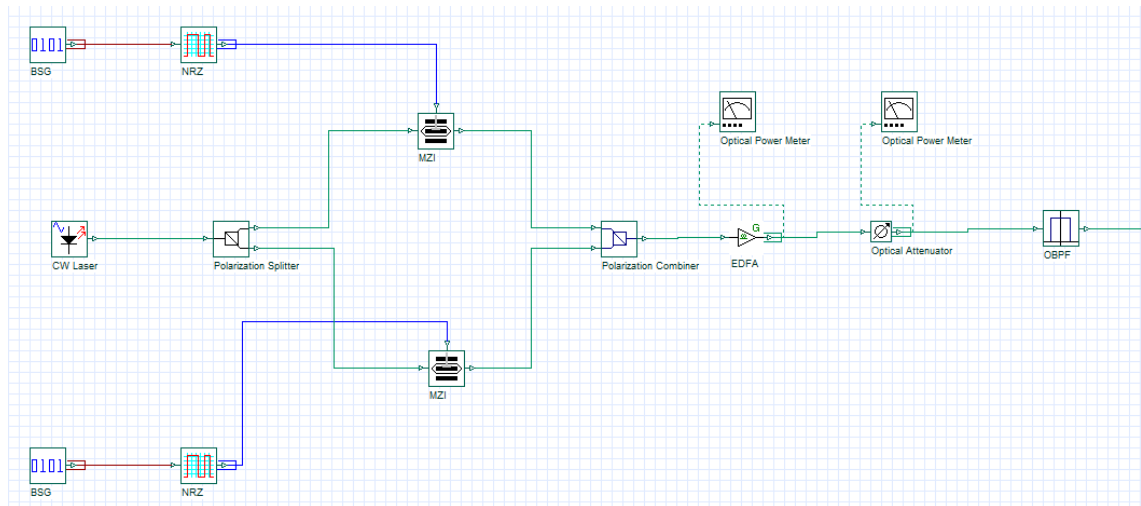
Figure (4.2): Transmitter for a single channel including Binary sequence generator (BSG), non-return-to-zero pulse generator (NRZ), Mach–Zehnder modulator (MZM), polarization splitter, polarization combiner, erbium-doped fiber amplifier (EDFA), and optical attenuator.

Figure (4.3) illustrates the receiver structure of the NRZ-OOK signaling. It consists of polarization splitter to separate X and Y polarization components. Each polarization part has a PIN Photodetector to convert the received signal from optical to electrical domain. Finally, the converted electrical signal is filtered using low pass filter.
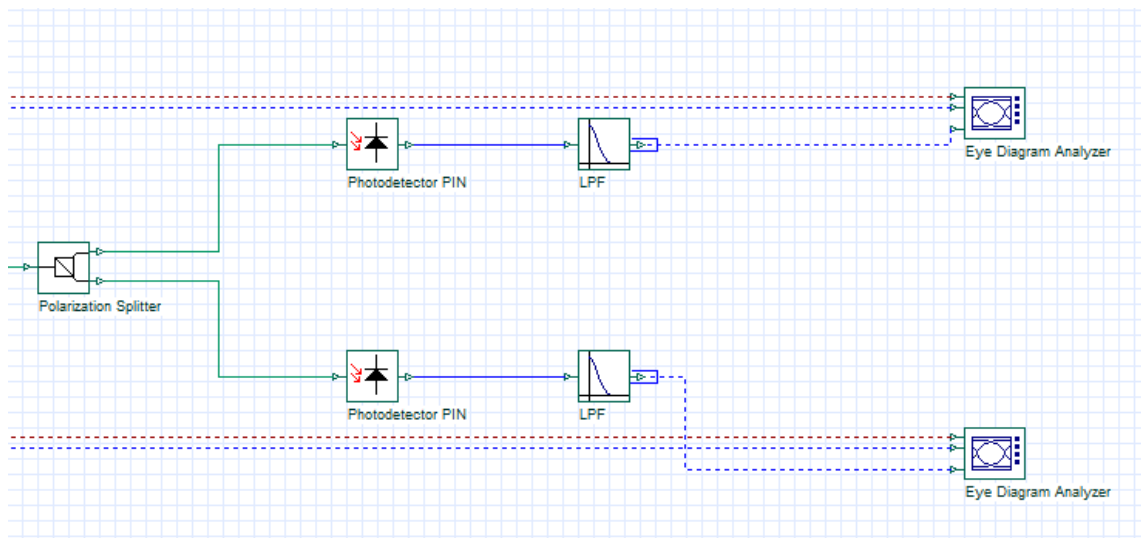
Figure (4.3): Receiver for a single channel including polarization splitter (PS), photodetector PIN, optical low-pass filter (LPF), and eye diagram analyzer.

Figures (4.4a) and (4.4b) show the spectrum of the transmitted optical signal at frequency of 190.2 THz (λ= 1576.2 nm) before and after the OBPF, respectively.
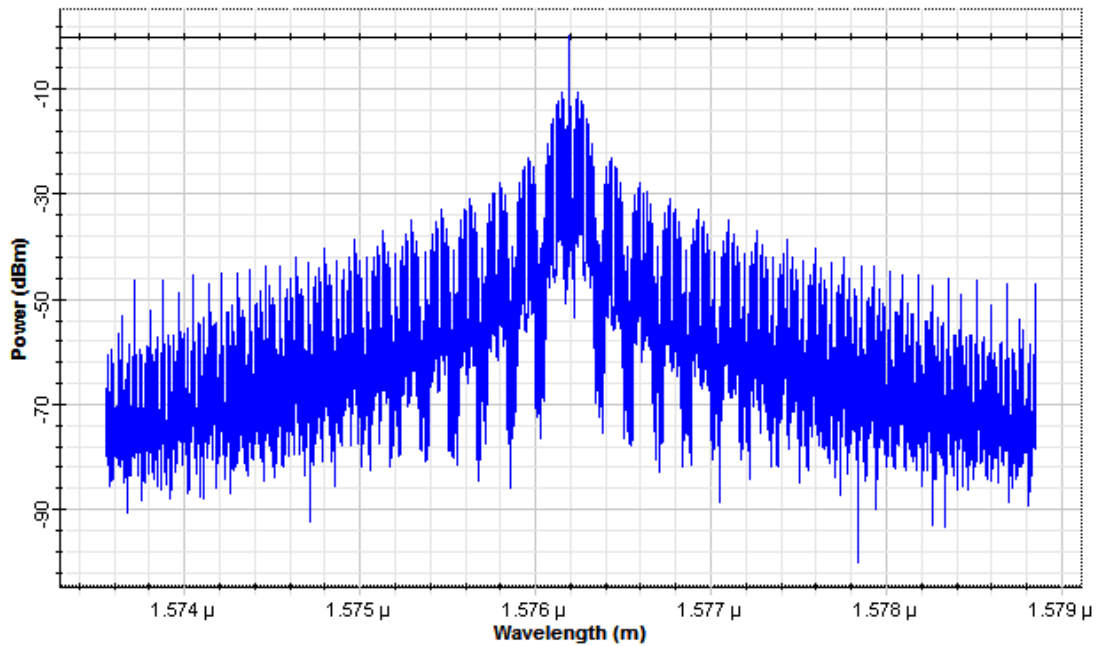
Figure (4.4): Spectrum of the transmitted optical signal.

Figure (4.5) shows the spectrum of the pump1 and pump2 at frequency of 191.3 THz (λ= 1567.06 nm) and 188.58 THz (λ= 1589.74 nm), respectively.
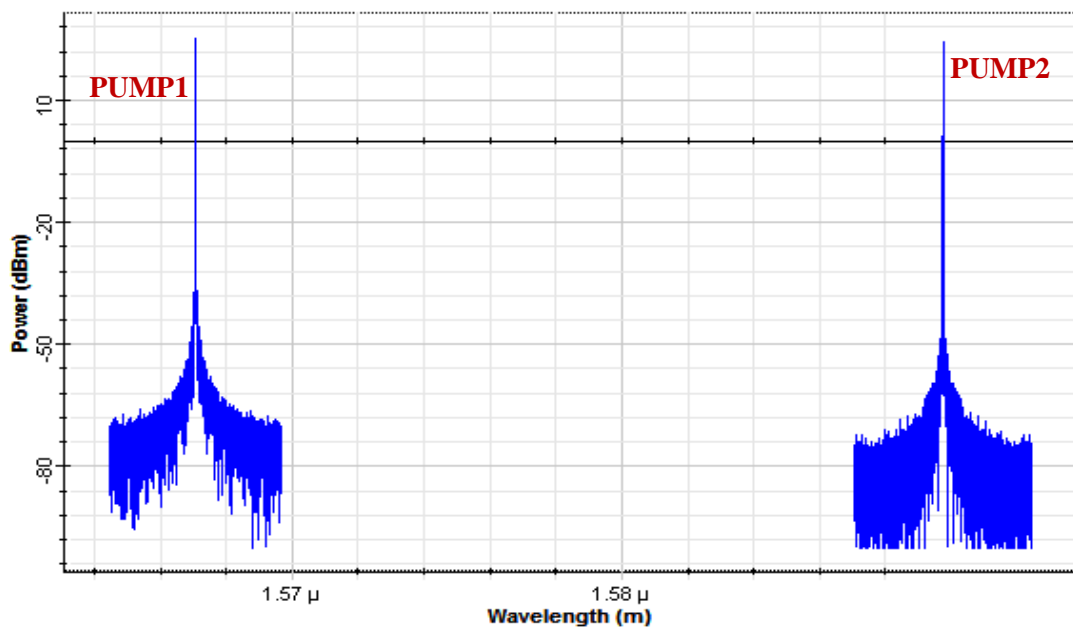
Figure (4.5): Spectrum of the pump1 and pump2.

Figures (4.6a) and (4.6b) show the waves spectrum at the HNLF input and output, respectively. In fig. (4.6b), it can be seen the generation of the conjugated idler at the output of the HNLF due to the FWM process at frequency 189.68 THz (1580.52 nm) based on the FWM equation ($\omega_i = \omega_{p1} + \omega_{p2} - \omega_s$).
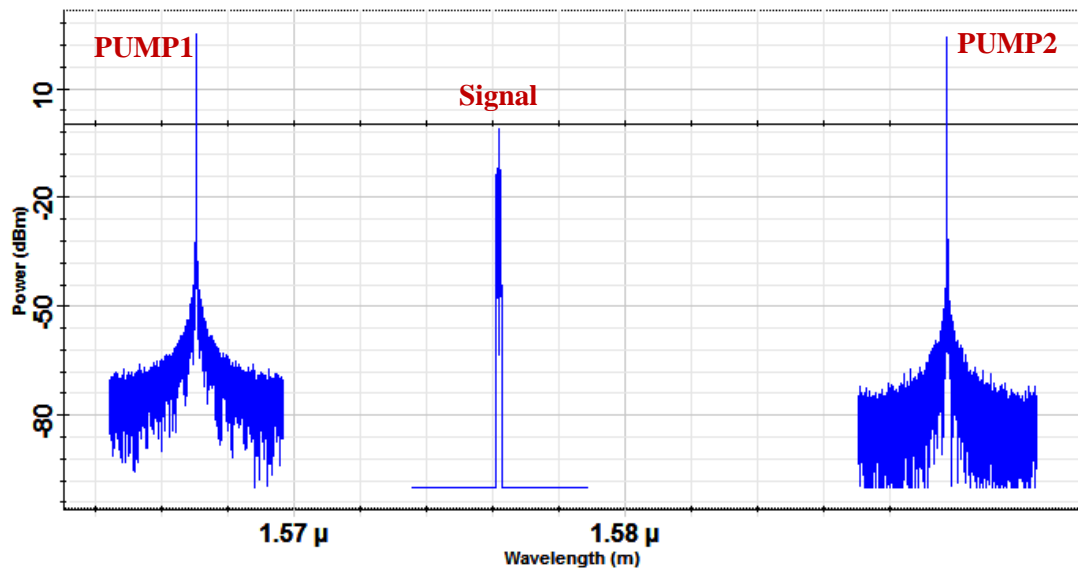
(a)
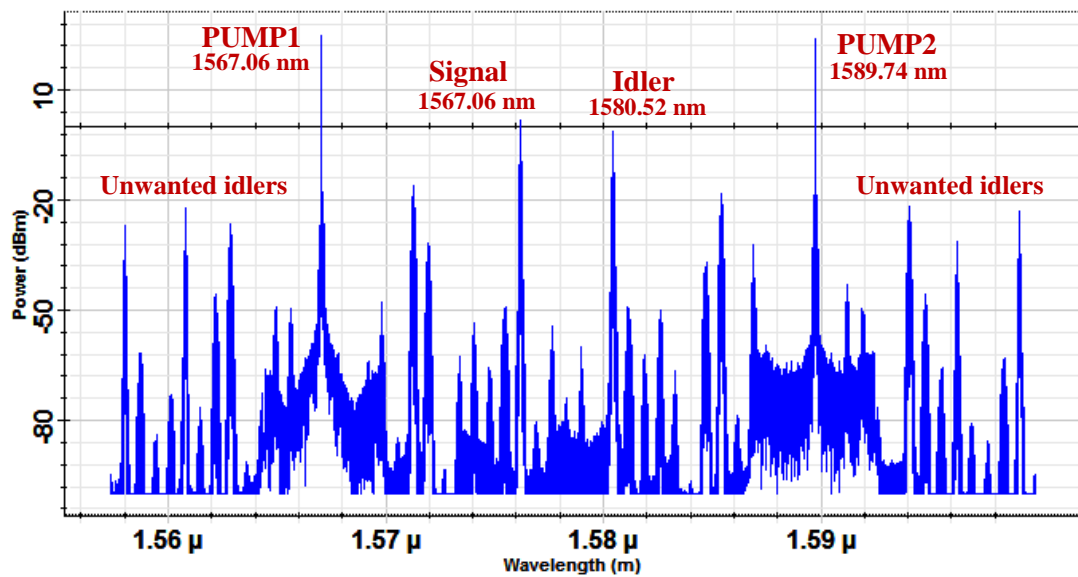
(b)

Figure (4.6): Waves spectrum at (a) HNLF input and (b) HNLF output.

The preceding discussion assumes that only the nondegenerate FWM process, contributes in the HNLF. In reality, the situation is much more complicated because the degenerate FWM process associated with each pump occurs simultaneously. In fact, it turns out that the combination of degenerate and nondegenerate FWM processes can create many other unwanted idlers as shown in fig. (4.6b).

Figure (4.7) shows the spectrum of the conjugated idler at the output of OPC device.
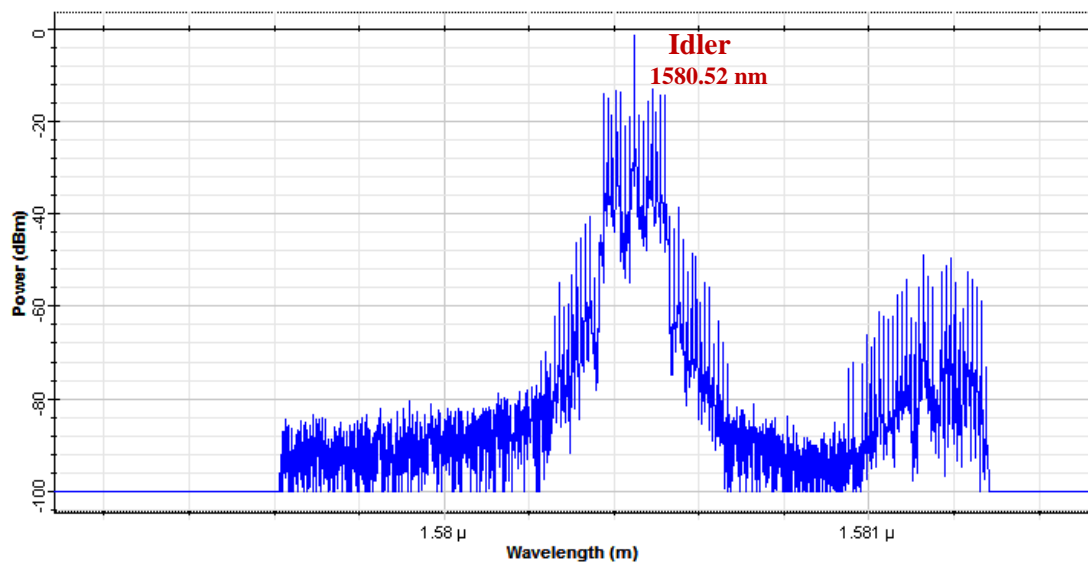
Figure (4.7): Spectrum of the conjugated idler at the output of the first OPC device.

The conjugated idler then transmitted across a second part of the optical link. At the second OPC device, the process of OPC will repeated again.

Figures (4.8a) and (4.8b) show the waves spectrum of the HNLF input and output at the second OPC device, respectively. In fig. (4.8b), a new conjugated idler at the output of the HNLF due to the FWM process was generated at frequency 190.2 THz (1576.2 nm), which is similar to the original transmitted signal.
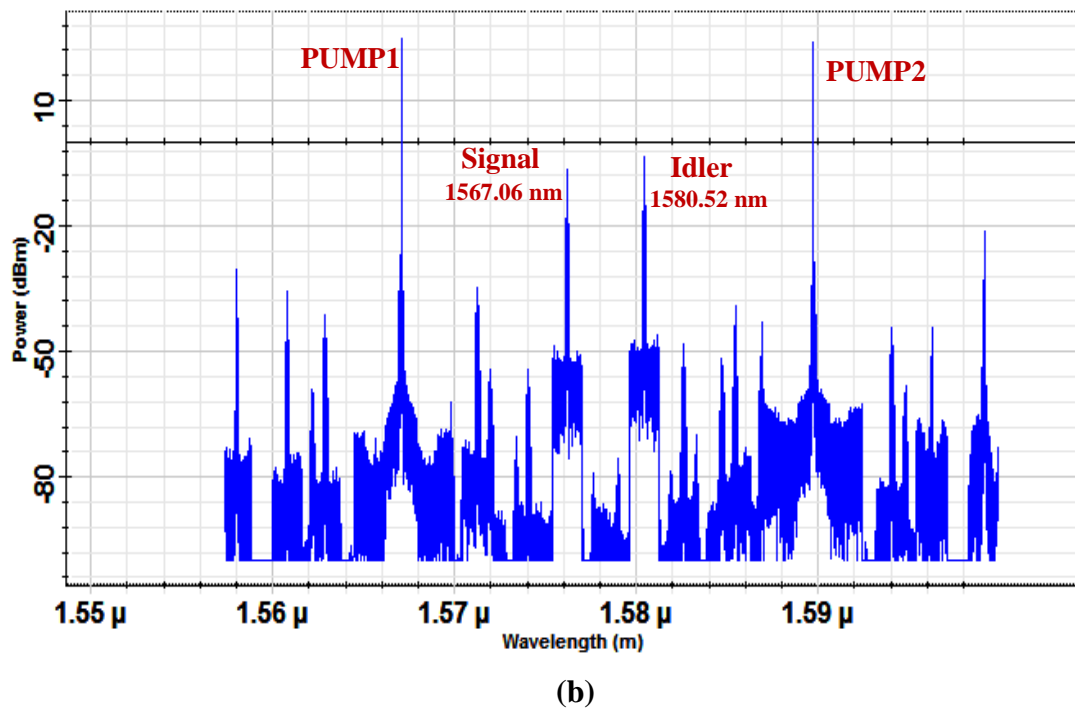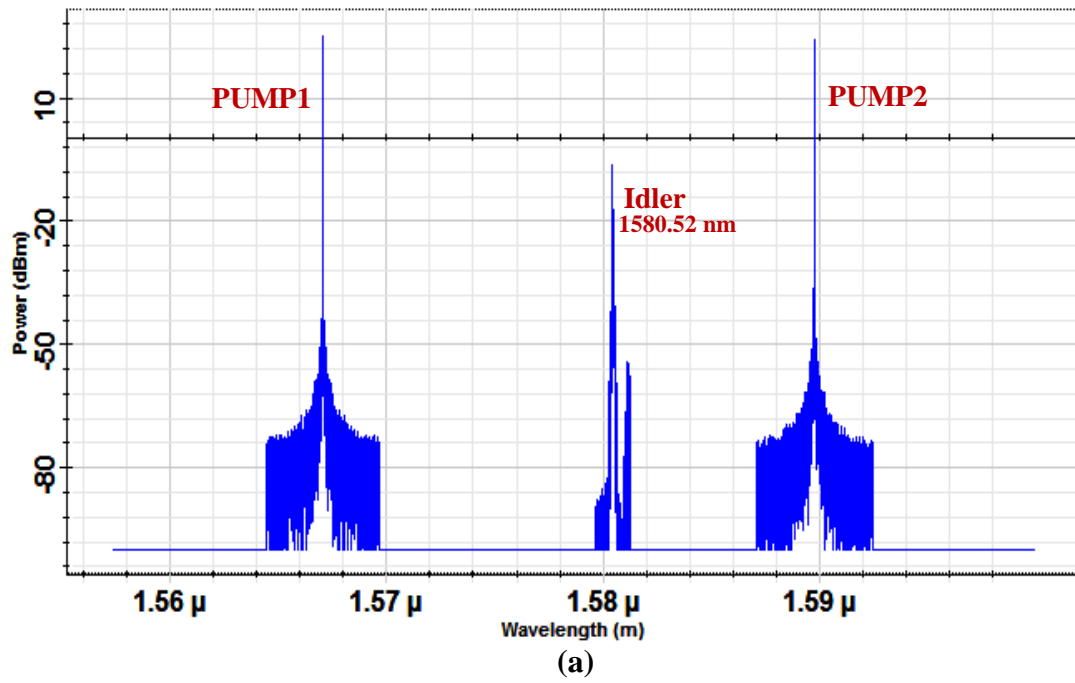
Figure (4.8): Waves spectrum at (a) HNLF input and (b) HNLF output at the second OPC device.

Figure (4.9) shows the spectrum of the received optical signal.
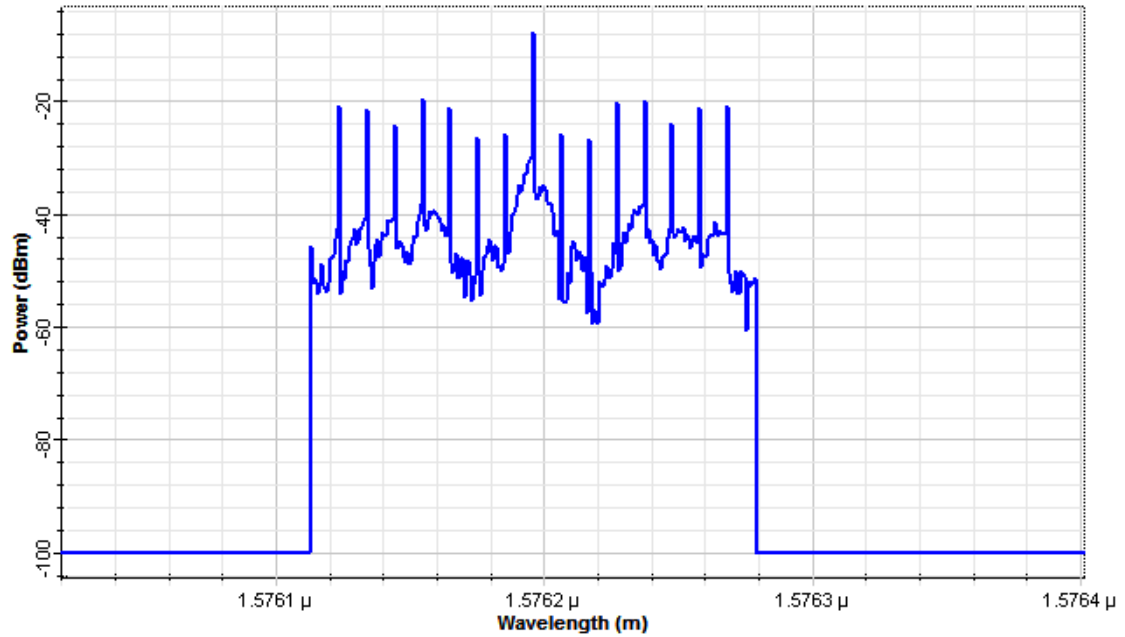
Figure (4.9): Spectrum of the received optical signal.

Figure (4.10a) displays the variation of the Q-factor with launched power. It can be seen from this figure that the maximum Q-factor of X-polarization component for the case with multiple-OPC compensation scheme is 17 dB at a launch power of 3 dBm. This indicates an improvement in performance of 1.2 dB compared to the maximum Q-factor for the MS-OPC compensation scheme.

For the Y-polarization component (see Fig (4.4b)), the maximum Q-factor with the multiple-OPC compensation scheme is 17.7 dB at a launch power of 4 dBm showing 1.8 dB improvement compared to the case of MS-OPC compensation scheme. The insets in the Figs. (4.10a) and (4.10b) illustrate the eye diagrams of the received signal (X and Y– Polarization components) at the corresponding optimum launched powers.

X - Polarization

(a)

Y - Polarization

(b)
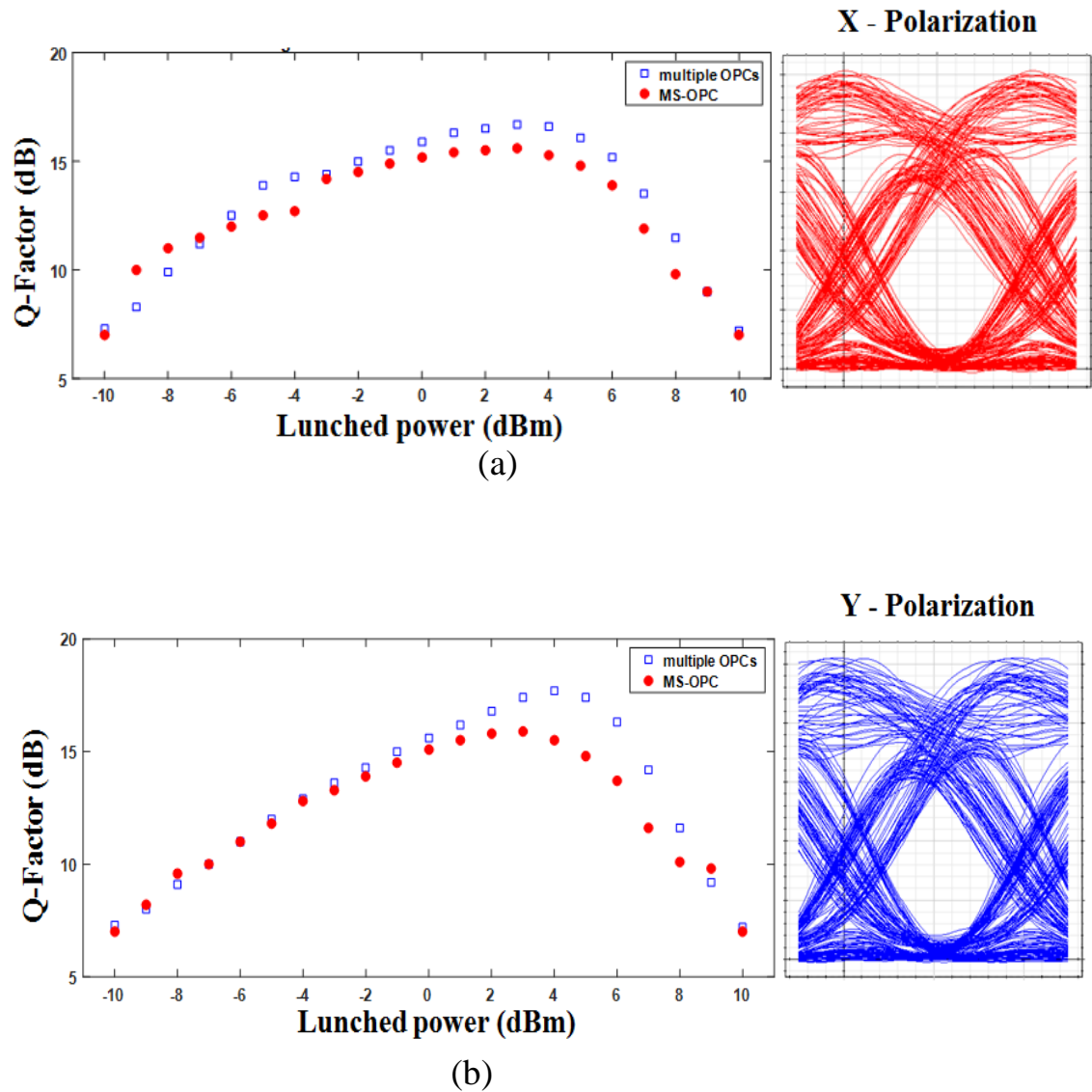
Figure (4.10): Calculated Q-factor as a function of a signal launched power for (a) (X-Polarization), and (b) (Y-Polarization), for single channel transmission after 912 km. The insets represent the eye diagrams of the received signal at the optimum launched powers.

Figures (4.11a) and (4.11b) compare the performance of the multiple-OPC and MS-OPC confgurations in terms of the total length of the optical link for the single channel transmission for both polarization components. The results show that the transmission reach at the HD-FEC limit (BER=3.85×10^{-3}) is enlarged by 24.2% when the multiple-OPC configuration is used.

Single channel transmission reach

(a)

Single channel transmission reach

(b)
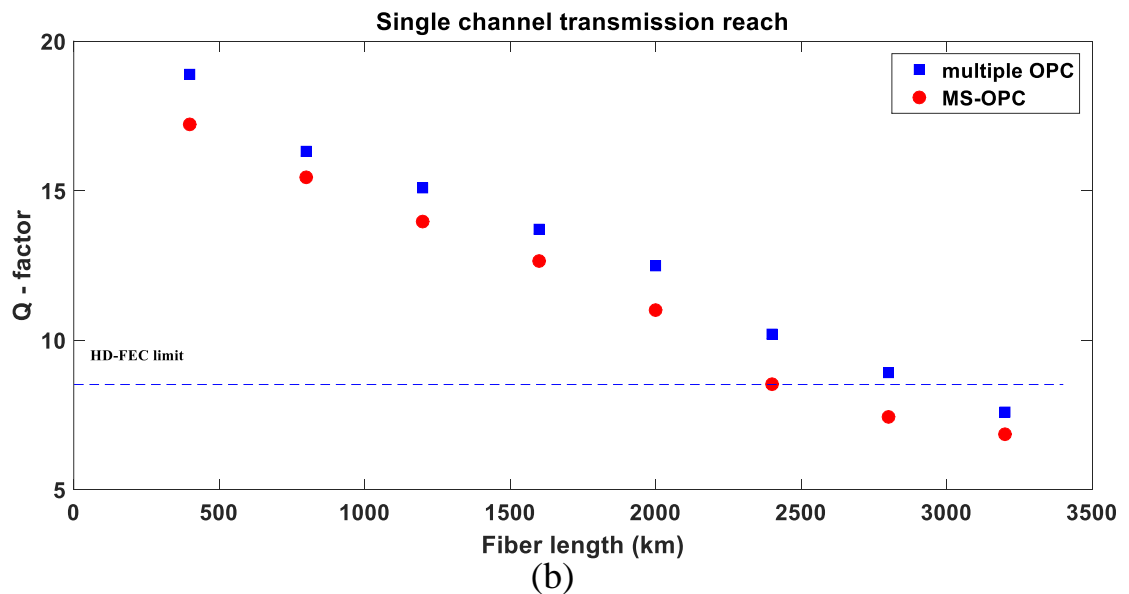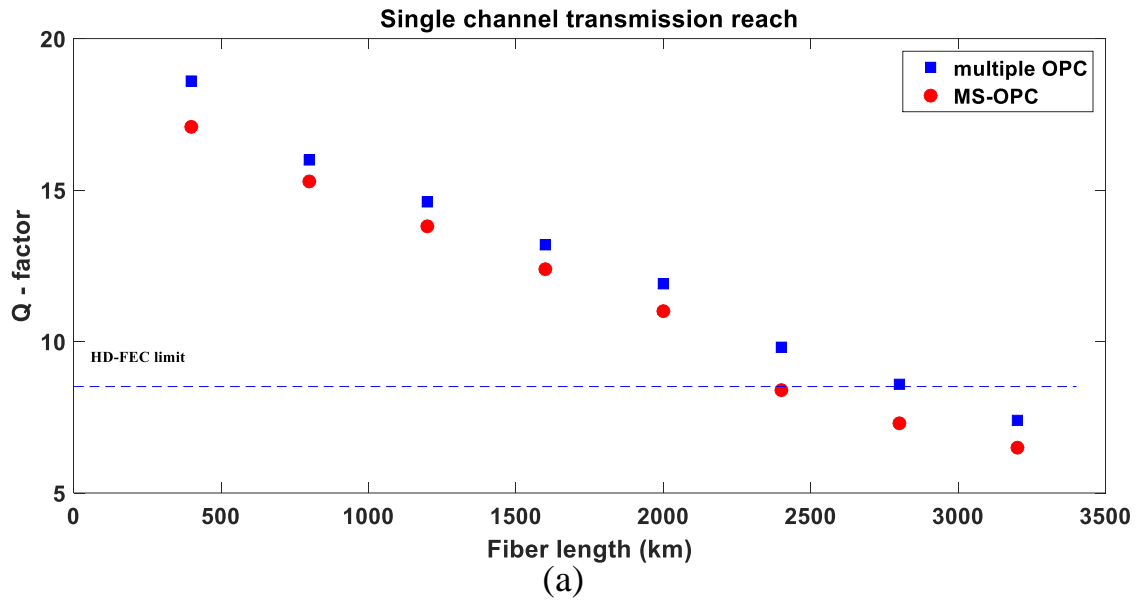
Figure (4.11): Variation Q-factors as a function of a transmission reach for single channel, (a) X-Polarization and (b) Y-Polarization.

The calculations are performed further to investigate the performance of the 8-channel WDM system. At the transmitter, eight channels at frequencies extending from 190 THz to 190.35 THz (50-GHz channel spacing). Figure (4.12) shows the spectrum of the multiplexed eight channels.
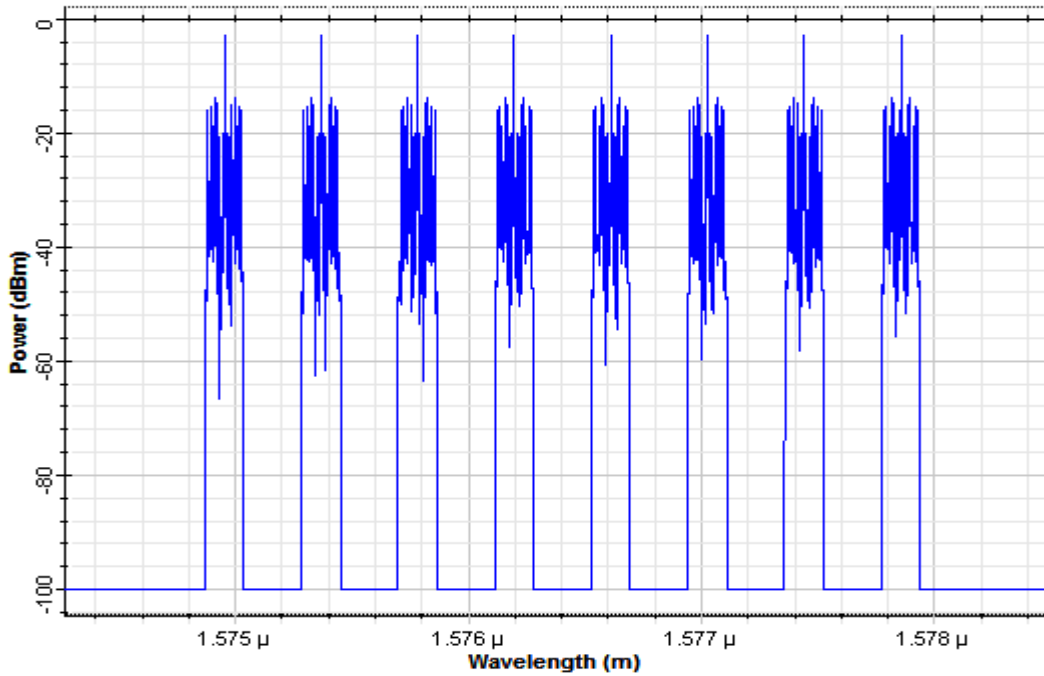
Figure (4.12): Spectrum of the multiplexed 8-channels of the WDM signal.

Figures (4.13a) and (4.13b) show the spectrum of the HNLF input and output at the first OPC device, respectively. An eight conjugated idlers were generated due to the process of FWM in the HNLF with frequencies extending from 189.86 THz to 189.51 THz (50 GHz channel spacing).

(a)
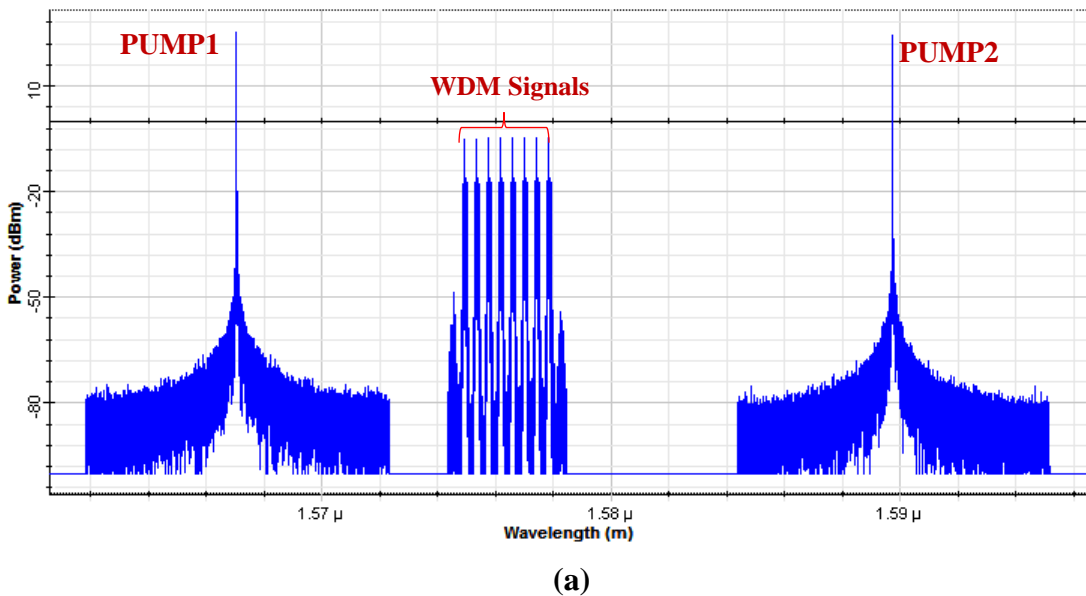
Figure (4.13): Waves spectrum at (a) HNLF input and (b) HNLF output at the first OPC device.

(b)
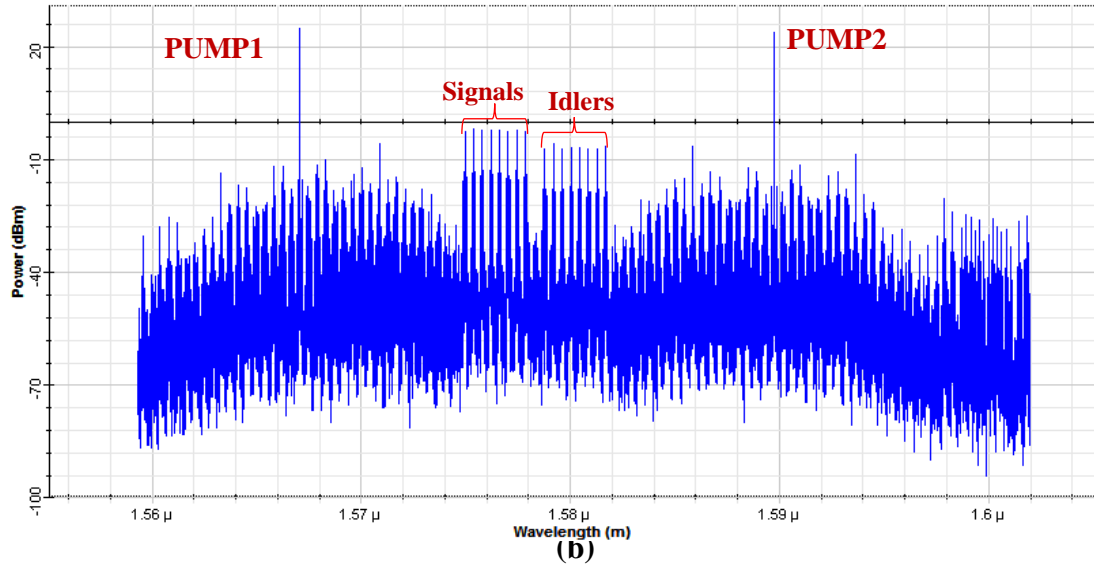
(b)

Figure (4.13): Continued.

After transmitting the output signals of the first OPC device over a second part of the optical link, an OPC process is performed again at the second OPC device generating new eight idlers similar in frequency to the original input signals. Figures (4.14a) and (4.14b) show the spectrum of the HNLF input and output at the second OPC device, respectively.
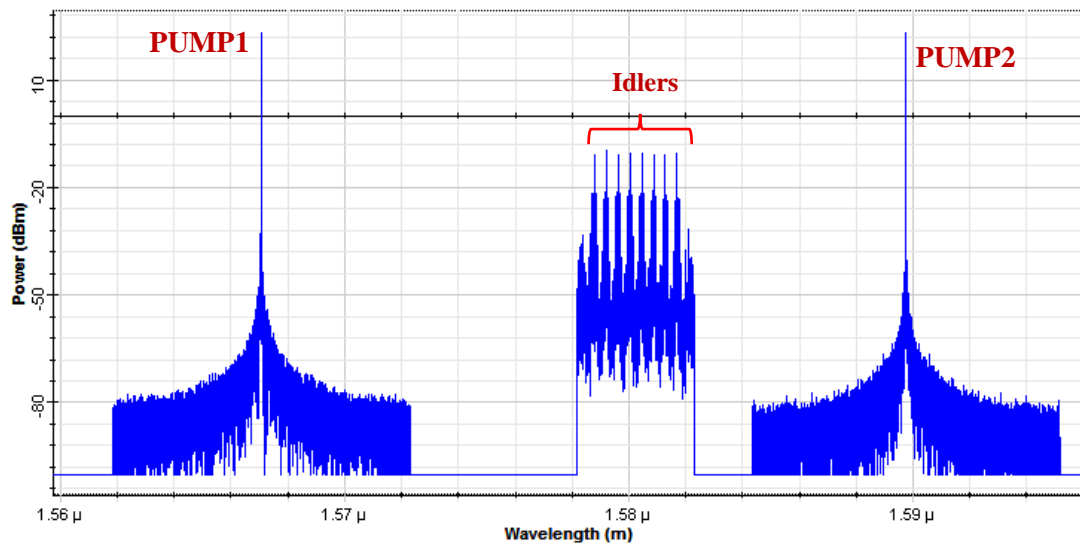
(a)

Figure (4.14): Waves spectrum at (a) HNLF input and (b) HNLF output at the second OPC device.
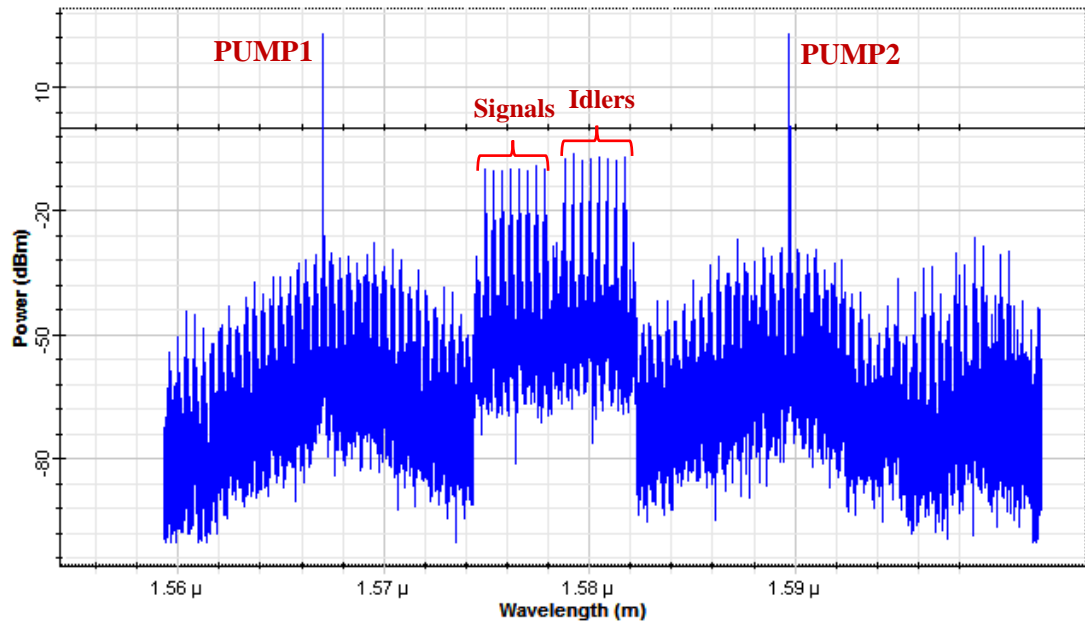
(b)
Figure (4.14): continued

Figure (4.15) shows the spectrum of the received signals before the demultiplexing.
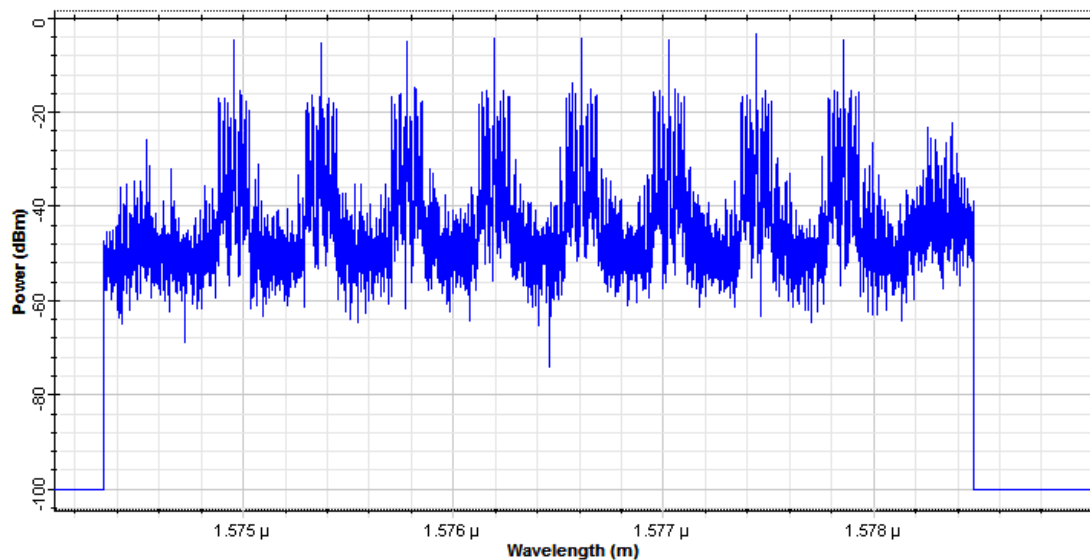
Figure (4.15): Spectrum of the received WDM signals.

The performance of the middle channel at frequency 190.2 THz of the WDM signal is deduced after transmission of 912 km for signal launched powers ranging from -10 dBm to +10 dBm, as shown in Fig. (4.16). The Q-factor improves by 0.62 dB when a multiple-OPC compensation scheme is used as compared with the MS-OPC scheme.
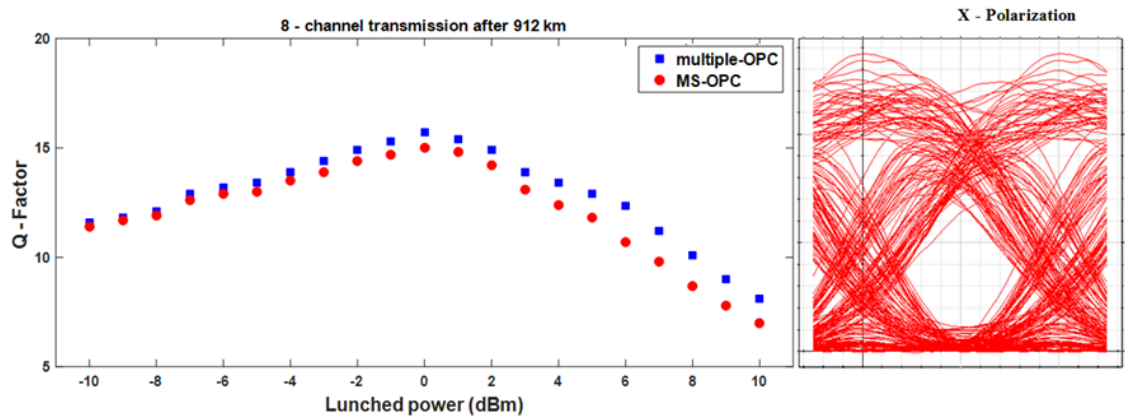
(a)
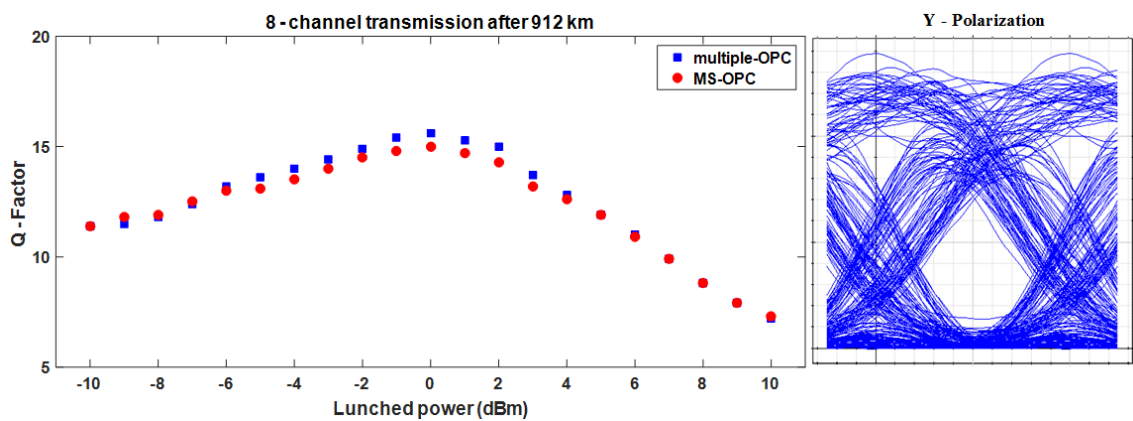
(b)

Figure (4.16): Calculated Q-factor as a function of a signal launched power (a) X – Polarization (b) Y – Polarization, for a middle channel operating at frequency of 190.2 THz for an 8-channel WDM signal transmission after 912 km.

4.3.2 16-QAM Signaling

The system under investigation in this subsection operates with 16-QAM signaling and 256 Gb/s bit rate. Figures (4.17a) and (4.17b) show the simulation setup using MS-OPC and multiple-OPC, respectively. The corresponding transmitter and receiver block diagrams are illustrated in Figs. (4.17c) and (4.17d), respectively.

The MS-OPC configuration consists of a 8×256 Gb/s WDM PDM 16-QAM transmitter, six 76 km SSMF spans forming the first half of the link, the OPC device, another six 76 km SSMF spans forming the second half of the link, and a coherent receiver. The multiple-OPC configuration uses the same transmitter and receiver, but the optical link consists of three parts

separated by two OPC devices each of the first and the last parts consist of three 76 km SSMF, while the middle part consists of six 76 km SSMF. Each span in both configurations is backward pumped with a Raman pump to achieve a symmetric power profile along the fiber spans. The transmitter has eight CW laser sources (from 190 THz to 190.35 THz with 50 GHz channel spacing) modulated by the corresponding data to generate the WDM signals (see Fig. 4.17c). After combining all the eight WDM channels by the WDM multiplexer, the 8×256 Gb/s WDM PDM 16-QAM signal is amplified with an EDFA. The ASE noise is suppressed by an optical BPF. An EDFA and optical attenuator are used to control the signal power launched to the fiber spans.

At the receiving end, (Fig. 4.17d), the received WDM signal is demultiplexed and each of the channels is polarization-demultiplexed and converted into an electrical domain using coherent 16-QAM dual polarization receiver. The DSP used for each single channel helps in recovering the incoming transmission signal after coherent detection. The decision component processes the electrical signal channels received from the DSP stage, normalizes the electrical amplitudes of both polarization channels to the respective 16-QAM grid and performs a decision on each received symbol based on normalized threshold settings. Finally, 16-QAM decoders are used to decode the two parallel 16-QAM M-ary symbol sequences into binary output signals.
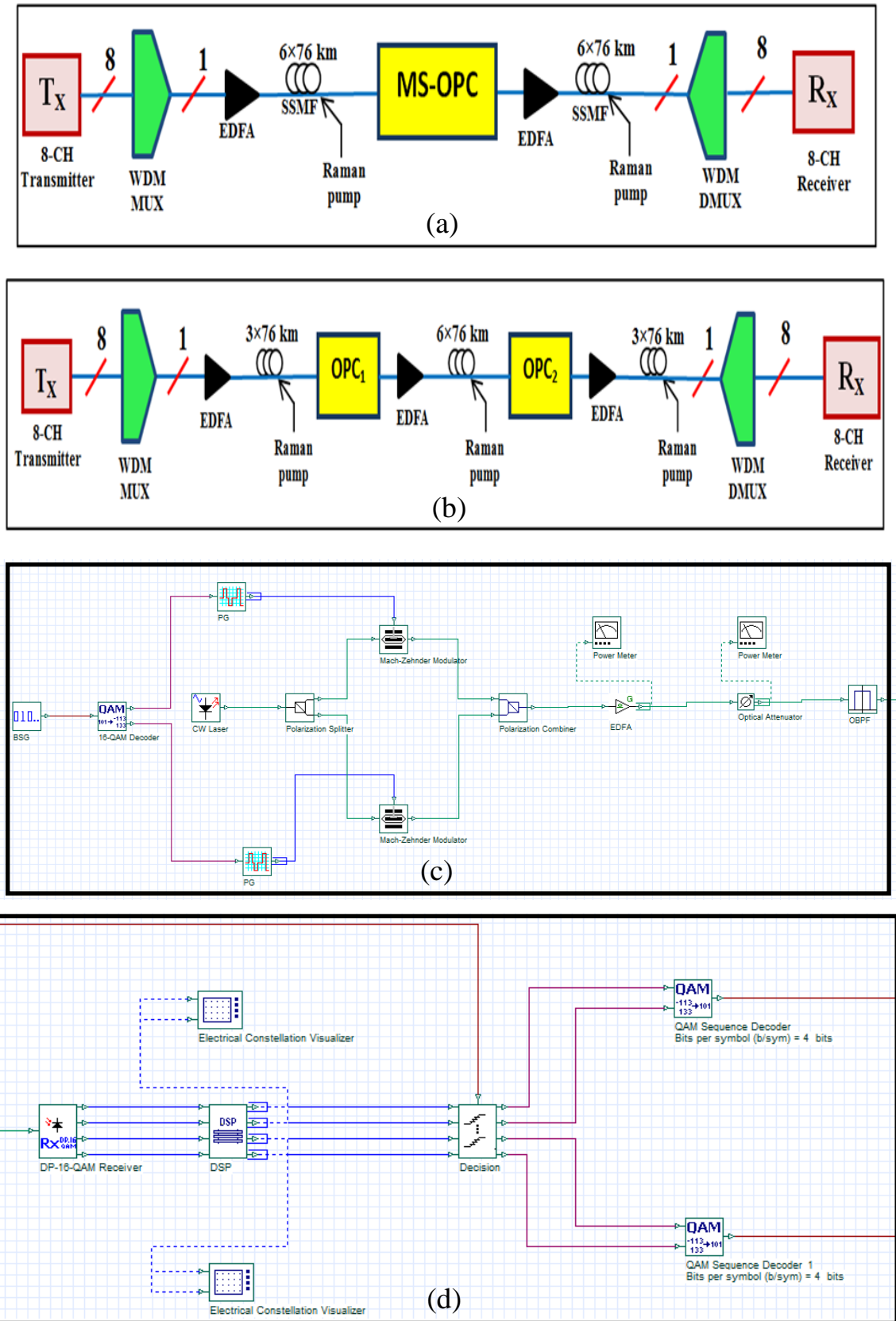
Figure (4.17): Schematic of the simulation setup corresponding to 8-channel WDM system (a) MS-OPC configuration, (b) multiple-OPC configuration, (c) Transmitter for a single channel including sequence generator (SG), pulse generator (PG), Mach-Zehnder modulator (MZM), polarization combiner (PC), polarization splitter (PS), and optical attenuator, and (d) Receiver for a single channel.

First, the BER of a single-channel (at 190.2 THz) is deduced. The launched signal power to the fiber link is adjusted from -9 dBm to +3 dBm by tuning the gain of the EDFA and the optical attenuator located at the transmitter output. Figure (4.18) shows the Q-factor for the single channel after 912 km transmission versus launched signal power. For the case of MS-OPC, the optimum launched power is about −2 dBm, while in the multiple-OPC scenario, it increases by 4 dB to be about 2 dBm with a 1.35 dB improvement in Q-factor. These results are compared with experimental ones that is given in [26] showing good agreement.
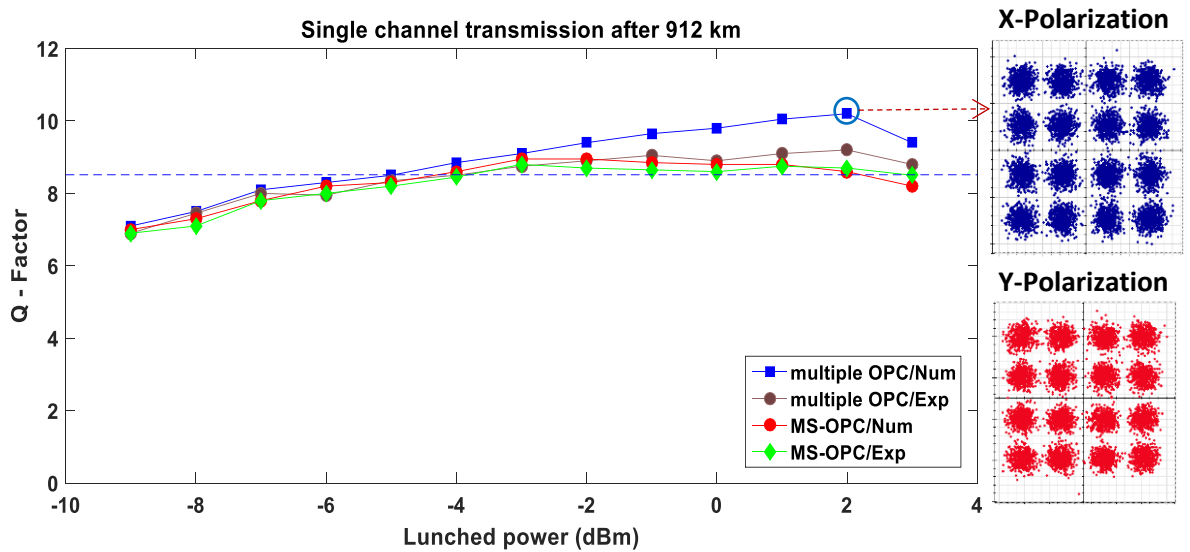
Figure (4.18): Calculated Q-factor as a function of a signal launched power for single channel scenario after 912 km transmission. The insets show the recovered constellation diagrams for both polarization components corresponding to multiple-OPCs configuration at the optimum signal launched power.

Figure (4.19) compares the performance of the multiple-OPC and MS-OPC confgurations in terms of the total length of the optical link for the single channel transmission. The results show that the transmission reach at the HD-FEC limit is enlarged by 30.7% when the multiple-OPC configuration is used.
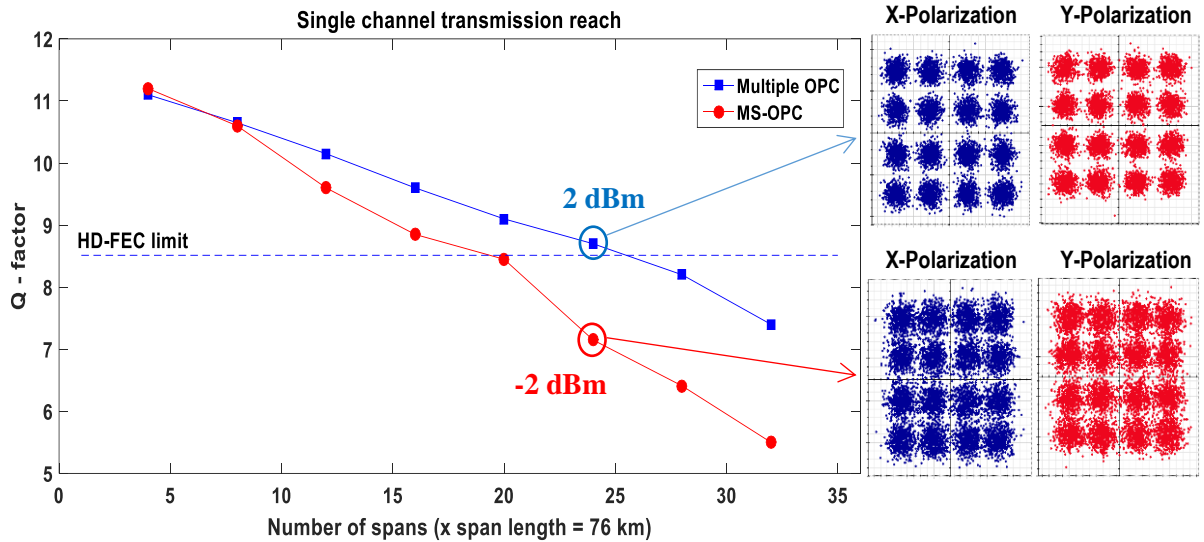
Figure (4.19): Calculated Q factor as a function of number of fiber spans for a single channel transmission. Insets show the recovered constellation diagrams for the multiple OPCs and MS-OPC after 1824 km transmission (24 spans).

The calculations are carried further to investigate the performance of the 8-channel WDM system. The performance of the central channel at frequency 190.2 THz of the WDM signal is deduced after transmission of 912 km for signal launch powers started from -9 dBm to +3 dBm, as shown in Fig. (4.20). For the case of MS-OPC, the optimum launch power is around −2 dBm. For the case of multiple-OPC, the optimum launch power increases to 0 dBm, and the Q-factor is improved by 0.62 dB, deduced at optimum signal powers associated with the two cases.
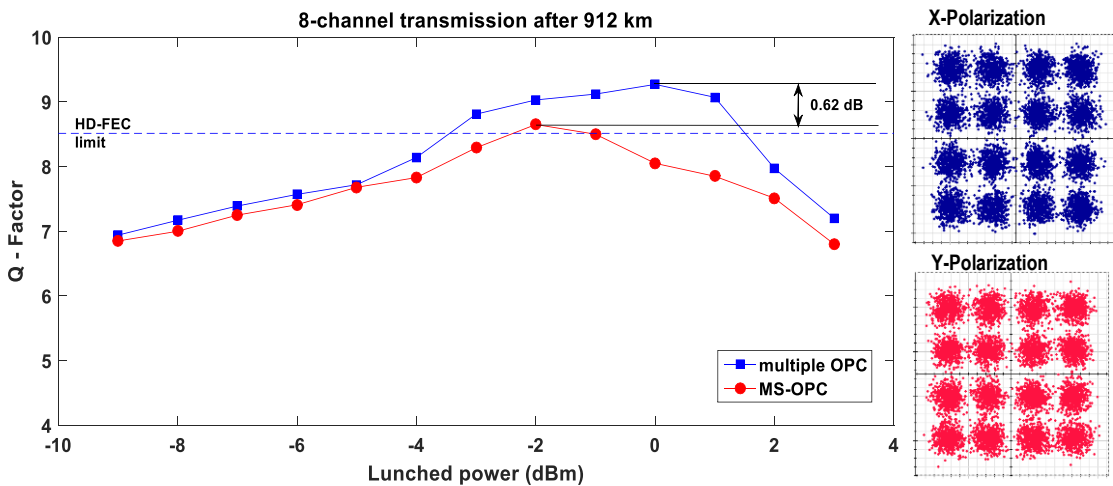
Figure (4.20): Calculated Q-factor as a function of launched signal power for the middle channel of an 8-channel WDM system after 912 km transmission. The insets show the recovered constellation diagrams for both polarization components corresponding to multiple OPCs configuration at the optimum signal launched power.

Figure (4.21) shows the BER for all the 8 channels after 912 km at the optimum signal launched power for each configuration. For the multiple-OPC system, the BERs of all channels except channel 8, are under the HD-FEC limit. A minimum BER of 1.14×10^{-3} is observed in channel 7.
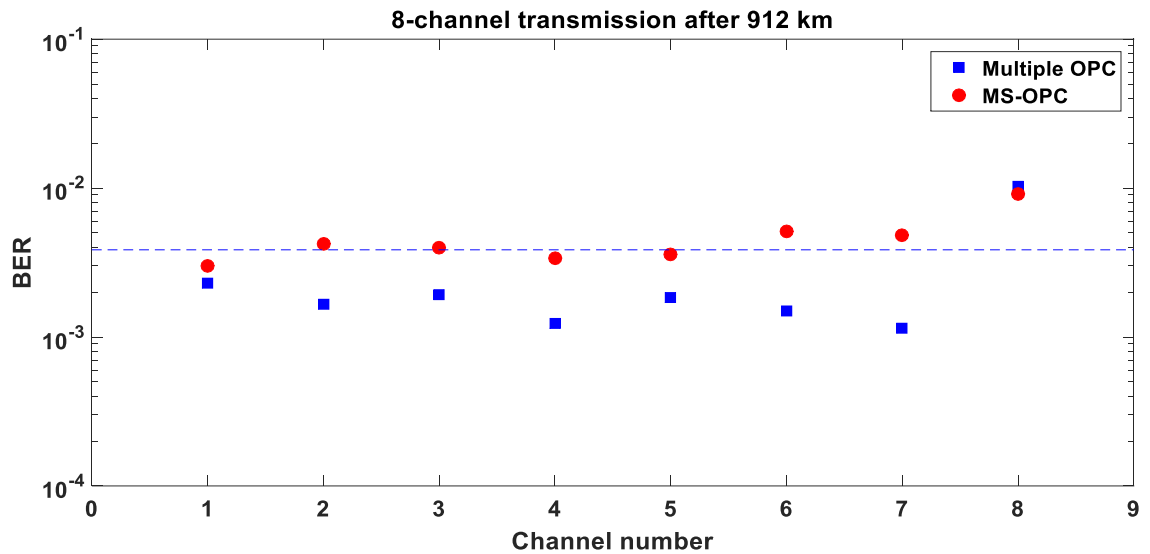
Figure (4.21): BER as a function of WDM channel number evaluated at the corresponding optimum signal launched powers.

4.4 Thesis Conclusions

Mitigation of fiber dispersion and nonlinear distortions in advanced fiber-optic communication systems have been investigated both theoretically and by simulation. The effect of SOP on the performance of a dual-pump HNLF-OPC has been analyzed using a set of eight coupled NLSEs. Further, the transmission performance of two long-haul fiber-optic communication systems incorporating multiple-OPC compensation scheme has been simulated and the results are compared with published experimental data. The two systems use 8-channel WDM technique with each channel adopting PDM NRZ-OOK and PDM-16QAM modulation with bit rates of 40 Gb/s and 256 Gb/s, respectively.

The main conclusions drawn from investigation of polarization effect in a dual-pump OPC are

(i) The maximum conversion efficiency is obtained when the signal and the two pumps are all copolarized, while the conversion efficiency becomes almost zero when the signal wave is orthogonal to the two copolarized pumps.

(ii) The analytical investigation shows that the use of a pair of orthogonally polarized pumps can provide polarization-independent conversion efficiency, but this conversion efficiency is lower compared with the case of copolarized waves and this efficiency can be increased by increasing the pump powers.

The simulation of the two advanced optical systems reveals the following main findings

(i) In PDM-NRZ-OOK signal transmission, the use of multiple-OPC provides better transmission performance when compared to MS-OPC in both, single channel and WDM signal transmission. Moreover, the results show that the transmission reach at the HD-FEC limit can be enlarged when the multiple-OPC configuration is used.

(ii) In PDM-16QAM signal, single channel transmission using multiple-OPC shows a 1.35 dB improvement in Q-factor over the MS-OPC case. In the WDM system, using multiple-OPC increases the nonlinear threshold by ~2 dB compared with the case of MS-OPC, showing 0.62 dB improvement in Q-factor over the MS-OPC compensation scheme.

4.5 Suggestions for Future Work

Possible future extension for the work included in this thesis may cover the following points

(i) This thesis provides theoretical analysis and simulation results of fiber nonlinear effects in the presence of the polarization effects and discusses the optical compensation techniques. Experimental research

is one of the most important future works to validate the theoretical models and to measure the performance of different optical compensation schemes for mitigating fiber nonlinear effects.

(ii) The research described in this thesis is focused on the investigation of single-carrier transmission, where a single optical carrier is modulated and transmitted in wavelength window, significantly broader than the symbol rate. To increase spectral efficiency it is possible to pack channels at a symbol rate spacing, which is denoted OFDM with presence of the polarization effect. Although, nonlinear compensation algorithms were already applied in the literature to OFDM, the effect of the polarization has not been investigated and a comprehensive study on potential performance improvement is not available in either case.

(iii) The system under investigation in this thesis can be expanded to be has higher-order modulation formats, hence increase the transmitted data bit rate. Furthermore, the transmission reach can be enlarged to cover a wide area.

(iv) Design of an OPC device using photonic crystal fiber instead of the HNLF.

References

[1]   H. Grupp, "Dynamics of Science-Based Innovation," Sprinter-Verlq Berlin · Heidelberg 1992.

[2]   G. P. Agrawal, "Fiber-optic communication systems," John Wiley & Sons, 4th edition, 2010.

[3]   G. P. Agrawal, "Light wave technology telecommunication Systems," John Wiley & Sons, Inc. 2005.

[4]   O. D. D. Soares, " Trends in optical fibre metrology and standards," Springer-Science & Business Media, BV. 1994.

[5] S. Olonkins, I. Stankunovs, A. Alsevska, L. Gegere, and V. Bobrovs, "Investigation of in-line Distributed Raman Amplifiers with Co and Counter-propagating Pumping Schemes," Progress In Electromagnetic Research Symposium (PIERS), Shanghai, China, Aug. 2016.

[6] B. Bouzid, "Analysis and review of erbium doped fiber amplifier," Electronics, Communications and Photonics Conference (SIECPC), Fira, Greece, April 2013.

[7] S. Aleksic, "Towards Fifth-Generation (5G) Optical Transport Networks" 17th International Conference on Transparent Optical Networks (ICTON), Budapest, Hungary, Jul. 2015.

[8] K. Kikuchi, "Fundamentals of coherent optical fiber communications," IEEE Journal of Lightwave Technology, vol. 34, no. 1, pp. 157-179, Jan. 2016.

[9] M. Nakazawa, K. Kikuchi, T. Miyazaki, "High spectral density optical communication technologies," Springer-Verlag Berlin Heidelberg, 2010.

[10] M. Seimetz, " High-Order modulation for optical fiber transmission," Springer-Verlag Berlin Heidelberg, 2009.

[11] R. J. Essiambre and R. W. Tkach, "Capacity Trends and Limits of Optical Communication Networks," in Proceedings of the IEEE, vol. 100, no. 5, pp. 1035-1055, May 2012.

[12] M. Asvial and A. A. S. Paramitha M. P, "Analysis of high order dispersion and nonlinear effects in fiber optic transmission with Non Linear Schrodinger Equation model," 2015 International Conference on Quality in Research (QiR), Lombok, pp. 145-150, Aug. 2015.

[13] C. Behrens, R. I. Killey, S. J. Savory, M. Chen and P. Bayvel, "Nonlinear Distortion in Transmission of Higher Order Modulation Formats," in IEEE Photonics Technology Letters, vol. 22, no. 15, pp. 1111-1113, Aug. 2010.

[14] G. P. Agrawal, "Nonlinear Fiber Optics: Academic Press," 1995.

[15] Y. Yamamoto, Y. Kawaguchi and M. Hirano, "Low-Loss and Low-Nonlinearity Pure-Silica-Core Fiber for C- and L-band Broadband Transmission," in Journal of Lightwave Technology, vol. 34, no. 2, pp. 321-326, Jan. 2016.

[16] C. Behrens, "Mitigation of nonlinear impairments for advanced optical modulation formats," UCL (University College London), 2012.

[17] G. J. Foschini and C. D. Poole, "Statistical theory of polarization dispersion in single mode fibers," IEEE Journal of Lightwave Technology, vol. 9, no. 11, pp. 1439-1456, Nov. 1991.

[18] J. Toulouse, "Optical nonlinearities in fibers: review, recent examples, and systems applications," IEEE Journal of Lightwave Technology, vol. 23, no. 11, pp. 3625-3641, Nov. 2005.

[19] L. He, J. Niu, Y. Sun and Y. Ji, "The four wave mixing effects in quantum key distribution based on conventional WDM network," International Conference on Optical Internet (COIN), Jeju, South Korea, pp. 1-2, Aug. 2014.

[20]   J. M. Senior, "Optical fiber communications principles and practice," Pearson Education Limited, 3rd edition, 2009.

[21]   M. Secondini, S. Rommel, F. Fresi, E. Forestieri, G. Meloni, and L. Potì," Coherent 100G nonlinear compensation with single-step digital backpropagation", International Conference on Optical Network Design and Modeling (ONDM), Pisa, Italy, pp. 63-67 May, 2015.

[22]   I. Sackey, F. D. Ros, J. K. Fischer, T. Richter, M. Jazayerifar, C. Peucheret, K. Petermann, and C. Schubert, "Kerr nonlinearity mitigation: mid-link spectral inversion versus digital backpropagation in 5×28-GBd PDM 16-QAM signal transmission," IEEE Journal of Lightwave Technology, vol. 33, no. 9, pp. 1821-1827, May1, 1 2015.

[23] E. Porto da Silva, F. da Ros and D. Zibar, "Performance of multi-channel DBP with long-haul frequency-referenced transmission," Optical Fiber Communications Conference and Exhibition (OFC), Anaheim, USA, pp. 1-3, Aug. 2016.

[24] X. Liu, A. R. Chraplyvy, P. J. Winzer, R. W. Tkach, and S. Chandrasekhar, "Phase-conjugated twin waves for communication beyond the Kerr nonlinearity limit," National Photonics, vol. 7, no. 7, pp. 560–568, May 2013.

[25]   U. Sahu and B. C. Jinaga." Compensation of fiber nonlinear impairments using optical back propagation", International Conference on Microwave, Fiber-optic communication Engineering, December 2015.

[26]   H. Hu, R. M. Jopson, A H. Gnauck, S. Randel,and S. Chandrasekhar "Fiber nonlinearity mitigation of WDM-PDM QPSK/16-QAM signals using fiber-optic parametric amplifiers based multiple optical phase conjugations," Optical Express, vol. 25, no. 3, pp. 1618-1628, Feb. 2017.

[27]   S. L. Jansen, D. van den Borne, P. M. Krummrich, S. Spalter, G. D. Khoe and H. de Waardt, "Long-haul DWDM transmission systems

employing optical phase conjugation," IEEE Journal of Selected Topics in Quantum Electronics, vol. 12, no. 4, pp. 505-520, Jul.-Aug. 2006.

[28] P. Kaewplung and K. Kikuchi, "Simultaneous cancellation of fiber loss, dispersion, and Kerr effect in ultra-long-haul optical fiber transmission by midway optical phase conjugation incorporated with distributed Raman amplification," IEEE Journal of Lightwave Technology, vol. 25, no. 10, pp. 3035-3050, Oct. 2007.

[29] M. Morshed, A. J. Lowery, and L. B. Du, "Improving performance of optical conjugation by splitting the nonlinear element," Optics Express, vol. 21, no. 4, pp. 4567–4577, Feb. 2013.

[30] F. Da Ros, I. Sackey, R. Elschner, T. Richter, C. Meuer, M. Nölle, M. Jazayerifar, K. Petermann, C. Peucheret, and C. Schubert, "Kerr nonlinearity compensation in a 5×28-GBd PDM 16-QAM WDM system using fiber-based optical phase conjugation," The European Conference on Fiber-optic communication (ECOC), pp. 1-3, Cannes, France, Sept. 2014.

[31] I. Sackey, F. D. Ros, M. Jazayerifar, T. Richter, C. Meuer, M. Nölle, L. Molle, C. Peucheret, K. Petermann, and C. Schubert, "Kerr nonlinearity mitigation in 5 × 28-GBd PDM 16-QAM signal transmission over a dispersion-uncompensated link with backward-pumped distributed Raman amplification", Optical Express vol. 22, no. 22, pp. 27381-27391, Oct. 2014.

[32] H. Hu et al., "Fiber nonlinearity compensation of an 8-channel WDM PDM-QPSK signal using multiple phase conjugations," Optical Fiber Communications Conference and Exhibition (OFC), pp. 1-3, San Francisco, USA, Mar. 2014.

[33] I. Sackey, F. D. Ros, T. Richter, R. Elschner, M. Jazayerifar, C. Meuer, C. Peucheret, K. Petermann, and C. Schubert, "Design and performance evaluation of an OPC device using a dual-pump polarization-independent FOPA," The European Conference on Fiber-optic communication (ECOC), pp. 1-3, Cannes, France, 2014.

[34] F. D. Ros, I. Sackey, M. Jazayerifar, T. Richter, C. Meuer, M. Nölle, L. Molle, K. Petermann, J. K. Fischer, and C. Schubert, "Optical phase conjugation for nonlinearity compensation in WDM PDM 16-QAM transmission over dispersion-compensated and dispersion uncompensated links," IEEE Summer Topicals Meeting Series (SUM), pp. 1-3, Nassau, Bahamas, Jul. 2015.

[35] S. Yoshima, Z. Liu, Y. Sun, K. R. Bottrill, F. Parmigiani, P. Petropoulos, and D. J. Richardson, "Nonlinearity mitigation for multi-channel 64-QAM signals in a deployed fiber link through optical phase conjugation," Optical Fiber Communication Conference, pp. 1-3, Anaheim, USA, Mar. 2016.

[36] H. Hu, R. M. Jopson, A. H. Gnauck, D. Pilori, S. Randel and S. Chandrasekhar, "Fiber nonlinearity compensation by repeated phase conjugation in 2.048-Tbit/s WDM transmission of PDM 16-QAM channels," Optical Fiber Communications Conference and Exhibition (OFC), pp. 1-3, Anaheim, USA, Mar. 2016.

[37] L. N. Binh,"Advanced digital fiber-optic communications", Taylor & Francis Group, LLC, 2nd edition, 2015.

[38] J. K. Show," Mathematical Principles of Optical Fiber Communications", the Society for Industrial and Applied Mathematics, 2004.

[39] J. A. Buck, "Fundamentals of Optical Fibers," John wiely & Sons, Inc., 1995.

[40] M. Karasek, J. Kanka, P. Honzatko, J. Vojtech and J. Radil, "10 Gb/s and 40 Gb/s Multi-Wavelength Conversion Based on Nonlinear

Effects in HNLF," International Conference on Transparent Optical Networks, Nottingham, 2006.

[41]   H. Hu, R. M. Jopson, A. H. Gnauck, M. Dinu, S. Chandrasekhar, C. Xie, and S. Randel, "Parametric Amplification, Wavelength Conversion, and Phase Conjugation of a 2.048-Tbit/s WDM PDM 16-QAM Signal," IEEE Journal of Lightwave Technology, vol. 33, no. 7, pp. 1286-1291, Apr. 2015.

[42]   M. Baillot, T. Chartier and M. Joindot, "Multiple four-wave mixing in optical fibres," 2014 The European Conference on Fiber-optic communication (ECOC), Cannes, France, pp. 1-3, Sept. 2014.

[43]   Casimer DeCusatis, "Handbook of Fiber Optic Data communications, A Practical Guide to Optical Networking," Elsevier Inc. 3rd edition, 2008.

[44]   Reinhold Noé, "Essentials of Modern Optical Fiber Communication," Springer, 2010.

[45]   G. W. Lu, T. Sakamoto, A. Chiba, T. Kawanishi, T. Miyazaki, K. Higuma, M. Sudo, and J. Ichikawa, "Monolithically integrated quad mach-zehnder IQ modulator for generation of advanced optical modulation formats," 9th International Conference on Fiber-optic communications and Networks (ICOCN 2010), Nanjing, China, pp. 222-224, Oct. 2010.

[46] G. W. Lu, "Optical signal processing for advanced optical modulation format," IEEE Photonics Society Summer Topics, pp. 170-171, Playa del Carmen, Mexico, Jul. 2010.

[47]   B. B. Purkayastha, and K. K. Sarma, "A Digital Phase Locked Loop based Signal and Symbol Recovery System for Wireless Channel," Springer, 2015.

[48]   Y. Zhang, F. Zhang and S. Pan, "Generation of Frequency-Multiplied and Phase-Coded Signal Using an Optical Polarization Division

Multiplexing Modulator," IEEE Transactions on Microwave Theory and Techniques, vol. 65, no. 2, pp. 651-660, Feb. 2017.

[49] B. Zhu et al., "Large-area low-loss fibers and advanced amplifiers for high-capacity long-haul optical networks [Invited]," in IEEE/OSA Journal of Fiber-optic communications and Networking, vol. 8, no. 7, pp. A55-A63, Jul. 2016.

[50] Afsal S. et al., "A novel approach for the enhancement of Fiber optic communication using EDFA," 2016 International Conference on Wireless Communications, Signal Processing and Networking (WiSPNET), pp. 23-27, Chennai, India, March 2016.

[51] C. Clivati et al., "Distributed Raman Optical Amplification in Phase Coherent Transfer of Optical Frequencies," IEEE Photonics Technology Letters, vol. 25, no. 17, pp. 1711-1714, Sept. 2013.

[52] A. F. Evans, J. Grochocinski, A. Rahman, C. Reynolds and M. Vasilyev, "Distributed amplification: how Raman gain impacts other fiber nonlinearities," Optical Fiber Communication Conference and Exhibit, pp. MA7-MA7, Anaheim, USA, Mar. 2001.

Publications and Conferences

1. Adnan A. Abbas, Mazin M. Elias, and Raad S. Fyath, "Fiber nonlinearity compensation of WDM-PDM 16-QAM signaling using multiple optical phase conjugations over a distributed Raman-amplified link," Photonic Network Communications**, Accepted**.

2. Adnan A. Abbas, Mazin M. Elias, and Raad S. Fyath, "Comprehensive Analysis of HNLF-Based Optical Phase Conjugation in the Presence of Polarization Misalignment," Journal of Engineering and Applied Science, **Accepted**.

3. Adnan A. Abbas, Mazin M. Elias, and Raad. S. Fyath, "Investigation of Polarization Effects on Highly Nonlinear Fiber-Based Optical Phase Conjugation" **Presented** on the second conference of postgraduate researchers (CPGR2017), Al-Nahrain university, October 2017.

Appendix A

Detailed Analysis of Dual-Pump Polarization-Aligned HNLF-OPC

The aim of this appendix is to present an analytical solution for the pumps, signal, and conjugated idler waves equations in the absences of the polarization effect. The analytical solution of the pumps equations starts from Eqns. (3.2a) and (3.2b) as follow

$$\frac{dA_{p1}(z)}{dz} = j\gamma[P_{p1} + 2P_{p2}]A_{p1}(z) \tag{A1}$$

$$\frac{dA_{p2}(z)}{dz} = j\gamma[2P_{p1} + P_{p2}]A_{p2}(z) \tag{A2}$$

where $P_{p1} = |A_{p1}(0)|^2$ and $P_{p2} = |A_{p2}(0)|^2$ are the incident pump powers at $z = 0$.

Integrating both side of Eqns. (A1) and (A2) with respect to z yields

$$\int \frac{1}{A_{p1}(z)} dA_{p1}(z) = \int j\gamma[P_{p1} + 2P_{p2}]dz \tag{A3}$$

$$\int \frac{1}{A_{p2}(z)} dA_{p2}(z) = \int j\gamma[2P_{p1} + P_{p2}]dz \tag{A4}$$

Solutions of Eqns. (A3) and (A4) are given by

$$ln\left(A_{p1}(z)\right) = j\gamma[P_{p1} + 2P_{p2}]z + C_1 \tag{A5}$$

$$ln\left(A_{p2}(z)\right) = j\gamma[2P_{p1} + P_{p2}]z + C_2 \tag{A6}$$

Taking exponential for both side in the Eqns. (A5) and (A6) with $C_{11} = \exp(C_1)$ and $C_{22} = \exp(C_2)$ gives

$$A_{p1}(z) = C_{11} \exp(j\gamma[P_{p1} + 2P_{p2}]z) \tag{A7}$$

$$A_{p2}(z) = C_{22} \exp(j\gamma[2P_{p1} + P_{p2}]z) \tag{A8}$$

where $C_{11} = A_{p1}(0)$ and $C_{22} = A_{p2}(0)$ are the integration constant and they are obtained from the initial conditions at $z = 0$. Therefore, pumps powers equations can be given by

$$A_{p1}(z) = A_{p1}(0) \, exp(j\gamma[P_{p1} + 2P_{p2}]z) \tag{A9}$$

$$A_{p2}(z) = A_{p2}(0) \, exp(j\gamma[2P_{p1} + P_{p2}]z) \tag{A10}$$

The analytical solution of the signal and conjugated idler equations starts from Eqns. (3.4a) and (3.4b)

$$\frac{dA_s(z)}{dz} = 2j\gamma([P_{p1} + P_{p2}]A_s(z) + A_i^*(z)A_{p1}(z)A_{p2}(z) \; exp(-j\Delta kz)) \tag{A11}$$

$$\frac{dA_i^*(z)}{dz} = -2j\gamma([P_{p1} + P_{p2}]A_i^*(z) + A_s(z)A_{p1}^*(z)A_{p2}^*(z) \; exp(j\Delta kz)) \tag{A12}$$

Substituting Eqns. (A9) and (A10) into Eqns. (A11) and (A12) yields

$$\begin{aligned}
\frac{dA_s(z)}{dz} = 2j\gamma([P_{p1} + P_{p2}]A_s(z) \\
+ A_i^*(z)A_{p1}(0) \, exp(j\gamma[P_{p1} + 2P_{p2}]z) \, A_{p2}(0) \, exp(j\gamma[2P_{p1} \\
+ P_{p2}]z) \; exp(-j\Delta kz))
\end{aligned} \tag{A13}$$

$$\begin{aligned}
\frac{dA_i^*(z)}{dz} = -2j\gamma([P_{p1} + P_{p2}]A_i^*(z) \\
+ A_s(z)A_{p1}^*(0) \, exp(-j\gamma[P_{p1} + 2P_{p2}]z)A_{p2}^*(0) \; exp(-j\gamma[2P_{p1} \\
+ P_{p2}]z) \; exp(j\Delta kz))
\end{aligned} \tag{A14}$$

For simplification, let $\theta = (\Delta k - 3\gamma(P_{p1} + P_{p2}))$, Eqns. (A13) and (A14) will be

$$\frac{dA_s(z)}{dz} = 2j\gamma \left((P_{p1} + P_{p2})A_s(z) + A_i^*(z)A_{p1}(0) \, A_{p2}(0) \; exp(-j\theta z) \right) \tag{A15}$$

$$\frac{dA_i^*(z)}{dz} = -2j\gamma \left((P_{p1} + P_{p2})A_i^*(z) + A_s(z)A_{p1}^*(0) \, A_{p2}^*(0) \, exp(j\theta z) \right) \tag{A16}$$

To solve Eqns. (A15) and (A16), let

$$B_s(z) = A_s(z)exp\left(-2j\gamma\left(P_{p1} + P_{p2}\right)z\right) \tag{A17}$$

$$B_i^*(z) = A_i^*(z)exp\left(2j\gamma\left(P_{p1} + P_{p2}\right)z\right) \tag{A18}$$

Differentiating Eqns. (A17) and (A18) with respect to z yields

$$\frac{dB_s(z)}{dz} = A_s(z)\left(-2j\gamma\left(P_{p1} + P_{p2}\right)\right)exp\left(-2j\gamma\left(P_{p1} + P_{p2}\right)z\right)$$
$$+ \frac{dA_s(z)}{dz}\,exp\left(-2j\gamma\left(P_{p1} + P_{p2}\right)z\right) \tag{A19}$$

$$\frac{dB_i^*(z)}{dz} = A_i^*(z)\left(2j\gamma\left(P_{p1} + P_{p2}\right)\right)exp\left(2j\gamma\left(P_{p1} + P_{p2}\right)z\right)$$
$$+ \frac{dA_i^*(z)}{dz}\,exp\left(2j\gamma\left(P_{p1} + P_{p2}\right)z\right) \tag{A20}$$

Substituting Eqns. (A15) and (A16) into Eqns. (A19) and (A20)

$$\frac{dB_s(z)}{dz} = A_s(z)\left(-2j\gamma\left(P_{p1} + P_{p2}\right)\right)exp\left(-2j\gamma\left(P_{p1} + P_{p2}\right)z\right)$$
$$+ 2j\gamma\left(P_{p1} + P_{p2}\right)A_s(z)\,exp\left(-2j\gamma\left(P_{p1} + P_{p2}\right)z\right)$$
$$+ 2j\gamma\,A_i^*(z)A_{p1}(0)\,A_{p2}(0)\,exp(-j\theta z)\,exp\left(-2j\gamma\left(P_{p1}\right.\right.$$
$$\left.\left. + P_{p2}\right)z\right) \tag{A21}$$

$$\frac{dB_i^*(z)}{dz} = A_i^*(z)\left(2j\gamma\left(P_{p1} + P_{p2}\right)\right)exp\left(2j\gamma\left(P_{p1} + P_{p2}\right)z\right)$$
$$- 2j\gamma\left(P_{p1} + P_{p2}\right)A_i^*(z)\,exp\left(2j\gamma\left(P_{p1} + P_{p2}\right)z\right)$$
$$- 2j\gamma\,A_s(z)A_{p1}^*(0)\,A_{p2}^*(0)\,exp(j\theta z)\,exp\left(2j\gamma\left(P_{p1}\right.\right.$$
$$\left.\left. + P_{p2}\right)z\right) \tag{A22}$$

Equations (3.19) and (3.20), after simplification, can be written as follow

$$\frac{dB_s(z)}{dz} = 2j\gamma A_{p1}(0)\,A_{p2}(0)\,exp(-j\theta z)A_i^*(z)\,exp\left(-2j\gamma\left(P_{p1} + P_{p2}\right)z\right) \tag{A23}$$

$$\frac{dB_i^*(z)}{dz} = -2j\gamma\,A_{p1}^*(0)\,A_{p2}^*(0)\,exp(j\theta z)\,A_s(z)\,exp\left(2j\gamma\left(P_{p1} + P_{p2}\right)z\right) \tag{A24}$$

From Eqns. (A17) and (A18), $A_s(z)$ and $A_i^*(z)$ can be given by

$$A_s(z) = B_s(z)exp\left(2j\gamma\left(P_{p1} + P_{p2}\right)z\right) \tag{A25}$$

$$A_i^*(z) = B_i^*(z) exp\left(-2j\gamma(P_{p1} + P_{p2})z\right) \tag{A26}$$

Substituting Eqns. (A26) and (A25) into Eqns. (A23) and (A24) respectively, yields

$$\frac{dB_s(z)}{dz} = 2j\gamma\, A_{p1}(0)\, A_{p2}(0)\, \exp(-jkz)\, B_i^*(z) \tag{A27}$$

$$\frac{dB_i^*(z)}{dz} = -\, 2j\gamma\, A_{p1}^*(0)\, A_{p2}^*(0)\, exp(jkz)\, B_s(z) \tag{A28}$$

where k is the effective phase mismatch which is given by

$$k = \Delta k + \gamma(P_{p1} + P_{p2}) \tag{A29}$$

Differentiating Eqns. (A27) and (A28) a second time with respect to z yields

$$\frac{d^2 B_s(z)}{dz^2} = 2j\gamma\, A_{p1}(0)\, A_{p2}(0)\, \exp(-jkz)\, \frac{dB_i^*(z)}{dz}$$
$$+ 2\gamma k\, A_{p1}(0)\, A_{p2}(0)\, exp(-jkz)B_i^*(z) \tag{A30}$$

$$\frac{d^2 B_i^*(z)}{dz^2} = -\, 2j\gamma\, A_{p1}^*(0)\, A_{p2}^*(0)\, exp(jkz)\frac{dB_s(z)}{dz}$$
$$+ 2\gamma k\, A_{p1}^*(0)\, A_{p2}^*(0)\, \exp(jkz)\, B_s(z) \tag{A31}$$

From Eqns. (A27) and (A28)

$$B_i^*(z) = \frac{1}{2j\gamma\, A_{p1}(0)\, A_{p2}(0)\, \exp(-jkz)}\, \frac{dB_s(z)}{dz} \tag{A32}$$

$$B_s(z) = -\frac{1}{2j\gamma\, A_{p1}^*(0)\, A_{p2}^*(0)\, exp(jkz)}\, \frac{dB_i^*(z)}{dz} \tag{A33}$$

Substituting Eqns. (A28) and (A32) into Eqn. (A30) yields

$$\frac{d^2 B_s(z)}{dz^2}$$
$$= 2j\gamma A_{p1}(0)\, A_{p2}(0)\, \exp(-jkz)\, [-\, 2j\gamma\, A_{p1}^*(0)\, A_{p2}^*(0)\, exp(jkz)\, B_s(z)]$$
$$+ 2\gamma k A_{p1}(0)\, A_{p2}(0)\, exp(-jkz)\left[\frac{1}{2j\gamma\, A_{p1}(0)\, A_{p2}(0)\, \exp(-jkz)}\frac{dB_s(z)}{dz}\right] \tag{A34}$$

Then Substituting Eqns. (A27) and (A33) into Eqn. (A31) yields

$$\frac{d^2 B_i^*(z)}{dz^2}$$

$$= -2j\gamma\, A_{p1}^*(0)\, A_{p2}^*(0)\, exp(jkz)\, [2j\gamma\, A_{p1}(0)\, A_{p2}(0)\,\, exp(-jkz)\, B_i^*(z)]$$

$$+ 2\gamma k\, A_{p1}^*(0)\, A_{p2}^*(0)\, exp(jkz) \left[\frac{-1}{2j\gamma\, A_{p1}^*(0)\, A_{p2}^*(0)\, exp(jkz)}\, \frac{dB_i^*(z)}{dz}\right] \quad (A35)$$

Then, from Eqns. (A34) and (A35) the following second-order ordinary differential equations can be obtained

$$\frac{d^2 B_s(z)}{dz^2} + jk\,\frac{dB_s(z)}{dz} - 4\gamma^2 P_{p1}P_{p2}\, B_s(z) = 0 \qquad\qquad (A36)$$

$$\frac{d^2 B_i^*(z)}{dz^2} - jk\,\frac{dB_i^*(z)}{dz} - 4\gamma^2 P_{p1}P_{p2}\, B_i^*(z) = 0 \qquad\qquad (A37)$$

The general solutions of Eqns. (A36) and (A37) can be found as follow

$$B_s(z) = [C_1 \exp(gz) + C_2 \exp(-gz)] \exp(-j\tfrac{k}{2}z) \qquad\qquad (A38)$$

$$B_i^*(z) = [C_3 \exp(gz) + C_4 \exp(-gz)] \exp(j\tfrac{k}{2}z) \qquad\qquad (A39)$$

where the parametric gain coefficient $g = \sqrt{4\gamma^2 P_{p1}P_{p2} - (k/2)^2}$. Further, C_1, C_2, C_3, and C_4 are constants determined from the boundary conditions. Applying $z = 0$ in Eqn. (A38), yields

$$B_s(0) = C_1 + C_2 \qquad\qquad (A40)$$

Differentiating Eqn. (A38) with respect to z gives

$$\frac{dB_s(z)}{dz} = [C_1 \exp(gz) + C_2 \exp(-gz)] \exp(-j\tfrac{k}{2}z)\left(-j\tfrac{k}{2}\right)$$

$$+ \exp\left(-j\tfrac{k}{2}z\right) [gC_1 \exp(gz) - gC_2\exp(-gz)] \qquad\qquad (A41)$$

Equating Eqns. (A41) and (A27) with the primary condition $z = 0$ gives

$$2j\gamma \, A_{p1}(0) \, A_{p2}(0) \, \exp(-jkz) \, B_i^*(0) = [C_1 + C_2]\left(-j\frac{k}{2}\right) + g[C_1 - C_2] \quad (A42)$$

Applying $B_i^*(0) = 0$, (idler wave at $z = 0$)

$$g[C_1 - C_2] = [C_1 + C_2]\left(j\frac{k}{2}\right) \quad\quad (A43)$$

Solving Eqns. (A40) and (A43) produces

$$C_1 = \frac{1}{2}\left(1 + \frac{jk}{2g}\right) B_s(0) \quad \text{and} \quad C_2 = \frac{1}{2}\left(1 - \frac{jk}{2g}\right) B_s(0)$$

Now, similar method is used to find C_3 and C_4, therefore

$$C_3 = \frac{-j\gamma \, A_{p1}^*(0) \, A_{p2}^*(0) \, B_s(0)}{g} \quad \text{and} \quad C_4 = \frac{j\gamma \, A_{p1}^*(0) \, A_{p2}^*(0) \, B_s(0)}{g}$$

Substituting $C_1 \; and \; C_2$ into Eqn. (A38) and $C_3 \; and \; C_4$ into Eqn. (A39) and simplifying these equations yields

$$B_s(z) = B_s(0)\left[\left(\frac{exp(gz) + exp(-gz)}{2}\right)\right.$$
$$\left. + \frac{jk}{2g}\left(\frac{exp(gz) - exp(-gz)}{2}\right)\right] exp\left(-j\frac{k}{2}z\right) \quad\quad (A44)$$

$$B_i^*(z) = \left[\frac{-j\gamma \, A_{p1}^*(0) \, A_{p2}^*(0) \, B_s(0)}{g} \, exp(gz)\right.$$
$$\left. + \frac{j\gamma \, A_{p1}^*(0) \, A_{p2}^*(0) \, B_s(0)}{g} \, exp(-gz)\right] exp\left(j\frac{k}{2}z\right) \quad\quad (A45)$$

Using the formulas

$$cosh(x) = \frac{exp(x) + exp(-x)}{2} \quad \text{and} \quad sinh(x) = \frac{exp(x) - exp(-x)}{2}$$

$$B_s(z) = B_s(0)\left[cosh(gz) + \frac{jk}{2g}\, sinh(gz)\right] exp\left(-j\frac{k}{2}z\right) \quad\quad (A46)$$

$$B_i^*(z) = \frac{-j2\gamma \, A_{p1}^*(0) \, A_{p2}^*(0) \, B_s(0) \, sinh(gz)}{g} \, exp(j\frac{k}{2}z) \quad\quad (A47)$$

Return back to Eqns. (A17) and (A18) to find $A_s(0)$ and $A_i^*(z)$ from $B_s(0)$ and $B_i^*(z)$, respectively

$$A_s(z) = B_s(z)exp\left(2j\gamma\left(P_{p1} + P_{p2}\right)z\right) \tag{A48}$$

$$A_i^*(z) = B_i^*(z)exp\left(-2j\gamma\left(P_{p1} + P_{p2}\right)z\right) \tag{A49}$$

Substituting Eqns. (A48) and (A49) into Eqns. (A46) and (A47) yields

$$A_s(z) = A_s(0)\left(cosh(gz) + \frac{jk}{2g}\ sinh(gz)\right)$$
$$* exp\left(j\ \frac{3\gamma\left(P_{p1} + P_{p2}\right) - \Delta k}{2}z\right) \tag{A50}$$

$$A_i^*(z) = A_s(0)\left(\frac{-j2\gamma\ A_{p1}^*(0)\ A_{p2}^*(0)}{g}\right)sinh(gz)$$
$$* exp\left(-j\ \frac{3\gamma\left(P_{p1} + P_{p2}\right) - \Delta k}{2}z\right) \tag{A51}$$